

N 66-14376  
(ACCESSION NUMBER) (THRU)

133  
(PAGES) (CODE)

15  
(NASA CR OR TMX OR AD NUMBER) (CATEGORY)

GPO PRICE \$ \_\_\_\_\_

CFSTI PRICE(S) \$ \_\_\_\_\_

Hard copy (HC) 4.00

Microfiche (MF) 1.00

# 853 July 65

# DEVELOPMENT OF LARGE-INTERNAL-SURFACE-AREA NICKEL-METAL PLAQUES

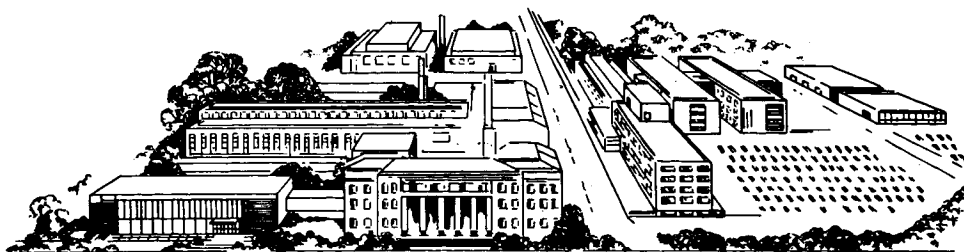
by

J. McCallum, G. R. Schaer, D. G. Trevethan, and C. L. Faust

prepared for

NATIONAL AERONAUTICS AND SPACE ADMINISTRATION  
LEWIS RESEARCH CENTER  
SPACE POWER SYSTEMS DIVISION

Contract NAS 3-6003



**BATTELLE**  
MEMORIAL INSTITUTE

### NOTICE

This report was prepared as an account of Government sponsored work. Neither the United States, nor the National Aeronautics and Space Administration (NASA), nor any person acting on behalf of NASA:

- A.) Makes any warranty or representation, expressed or implied, with respect to the accuracy, completeness, or usefulness of the information contained in this report, or that the use of any information, apparatus, method, or process disclosed in this report may not infringe privately owned rights; or
- B.) Assumes any liabilities with respect to the use of, or for damages resulting from the use of any information, apparatus, method or process disclosed in this report.

As used above, "person acting on behalf of NASA" includes any employee or contractor of NASA, or employee of such contractor, to the extent that such employee or contractor of NASA, or employee of such contractor prepares, disseminates, or provides access to, any information pursuant to his employment or contract with NASA, or his employment with such contractor.

Requests for copies of this report  
should be referred to:

National Aeronautics and Space Administration  
Office of Scientific and Technical Information  
Washington 25, D.C.  
Attention: AFSS-A

FINAL REPORT

DEVELOPMENT OF LARGE-INTERNAL-SURFACE-AREA  
NICKEL-METAL PLAQUES

by

J. McCallum, G. R. Schaer, D. G. Trevethan, and C. L. Faust

prepared for

NATIONAL AERONAUTICS AND SPACE ADMINISTRATION  
LEWIS RESEARCH CENTER  
SPACE POWER SYSTEMS DIVISION

September 30, 1965

CONTRACT NAS 3-6003

Technical Management  
NASA Lewis Research Center  
Cleveland, Ohio  
Space Power Systems Division  
Mr. W. A. Robertson  
MS 500-201

BATTELLE MEMORIAL INSTITUTE  
505 King Avenue  
Columbus, Ohio 43201

# Battelle Memorial Institute · COLUMBUS LABORATORIES

505 KING AVENUE COLUMBUS, OHIO 43201 · AREA CODE 614, TELEPHONE 299-3151 · CABLE ADDRESS: BATMIN

January 14, 1966

National Aeronautics and Space Administration  
Lewis Research Center  
Space Power Systems Procurement Section  
21000 Brookpark Road  
Cleveland, Ohio 44135

Attention John E. Dilley, MS 500-309  
Contracting Officer

Final Report  
"Development of Large-Internal-Surface-Area  
Nickel Metal Plaques"  

---

Contract NAS 3-6003

This is your copy of the Final Report on Contract NAS 3-6003. It covers the period between June 18, 1964, and September 30, 1965.

This report has been reviewed by Mr. Wm. A. Robertson (Technical Project Manager for your organization). All corrections suggested by Mr. Robertson are now included in the report. Printing and distribution are in accordance with your approval dated December 17, 1965. The distribution list for this report is identical with the list approved for the Third Quarterly Progress Report.

We appreciate having had the opportunity to work with NASA on this interesting project.

Yours sincerely,



John McCallum  
Project Leader

JM:bep  
cc: See Distribution List  
Enc.

DEVELOPMENT OF LARGE-INTERNAL-SURFACE-AREA  
NICKEL-METAL PLAQUES

by

J. McCallum, G. R. Schaer, D. G. Trevethan, and C. L. Faust

ABSTRACT

14976

Porous nickel electrodes having preselected pore sizes and pore shapes were made. They were impregnated with cadmium in various forms and evaluated as rechargeable cadmium electrodes. The results showed a need to understand the changes that occur with cycling of cadmium electrodes. Impregnation of active cadmium into the porous nickel plaque was found to be a critical variable. The use of fused cadmium nitrate hydrate followed by a hot soak in potassium hydroxide solution was found to be preferred. Additional ways to decrease the weight of cadmium electrodes were implied by the results obtained: (1) The weights of active positive and negative materials should be more closely balanced stoichiometrically. (2) Pore volumes should be filled more than the present commercial practice of about 40 percent. (3) Electrode plaques should have straight-through pores with electrode thickness equal to about twice the pore diameters.

*Author*

TABLE OF CONTENTS

	<u>Page</u>
SUMMARY . . . . .	1
INTRODUCTION . . . . .	4
EXPERIMENTAL RESULTS BY TASKS	
TASK A - RAW-MATERIAL CLASSIFICATION . . . . .	6
Objectives . . . . .	6
Item 1 - Average Size . . . . .	6
Powdered Plaques . . . . .	6
Electroformed Screens . . . . .	8
Item 2 - Size Tolerance . . . . .	8
Powdered Plaques . . . . .	8
Electroformed Screens . . . . .	8
Item 3 - Shape of Holes . . . . .	10
Powdered Plaques . . . . .	10
Electroformed Screens . . . . .	10
Comparisons . . . . .	10
Location of Data . . . . .	15
TASK B - POROUS MAT MANUFACTURE . . . . .	15
Objectives . . . . .	15
Item 1 - Thickness Ranges . . . . .	16
Item 2 - Techniques . . . . .	16
Electroforming . . . . .	16
Commercial Screens . . . . .	16
Screen Electroforming Mandrels . . . . .	17
Superimposing Electroformed Screens . . . . .	26
Superimposing Etched Screens . . . . .	32
Item 3 - Method of Controlling Pore Shapes . . . . .	32
Pore Shapes . . . . .	32
Control of Porosity . . . . .	36
Discussion of Manufacturing Porous Screen Electrodes . . . . .	42
Location of Data . . . . .	42
TASK C - SINTERED PLAQUE PROCESSING . . . . .	43
Objectives . . . . .	43
Item 1 - Temperature and Pressure . . . . .	43
Item 2 - Time and Resistivity . . . . .	44
Item 3 - Atmosphere and Special Precautions . . . . .	44
Location of Data . . . . .	45
TASK D - PLAQUE CLASSIFICATION . . . . .	45
Objectives . . . . .	45

TABLE OF CONTENTS  
(Continued)

	<u>Page</u>
Item 1 - Electrical Resistivity . . . . .	45
Edge to Edge . . . . .	45
Surface to Surface . . . . .	46
Item 2 - Pore-Size Distribution . . . . .	46
Item 3 - Pore Shapes . . . . .	47
Item 4 - Internal Surface Areas . . . . .	47
Item 5 - Density and Porosity . . . . .	48
Item 6 - Measurement of Interconnecting Pores . . . . .	49
Item 7 - Tensile Strength . . . . .	49
Item 8 - Flexibility . . . . .	49
Location of Data . . . . .	51
 TASK E - IMPREGNATION PROCEDURE . . . . .	 51
Objectives . . . . .	51
General Conditions . . . . .	52
Step 1 - Selection of Procedure . . . . .	52
Step 2 - Weight Gains . . . . .	53
Step 3 - Energy Density Comparison of Electrodes . . . . .	53
Step 4A - Weight Gains and Ampere-Minute Capacity for Chemical Impregnation of Screen Electrodes . . . . .	55
Fleischer's Method . . . . .	55
Modified Fleischer Method. . . . .	58
The Effect of Additives in the Impregnation Solution. . . . .	61
Wetting Agents . . . . .	61
Barium Hydroxide . . . . .	61
Passivation of Nickel . . . . .	62
Multiple Impregnations . . . . .	62
Effect of Multiple Chemical Impregnations of Sintered Powder Plaques on Energy Output . . . . .	64
Energy-Output Efficiencies . . . . .	66
Polarizing With Controlled Potential . . . . .	68
Fused-Salt Impregnation . . . . .	69
Step 4B - Weight Gains and Amp-Minute Capacity for Physical Impregnation of Screen Electrodes . . . . .	73
Physical Packing Materials . . . . .	73
Cadmium Oxide . . . . .	73
Cadmium Hydroxide . . . . .	74
Physical Impregnation of Screen Electrodes With Cadmium Metal . . . . .	74
Electrochemical Evaluation of Physical Impregnation . . . . .	75
Removal of Cd/Cd(OH) <sub>2</sub> From Screen Electrodes . . . . .	76
Discussion of Physical Impregnation . . . . .	76
Comparison of Energy Densities . . . . .	76
Location of Data . . . . .	77
 TASK F - ELECTROCHEMICAL EVALUATION . . . . .	 77
Objectives . . . . .	77
Summary of Electrochemical Evaluations . . . . .	78

TABLE OF CONTENTS

(Continued)

	<u>Page</u>
Item 1 - Energy Output . . . . .	79
Relationship of Commercial Batteries to Commercial Cells . . . . .	79
Relationship of Cell Components to Commercial Cells . . . . .	80
Weight and Size Breakdown . . . . .	80
Reproducibility and Effect of Flooding . . . . .	82
Energy Conversion Factors . . . . .	85
Commercial Single Positive Electrodes . . . . .	86
Effect of Rate of Discharge . . . . .	86
Oxygen Effect . . . . .	90
Commercial Single Negative Electrodes . . . . .	90
Chemical Analysis . . . . .	90
Experimental Method for Single Electrodes . . . . .	91
Effect of Rate of Discharge . . . . .	92
Hydrogen Effect . . . . .	93
Cycling Effect . . . . .	94
N/P Ratios . . . . .	95
Experimental Screen Electrodes . . . . .	99
Reproducibility . . . . .	104
Effect of Rates . . . . .	104
Effect of Pore Size and Electrode Thickness . . . . .	107
A Flat Plate Electrode . . . . .	109
The Effect of Carbonate Contamination . . . . .	109
Item 2 - Energy Input . . . . .	112
Input Efficiencies . . . . .	112
The Effect of Pore Shapes . . . . .	115
Effects of Pore Volume Filled and Plaques Areas on Electrode Performance . . . . .	116
TASK G - CORROSION STABILITY . . . . .	117
Objectives . . . . .	117

LIST OF TABLES

Table 1. Comparison of Average Pore Sizes for Electroformed Screens and Commercial Nickel Plaques . . . . .	9
Table 2. Comparison of Pore-Size Tolerance for Electroformed Screens and Commercial Sintered Nickel Plaques . . . . .	9
Table 3. Comparison of Size Tolerance . . . . .	9
Table 4. Photoprinting and Etching Copper Mandrels . . . . .	19
Table 5. Plating Nickel on Electroformed Screens . . . . .	25
Table 6. Control of Pore Shape in 250-Mesh Screen Plaques . . . . .	35



LIST OF TABLES  
(Continued)

		<u>Page</u>
Table 7.	Physical Dimensions, Weights, and Porosities of Stacked Screen Plaques . . . . .	40
Table 8.	Relationship of Hole Size and Porosity of Screens . . . . .	41
Table 9.	Nickel Etching Rates in Ferric Chloride Solutions . . . . .	42
Table 10.	Internal Surface Area of Nickel Plaques . . . . .	47
Table 11.	Relationships of Area to Volume for Sphere, Wires, and Sheets . . . . .	48
Table 12.	Density and Porosity of Commercial Electroformed Screens and Commercial Sintered Powder Plaques . . . . .	49
Table 13.	Tensile Strength of Commercial Powder Plaques and Superimposed Nickel Screens . . . . .	50
Table 14.	Total Amount of Cadmium Hydroxide Precipitated as a Function of the Number of Impregnations . . . . .	53
Table 15.	Coulombic Density Comparisons . . . . .	55
Table 16.	Chemical Impregnation of Semirandom Screen Structures . . . . .	56
Table 17.	Discharge Efficiency for Four-Cycle Impregnation . . . . .	60
Table 18.	Discharge Data for Screen Electrodes Chemically Impregnated Eight Times . . . . .	65
Table 19.	Energy Output as a Function of Percentage of Pore Volume Filled With Cd(OH) <sub>2</sub> for Commercial Electrodes . . . . .	66
Table 20.	Material Balance of Discharged-Screen Electrodes . . . . .	67
Table 21.	Activation of a Fused-Salt Impregnation for Electrode 38 . . . . .	68
Table 22.	Descriptive and Experimental Data for Physically Impregnated Screen Electrodes . . . . .	75
Table 23.	Energy Density Comparison of an Experimental Screen Electrode With a Commercial Sintered Nickel Electrode . . . . .	77
Table 24.	Physical Dimensions of a Commercial Nickel-Cadmium Battery to be Used for Comparison Purposes . . . . .	79
Table 25.	Physical Dimensions for Separate Components of a Commercial Nickel-Cadmium Cell . . . . .	81

LIST OF TABLES  
(Continued)

	<u>Page</u>
Table 26. Effect of Flooding in a Commercial Nickel-Cadmium Cell . . . . .	82
Table 27. Approximate Weight and Volume Factors for Estimating Performances From Individual Components . . . . .	86
Table 28. Electrochemical History of a Single Positive Electrode From a Commercial Nickel-Cadmium Battery . . . . .	87
Table 29. Electrochemical History of a Single Negative Electrode From a Commercial Nickel-Cadmium Battery . . . . .	93
Table 30. Electrochemical Data for Shaped Pore Electrodes . . . . .	99
Table 31. Typical Weights of Reused Electrodes . . . . .	103
Table 32. Reproducibility of Electrochemical Data . . . . .	105
Table 33. Relationship of Electrode Thickness and Pore Diameter to Electrochemical Efficiency . . . . .	107
Table 34. Capacity of Experimental Electrodes . . . . .	110
Table 35. Details of Carbon-Contamination Experiment . . . . .	112
Table 36. Effect of Electrode Shape on Electrode Efficiencies . . . . .	116
Table 37. Relationship of Electrode Efficiencies to Percent of Pore Volumes Filled and to the Internal Surface Area of the Electrodes . . . . .	117

LIST OF FIGURES

	<u>Page</u>
Figure 1. Cumulative Pore Volume, $\text{cm}^3/\text{g}$ , Measured by Mercury Porosimeter on Commercial Sintered Nickel-Powder Plaques . . .	7
Figure 2. Cross Section of Commercial Sintered Nickel Plaque Showing Structure at 100X . . . . .	11
Figure 3. Cross Section of Commercial Sintered Nickel Plaque Showing Structure at 250X . . . . .	11
Figure 4. Surface View of Center of 1000-Line-Per-Inch Electroformed Screen Showing Shapes of Holes . . . . .	12
Figure 5. Surface View of Center of 750-Line-Per-Inch Electroformed Screen Showing Shapes of Holes . . . . .	12
Figure 6. Surface View of Center of 500-Line-Per-Inch Electroformed Screen Showing Shapes of Holes . . . . .	13
Figure 7. Surface View of Center of 250-Line-Per-Inch Electroformed Screen Showing Shapes of Holes . . . . .	13
Figure 8. Surface View Near Corner of 1000-Line-Per-Inch Electroformed Screen Showing the Most Severe Hole Closure . . . . .	13
Figure 9. Cross Sections Near Corner of Electroformed Screen . . . . .	14
Figure 10. Sketch of Cross Section of Commercial Electroforming Mandrel . . .	17
Figure 11. Sketch of Cross Sections of Screen Electroforming Mandrel . . . .	20
Figure 12. Sectional View of Five Screens Electroformed on Glass-Filled Mandrel in Superimposed Position . . . . .	21
Figure 13. Cross Section of Copper Mandrel With Glass-Filled Holes . . . . .	22
Figure 14. Cross Section of Copper Mandrel With Glass Coating . . . . .	22
Figure 15. View Perpendicular to Surface of a Nickel Mandrel (Dark Area) With Cone-Shaped Rubber Protrusions (Light Circular Areas) . . . .	22
Figure 16. Cross Section Through Holes in Master Stainless Steel Screen . . .	24
Figure 17. Cross Section Through Holes in Electroformed Nickel Screen . . . .	24
Figure 18. Cross Section of One Wire of a 250-Line-Per-Inch Screen Plated With Three Layers of Nickel Plate to Increase the Thickness . . . .	26
Figure 19. Perspective View of Microscope, Alignment Mechanism, and Die. . .	27

LIST OF FIGURES  
(Continued)

	<u>Page</u>
Figure 20. Simplified Schematic Drawing Showing First Piece of Cut Foil Resting in Die With Second Cut Ready to be Made in Nickel Foil . . .	28
Figure 21. Surface View of 250-Mesh Screens Containing 32 Layers Stacked to 38.56-Mil Thickness Before Bonding . . . . .	30
Figure 22. Surface View of 250-Mesh Screens Containing 32 Layers After Bonding to 35.5-Mil Thickness . . . . .	30
Figure 23. Top Surface of Superimposed 250-Mesh Screens Before Bonding - Focused on Top Screen . . . . .	31
Figure 24. Top Surface of Superimposed 250-Mesh Screens Before Bonding - Focused on Underneath Layer . . . . .	31
Figure 25. Top Surface of Superimposed 250-Mesh Screens After Bonding . . .	31
Figure 26. Bottom Surface of Superimposed 250-Mesh Screens After Bonding . . .	31
Figure 27. Top Surface of Superimposed 250-Mesh Screens Before Bonding . . .	31
Figure 28. Top Surface of Superimposed 250-Mesh Screens After Bonding . . .	31
Figure 29. Bottom Surface of Superimposed 250-Mesh Screens After Bonding . . .	33
Figure 30. Top Surface of Superimposed 500-Mesh Screens Before Bonding . . .	33
Figure 31. Top Surface of Superimposed 500-Mesh Screens After Bonding . . .	33
Figure 32. Bottom Surface of Superimposed 500-Mesh Screens After Bonding . . .	33
Figure 33. Surface View of 250-Mesh Screens Stacked by Hand to 10.5-Mil Thickness . . . . .	33
Figure 34. Surface View of 250-Mesh Screens Containing 20 Layers Stacked by Hand to 35.5-Mil Thickness . . . . .	34
Figure 35. Cross Section of 250-Mesh Screens Containing 20 Layers Stacked by Hand to 35.5-Mil Thickness . . . . .	34
Figure 36. Surface View of 125-Mesh Etched Screens After Bonding to 10-Mil Thickness . . . . .	34
Figure 37. Surface View of Stacked and Bonded 250-Mesh Screens - Semirandom Orientation . . . . .	36
Figure 38. Surface View of Superimposed 500-Mesh Screens Before Bonding . . .	38

LIST OF FIGURES  
(Continued)

	<u>Page</u>
Figure 39. Surface View of Superimposed 500-Mesh Screens After Bonding . . .	38
Figure 40. Surface View of Superimposed 500-Mesh Screens After Bonding and Etching . . . . .	38
Figure 41. Cross Section of Electrode 44 After Fabrication - Parallel-Sided Structure . . . . .	39
Figure 42. Cross Section of Electrode 35 After Fabrication - Parallel-Sided Structure . . . . .	39
Figure 43. Cross Section of Electrode 49 After Fabrication - Keyed Structure .	39
Figure 44. Cross Section of Electrode 47 After Fabrication - Staggered-Taper Structure. . . . .	39
Figure 45. Drawing of Setup for Sintering Stacked Electroformed Nickel Screens . . . . .	44
Figure 46. Apparatus Used to Measure Surface-to-Surface Resistivity . . . . .	46
Figure 47. Tension-Test Specimen . . . . .	50
Figure 48. Percent Pore Volume Filled With $\text{Cd}(\text{OH})_2$ as a Function of the Number of Impregnations . . . . .	54
Figure 49. Capacity of Negative Plates as a Function of Charge-Discharge Cycles . . . . .	57
Figure 50. Cross Sections of Semirandom Porous Electrodes 15A, 15B, 16A, and 16B in Charged Condition . . . . .	59
Figure 51. Surface View of Screen Electrodes After Conventional Chemical Impregnation Showing Inactive Surface Deposits . . . . .	60
Figure 52. Photomicrograph of Electrode 31 After Impregnation and Charging and Discharging Showing Needles on Surface . . . . .	62
Figure 53. Surface View of Screen Electrode Number 37 After Several Charge-Discharge Cycles Showing Bare Nickel Exposed on Outside Screen . . . . .	63
Figure 54. Surface View of Cadmium-Plated Screen Electrode Number 24 After Several Charge-Discharge Cycles Showing Coverage of Screen With Cadmium Material . . . . .	63
Figure 55. Surface View of Screen Electrode 45 With 3.2-Mil Holes After Impregnation With 22 Percent of Pore Volume Filled, Test 106 . . .	69

LIST OF FIGURES  
(Continued)

	<u>Page</u>
Figure 56. Relationship of Input and Output Capacities as the Cadmium Hydroxide is Activated . . . . .	71
Figure 57. Surface View of Screen Electrode With 6-Mil Holes After Impregnation With 38 Percent of Pore Volume Filled . . . . .	73
Figure 58. Cross Section of a Physically Impregnated Stacked-Screen Electrode . . . . .	74
Figure 59. Discharge Data for Commercial Nickel-Cadmium Electrodes at 0.640-Amp Constant Current in a Sealed Cell and Under Flooded Conditions . . . . .	83
Figure 60. Half-Cell Discharge Data From Commercial Nickel-Cadmium Electrodes . . . . .	88
Figure 61. Half-Cell Discharge Data From Commercial Nickel-Cadmium Electrodes . . . . .	88
Figure 62. Average Voltage of Positive Half-Cell vs Current Density . . . . .	89
Figure 63. Cross Section of a Commercial Impregnated Battery Plate Before Cycling (Without Overlay) . . . . .	96
Figure 64. Cross Section of a Commercial Impregnated Battery Plate Before Cycling (With Overlay) . . . . .	96
Figure 65. Cross Section of a Commercial Impregnated Battery Plate After Five Charge-Discharge Cycles of 100 Percent Depth . . . . .	97
Figure 66. Cross Section of Battelle Impregnated Commercial Sintered Nickel Plate After Five Charge-Discharge Cycles of 100 Percent Depth . . . . .	97
Figure 67. Discharge Efficiency as a Function of Rate . . . . .	106
Figure 68. Relationship of Pore Length, L, and Pore Diameter, d, to Electrode Efficiency . . . . .	108
Figure 69. Effects of Cycling on the Charging of Commercial Cadmium Electrodes . . . . .	113
Figure 70. Voltage for Hydrogen Evolution as a Function of Cadmium Electrode Potential . . . . .	114
Figure 71. Charging Curves for Commercial and Screen Electrodes . . . . .	114
Figure 72. Anodic-Corrosion Measurements on Nickel Electrodes . . . . .	119

# DEVELOPMENT OF LARGE-INTERNAL-SURFACE-AREA NICKEL-METAL PLAQUES

by

J. McCallum, G. R. Schaer, D. G. Trevethan, and C. L. Faust

## SUMMARY

This report describes an investigation of porous nickel structures as inert plaques for cadmium electrodes. The overall project objective, to develop large-internal-surface-area nickel-metal plaques, was aimed toward plaques with controlled pore shapes. Accordingly, the program proceeded first to explore the possibilities for stacking electroformed screens into plaques with uniform pore distribution. Possibilities for controlling pore shapes by use of selective electroforming and stacking procedures were studied next. Finally, experiments were performed to demonstrate any physical and electrochemical advantages for the controlled pore dimensions. Results were as follows:

First, Stacking. Electroformed nickel screens were stacked into plaque structures with a uniform pore distribution. About 20 experimental electrodes 1 x 1 cm were made in thicknesses from 4.2 to 35.5 mil (0.01 to 0.09 cm) and with pore-size variations less than  $\pm 10$  percent of average for each electrode having pores from 0.6 to 6.0 mils in effective diameter.

Second, Shape. Control of pore shapes was achieved also by selective electroforming and stacking procedures. The most success was obtained with parallel-sided pores with and without constricted openings. The straight-through pores were made by superimposing identical layers of electroformed screens on top of one another. Constriction of openings was obtained by using screens with larger wires for the first few layers on both sides of a stack. Pores with an internal staggered taper were made by alternating screens with different wire width but the same mesh.

Third, Physical Advantage. Physical advantages for the controlled pore dimensions, compared to commercial sintered powder plaques, were demonstrated with (1) close tolerance on pore-size distribution, (2) greater tensile strength, (3) increased flexibility, and (4) lowered electrical resistivity. Apparent disadvantages were (1) lower internal surface area, (2) lower porosity, and (3) higher costs.

Fourth, Electrochemical Advantages. Electrochemical results led to some definite conclusions:

(1) Cadmium-impregnated porous electrodes are more efficiently charged and discharged as they are made thin relative to their pore diameters. This discovery may have practical significance because it implies that small pores are unnecessary. The result implies also that "Large-Internal-Surface-Area Nickel-Metal Plaques" may not be the most important criterion for improved electrodes. Rather, it seems that thin electrodes with large pores are preferred.

(2) Efficiency of cadmium electrodes depends more on rate of charging and discharging than on the apparent current density calculated with the geometric area. This result suggests that there is an "effective" area that controls performance, even though this effective area is neither synonymous with internal surface area nor with geometric area of an electrode. The effective area was found to change with cycling of the cadmium electrode even though the plaques remained unchanged.

(3) The uniform pores of stacked screens provided performances less sensitive to rates of charging or discharging than did the random pores of sintered nickel powders.

(4) The new electrodes permitted simplified impregnation procedures to be used. Electrochemical results showed that greater filling of plaques could decrease electrode weights per unit of capacity without decreasing performance.

Some of the work toward detailed objectives is summarized next.

From a contractual viewpoint, considerable research effort was given to the preparation and evaluation of electrodes: A special stacking machine was designed, made, and used to prepare electrodes. This machine permitted the alignment of consecutive screen layers and the cutting of 1 x 1-cm samples. A special holder in the machine permitted transport of a final stack through sintering operations.

The sintering operation was also investigated from the viewpoint of temperature, pressure, time, and atmosphere. Best results were obtained when the electroformed screens were diffusion bonded at 2150 F, for 2 hours, with a loading pressure on stacks of 175 g/cm<sup>2</sup>, and in a hydrogen atmosphere.

Electrodes were made to contract specifications of thicknesses, and pore sizes using commercial electroformed screens with the stacking machine. Research effort was given also to alternative techniques:

(1) A special plating process was used to selectively increase the thickness of commercial screen wires relative to their width. This process simplified stacking in two ways: (a) thicker screens are easier to handle, and (b) with thicker screens fewer layers are needed to make a given thickness of electrode.

(2) Means for increasing the reusability of electroforming mandrels were investigated because the photoresists used in the commercial processes are limited to a few reuses. A flat mandrel, in which conducting copper and the pattern-resist are made flush with one another, was found to be a good candidate for engineering development, providing less than 250 wires per inch is desired. Another mandrel process duplicated the holes in master plates with silicone rubber projections. The rubber projections permitted reusing of the mandrel.

(3) New corrugated mandrels were conceived for mass-producing special structures without a stacking machine. Future work will be needed to develop the concepts into practical hardware.



(4) Hand stacking of large screens, with the use of intermediate spot welding, was found to be feasible if screens were at least 1 mil thick.

After experimental screen electrodes had been made, it was found necessary to etch them to a common porosity for interelectrode comparisons because porosities varied with individual stacks of screens. An alcohol-iodine etching solution was found to give the best results. Aqueous etching solutions were observed to attack grain boundaries preferentially, thereby tending to disintegrate sintered screens. The above alcohol etchant required no agitation and uniformly removed nickel metal at a low enough rate for easy control of porosity. Porosities up to 76 percent were obtained.

Impregnation of electrodes was studied several ways. A general finding was that the impregnation process, itself, was sensitive to electrode-pore dimensions. The published chemical precipitation process used for commercial impregnation, for example, was duplicated in Battelle laboratories on commercial sintered powder plaques. The same commercial impregnation procedure was found to be completely inadequate for the experimental stacked screen electrodes - an unexpected result.

The presence of carbonate impurity present in reagent-grade potassium hydroxide used to make the electrolyte was found to seriously decrease efficiency (1) during cycling or (2) during standing in a discharged condition. Electrodes were charged and discharged up to four times with no loss in capacity when an electrolyte was used that had been freed of carbonate ions by the addition of barium hydroxide.

Physical methods for impregnating experimental electrodes were studied using  $\text{Cd}(\text{OH})_2$ ,  $\text{CdO}$ , and  $\text{Cd}$  metal as starting materials.

Active cadmium material in the form of very fine powder was less efficiently used during discharging than other electrodes which contained cadmium powder of larger size. This implies that larger metallic crystals are preferred both for efficient operation and for minimizing cycle losses. The cadmium hydroxide was always found to be too bulky for an efficient impregnation, that is, the bulk density, of  $\text{Cd}(\text{OH})_2$ , no matter how prepared, was too low to permit the pores to be 40 percent filled using physical methods for putting the hydroxide directly into pores. Results with cadmium oxide showed borderline utility for the same reason. That is, cadmium oxide physically pushed, or pulled, into pores always had a bulk density such that the effectiveness of impregnation remained questionable.

Impregnation by a process which electrodeposited cadmium metal from a slurry of cadmium hydroxide in potassium hydroxide, showed some promise. Weight gains with one cycle of this new process were equivalent to the weight gain brought about by four cycles of the conventional impregnation. The cadmium sponge so deposited was found, however, to require cycling and conditioning for its efficient electrochemical utilization. This complication was bypassed, rather than solved, by turning to impregnation with molten cadmium nitrate-hydrate:  $\text{Cd}(\text{NO}_3) \cdot 4\text{H}_2\text{O}$ .

The conditions for preparing porous and active  $\text{Cd}(\text{OH})_2$  using the molten nitrate impregnation procedure were worked out so that two impregnation cycles from the fused nitrate gave results equivalent to four conventional impregnation cycles from aqueous solutions. Soaking of the impregnated product in hot  $\text{KOH}$  was found to be preferred over the more usual cathodic polarization. When cathodic reduction of nitrate was desired, it was found preferable to adjust current densities so as to carry out the reduction at potentials positive with respect to cadmium metal.

A greater filling of voids in the nickel plaques, during impregnation with cadmium hydroxide, was found to be one way to increase the energy density of cadmium electrodes. An increase from the normal 40 percent to at least 50 percent of voids filled was observed to have no detrimental effect on electrode performance. Filling of voids up to 70 percent was indicated to be possible. Such increases in impregnation might decrease the weight of cadmium electrodes some 25 to 75 percent.

Experiments have shown that a cadmium electrode performance in a flooded condition is identical to its performance in sealed batteries.

Studies with commercial electrodes and battery components were made to provide a weight and size breakdown by separate parts. The negative electrodes were found to be the largest and heaviest single components of a battery. Therefore, any decrease in the weight and size of negative electrodes will provide significant decreases in the final battery.

A large excess of negative materials, N, relative to active positive material, P, is found in commercial cells. On the basis of theoretical capacities, an N/P ratio of 2.07 was found for two commercial electrodes. The literature reports N/P capacity ratios as high as 2.15. An ideal minimum was estimated to be an N/P capacity ratio of 1.08. If this ideal could be achieved by further research and development, the weight of cadmium electrodes might be nearly halved.

## INTRODUCTION

(a) Status of the Problem Prior to the Present Work. Presently used plaques, for the rechargeable cadmium electrode, are made with sintered nickel carbonyl powders, having porosities on the order of 80 percent. They have a range of random pore sizes and shapes. Not all of the pores can be filled with active cadmium and the impregnation procedures are lengthy and expensive. Active cadmium within the nickel pores tends to shift position during charge/discharge cycling. Effectiveness of contact between the uncharged cadmium oxide and the plaque is always uncertain because contacts are always changing. One of the results is that cadmium electrodes must be made oversize to allow for the uncertainties of and changes in their performances.

(b) Definition of the Purpose. This program is part of NASA's continuing effort to develop and improve electrochemical power-generating devices. The specific objective is the development of porous nickel-metal plaques for the rechargeable cadmium electrode to provide higher energy output per unit of weight than is presently available.

(c) Scope of Work and Its Relation to the General Problem. NASA has started this research project to investigate new opportunities for improving nickel-cadmium batteries through the use of nickel plaques with controlled pore structures. Experimental plaques were to be made from electroformed screens having from 62,500 to 1,000,000 pores per square inch. Such screens are available commercially. They approach perfection in that the pore sizes are within the range ordinarily encountered with the electrodes presently used. The selected range of electrode thicknesses, 5 to 35 mils, includes commercial thicknesses, 20 to 40 mils, as well as thinner electrodes, less than 20 mils. The improvements sought were to include (a) impregnation procedures and (b) energy and power outputs and inputs per unit of electrode weight.

(d) Unusual Conditions. Work was planned with small single electrodes to be evaluated when completely immersed in potassium hydroxide solution, using a minimum number of complete charge and discharge cycles. Experimentation with single and flooded electrodes is not an unusual procedure and results in this report show it is a sound procedure. On the other hand, complete charging and discharging of single cadmium electrodes simulates approximately 200 percent depth of discharge on commercial sealed cells. Such extreme depth of cycling was found to change electrode performance so drastically that cycling became a dominant variable.

(e) Similar Work. So far as can be determined, there has never been a study similar to that reported herein, in which pore dimensions were so carefully controlled. Numerous workers have tested electrodes made with a variety of powder sizes, powder shapes, fibers, or agglomerates.

Fleischer\* studied the effect of electrode thickness between 6 and 60 mils. He reported that percent of voids filled for four impregnation cycles increased with thickness up to 20 mils. Beyond 20 mils, thickness made little difference. He also reported more efficient use of active material, at higher permissible rates, with decreasing electrode thickness.

(f) Significance of the Material Presented. The material presented in this report is important because nickel-cadmium batteries yield less than 10 percent of their theoretical capacity for a limited number of cycles.\*\* This inefficiency is attributable to two factors. First, there is a relatively large amount of inert plaque material contained within the case as the battery is usually built. A second important factor is the shallow discharge that is required to obtain a long cycle life. Work in this report yields significant information about both of these inefficiency factors and shows internal surface area of the nickel-metal plaques is not the most important parameter, as is sometimes supposed. Rather, the results herein suggest that the cadmium particle sizes and their availability to react with electrolyte are the important parameters. The cadmium particles seem to be determined by the impregnation procedure and by the cycling history. The accessibility of cadmium to electrolyte seems to be determined by the diameters,  $d$ , of pores in an electrode, and electrode thickness,  $L$ . A large ratio for  $L/d$  seems to increase electrode efficiency. Therefore recommendations are made as follows:

I. "New Electrode Structures for Nickel-Cadmium Batteries", described in this report, should be made and used in sealed batteries to demonstrate the improvements predicted for them.

II. A fundamental study to understand "The Changes Occurring in Cadmium Electrodes" should be started toward attaining proper means for improving electrode performance.

---

\*Fleischer, A., Nickel-Cadmium Battery Company, "Nickel-Cadmium Batteries", Proceedings of the 10th Annual Battery Research and Development Conference (May 23, 1956), pp 37-41.

\*\*Sanders, N. D., et al, "Conference on New Technology", Lewis Research Center, Cleveland, Ohio, June 4-5, 1964, p 68.

## EXPERIMENTAL RESULTS BY TASKS

TASK A - RAW-MATERIAL CLASSIFICATIONObjectives

Task A of the contract reads as follows:

"Item 1 - Average Size

Electroformed nickel screens shall be compared with commercially available sintered nickel plaques.

Average pore sizes shall be determined by using a mercury porosimeter and gas adsorption techniques for the sintered powdered plaques and the microscope for the electroformed screens.

"Item 2 - Size Tolerance

Size tolerance shall be determined. One brand of commercial sintered electrode shall be characterized for comparison with four (4) sizes of screens. The screens selected shall be between 250 and 1000 lines per lineal inch.

"Item 3 - Shape of Holes

The shape of holes shall be shown in photomicrographs."

The objective of this work is to compare the structure of commercial nickel-powder plaques with the structure of electroformed screens that will be used to make new plaques. Raw materials were interpreted to mean commercial materials that were used in the preparation of plaques or used for comparison purposes.

Item 1 - Average SizePowdered Plaques

For the purpose of comparing pore dimensions, random samples from commercially available sintered nickel plaques were used in a mercury porosimeter. A duplicate measurement gave essentially the same results shown in Figure 1. The plaques were 21 mils thick.

An average pore size of 16 microns, or 0.63 mil, was deduced from Figure 1 as an equivalent cylindrical diameter. This number means that one-half the pore volume has pores with diameters greater than 0.63 mil, and one-half has diameters of less than 0.63 mil.

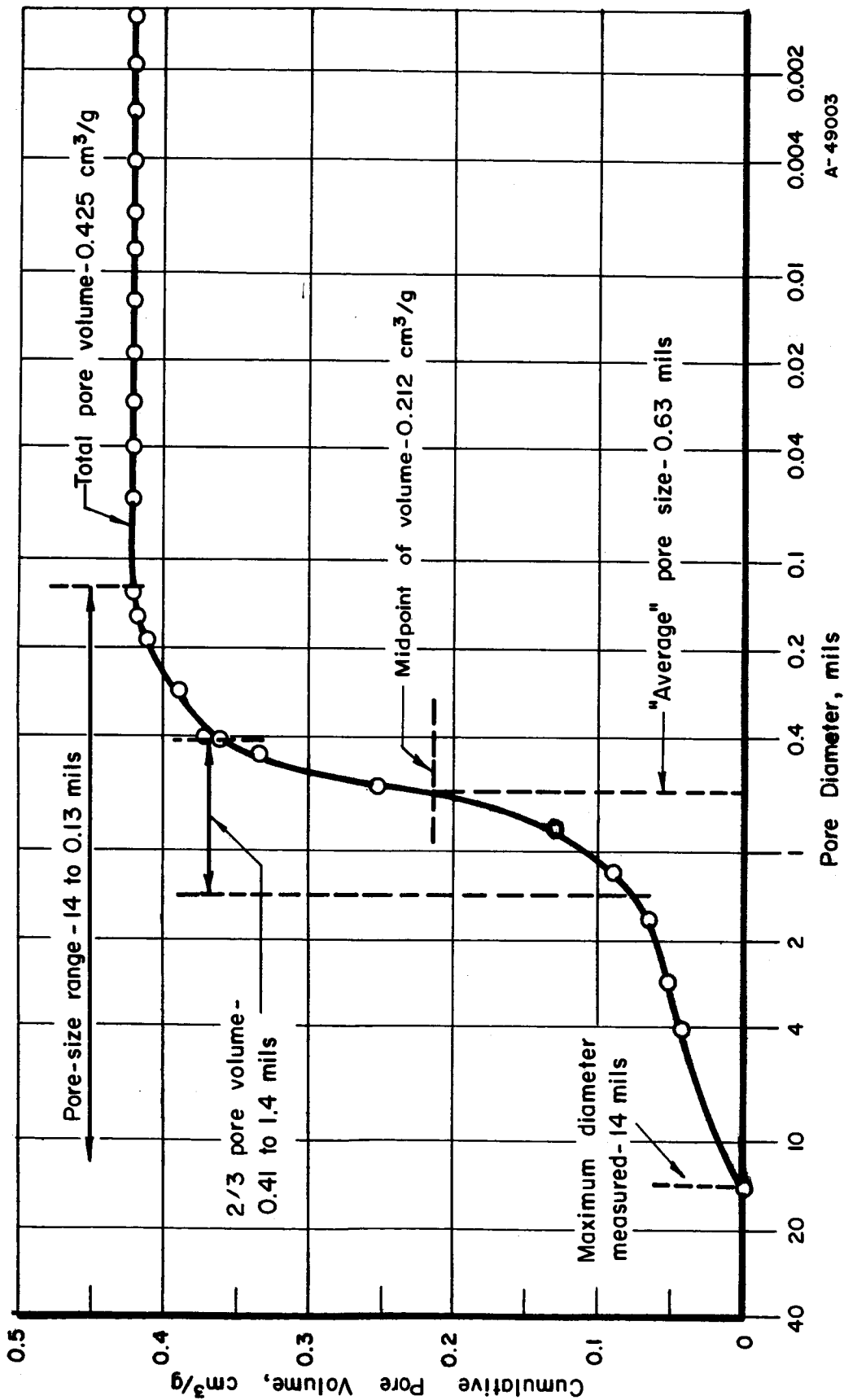


FIGURE 1. CUMULATIVE PORE VOLUME, CM<sup>3</sup>/G, MEASURED BY MERCURY POROSIMETER ON COMMERCIAL SINTERED NICKEL-POWDER PLAQUES

### Electroformed Screens

As raw materials to prepare new plaques, commercially available electroformed screens were purchased from Buckbee Mears Co., St. Paul, Minnesota. The four sizes, 1000-, 750-, 500-, and 250-line-per-inch screens, were checked microscopically for pore sizes.

These screens were remarkably uniform. Wire-to-wire spacing was excellent over all the surface and hole size was uniform over most of the surface. A linear accuracy of 0.01 mil over a length of 24 inches is reported by the manufacturer. The accuracy of screens was checked for distance from wire to adjacent wire and was found to be  $\pm 0.01$  mil, which is about the limit of the microscopic method used.

From measurement of hole sizes at several locations on the screens, the average widths of the square holes were estimated, as listed in Table 1. The size of the holes depended on the thickness of the nickel plate. Holes were larger in the center where the screen was thinner, and the holes were smaller at the edges where the screen was thicker than average.

### Item 2 - Size Tolerance

#### Powdered Plaques

Pore-size distribution was deduced also from Figure 1. First of all, at least 99 percent of the interconnecting pore volume is covered by the range of equivalent diameters between a maximum of 4 to 14 mils and a minimum of 0.13 mil. Secondly, two-thirds of the interconnecting pore volume has pores of equivalent diameters between 0.41 and 1.4 mils. The maximum pore size that can be measured by the mercury porosimeter is approximately 14 mils. Therefore, Figure 1 shows maximum diameter of 14 mils. During the measurement, the first diameter-volume point determined was 4 mils. This 4-mil value was selected for the comparison in Table 3 because microscopic examination of the surface of the plaques showed no openings larger than about 4 mils' equivalent cylindrical diameter.

#### Electroformed Screens

Pore-size tolerance was +5 to -10 percent for the majority of the screen area as noticed earlier. Table 2 shows the minimum pore sizes at the edges of screens and the maximum pore sizes. The average pore size given in Table 1 includes more than two-thirds of the total area. Pore sizes for screens are widths of square holes and for powdered plaques are equivalent cylindrical diameters. The numbers are comparable because the width of a square hole is equal to the equivalent cylindrical diameter that would be measured by mercury porosimetry.

TABLE 1. COMPARISON OF AVERAGE PORE SIZES FOR ELECTROFORMED SCREENS AND COMMERCIAL NICKEL PLAQUES

Screen Size, lines/inch	Width Average Hole, mils
1000	0.60
750	0.99
500	1.42
250	3.05
Powdered plaque	0.63

TABLE 2. COMPARISON OF PORE-SIZE TOLERANCE FOR ELECTROFORMED SCREENS AND COMMERCIAL SINTERED NICKEL PLAQUES

Screen Size, lines/inch	Minimum Wire Width, mil	Pore Size, mils	
		Maximum	Minimum
1000	0.37	0.63	0.53
750	0.34	0.99	0.94
500	0.55	1.45	1.40
250	0.80	3.2	2.96
Powdered plaques	--	<14.0	0.13

TABLE 3. COMPARISON OF SIZE TOLERANCE

Screen Size, lines/inch	Average Pore Diameter, mils	Maximum Percent Variation From Average	
		Larger	Smaller
1000	0.60	+5	-10
750	0.99	0	-5
500	1.42	+4	-1
250	3.05	+5	-3
Powdered plaque	0.63	+535(a)	-80

(a) Assuming maximum size of 4 mils.

### Item 3 - Shape of Holes

#### Powdered Plaques

The shapes of pores for the sintered powder nickel plaques are shown in Figures 2 and 3. The white areas in both figures are metallic nickel particles. The dark areas are the pores. The large white circle in Figure 2 is a cross section of one of the supporting grid wires in the commercial plaque. The shape of the pores is obviously random. Moreover, inspection of the dark areas shows the pore sizes have about the diameters predicted in Figure 1 from mercury porosimeter data.

#### Electroformed Screens

The shape of the holes in the electroformed screens was square when viewed from the surface. The holes as seen in cross section were not rectangular because the wires became rounded and changed shape during the electroforming process.

Figures 4, 5, 6, and 7 show surface pictures of the center area of screens with 1000, 750, 500, and 250 lines per inch, respectively. Some of the holes near the edges of the screen have holes partly closed because the nickel is too thick. Figure 8 is a photomicrograph of the screen with the most severe hole closure of all those examined. Of the 16 corners examined on the screens shown in Figures 4, 5, 6, and 7, only four of the corners showed a measurable hole closure. Duplicate screens were purchased and examined and appeared to be accurate reproductions of the first four screens.

Photomicrographs of cross sections are shown in Figure 9 for 1000, 750, 500, and 250 lines per inch, respectively. Thicknesses of these screens were, respectively, about 0.2, 0.1, 0.2, and 0.3 mil. Sections were made near the corners and are on the same screens shown in Figures 4 and 7.

#### Comparisons

Table 1 shows that the smallest mesh of screen has an average pore size about equal to the average pore size of commercial powdered plaques.

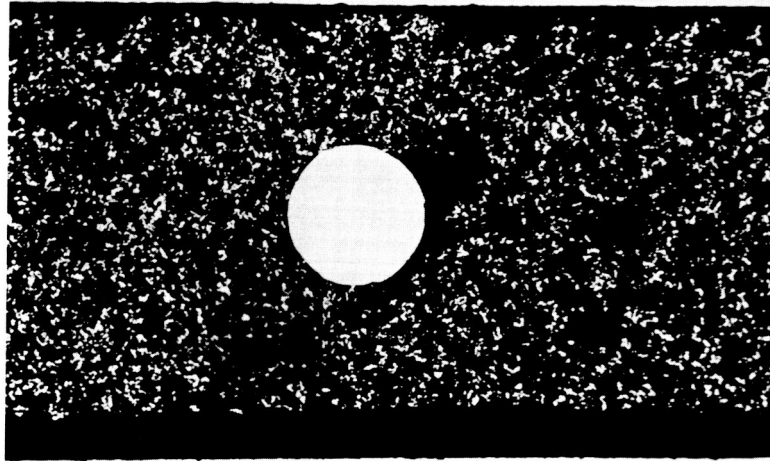
The chosen electroformed screens have a range of average pore sizes slightly larger than the range of pore sizes that contain two-thirds of the voids in the nickel plaques, as follows:

Range of pore sizes in electroformed screens, mils: 0.60 to 3.05 equivalent cylindrical diameter.

Range of pore sizes in powdered plaques that contain two-thirds of the volume, mils: 0.41 to 1.4, equivalent cylindrical diameter.

A striking difference between hole shapes is seen by comparing Figure 2, for the powdered plaque, with Figures 4 through 7, for the electroformed screens. The powdered plaques have pores of completely random shapes. The electroformed screens have pores that are identical in shape (square).

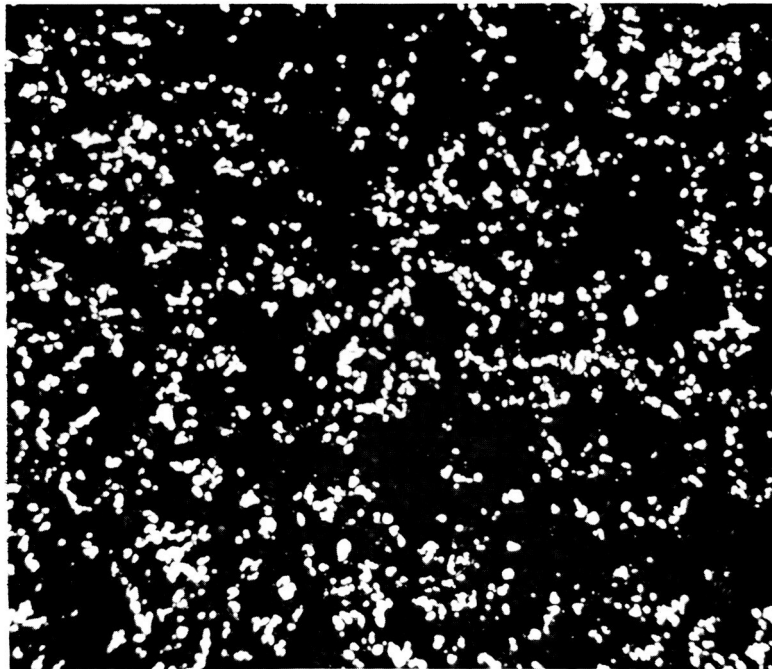




Polished Only

14027

FIGURE 2. CROSS SECTION OF COMMERCIAL SINTERED NICKEL PLAQUE SHOWING STRUCTURE AT 100X

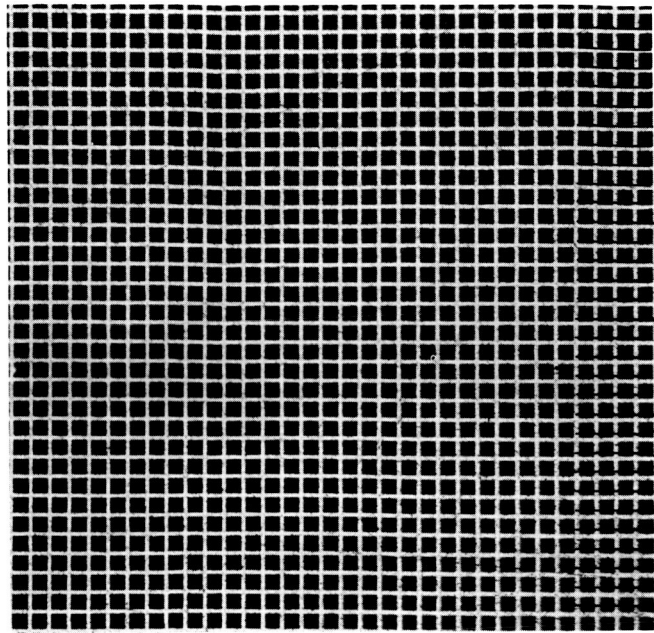


Polished Only

14029

FIGURE 3. CROSS SECTION OF COMMERCIAL SINTERED NICKEL PLAQUE SHOWING STRUCTURE AT 250X

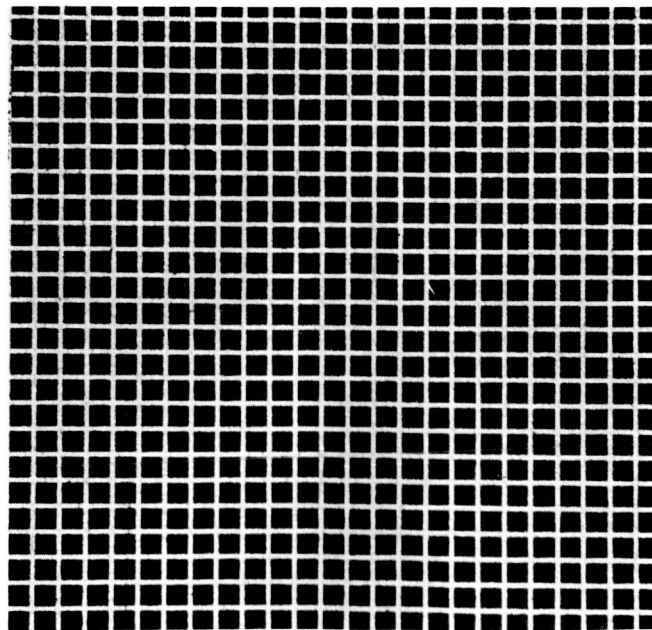
Black areas are voids; white areas are metallic nickel.



100X

13036

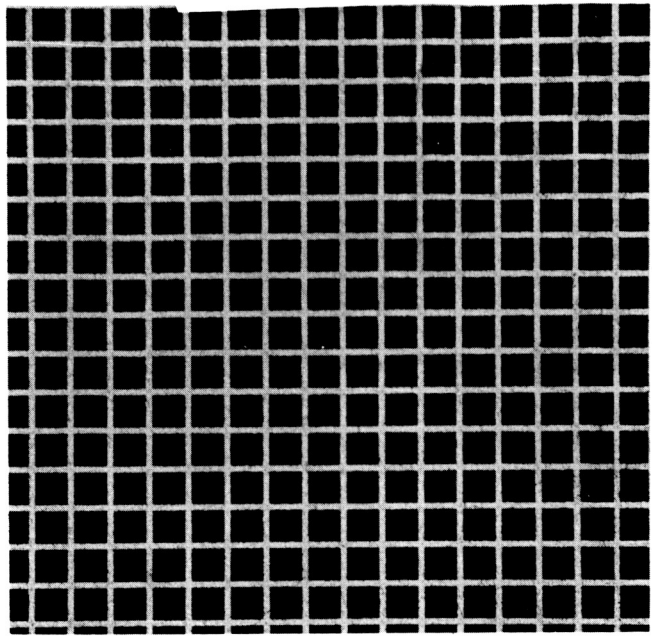
FIGURE 4. SURFACE VIEW OF CENTER OF 1000-LINE-PER-INCH ELECTROFORMED SCREEN SHOWING SHAPES OF HOLES



100X

13031

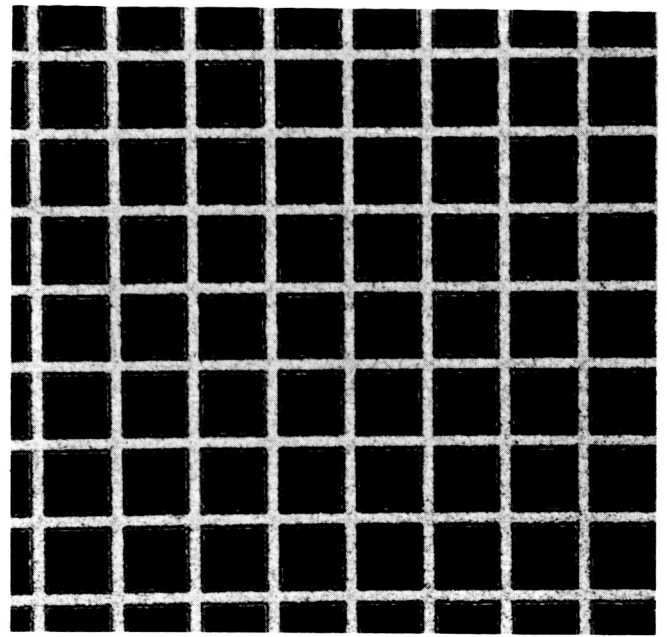
FIGURE 5. SURFACE VIEW OF CENTER OF 750-LINE-PER-INCH ELECTROFORMED SCREEN SHOWING SHAPES OF HOLES



100X

13026

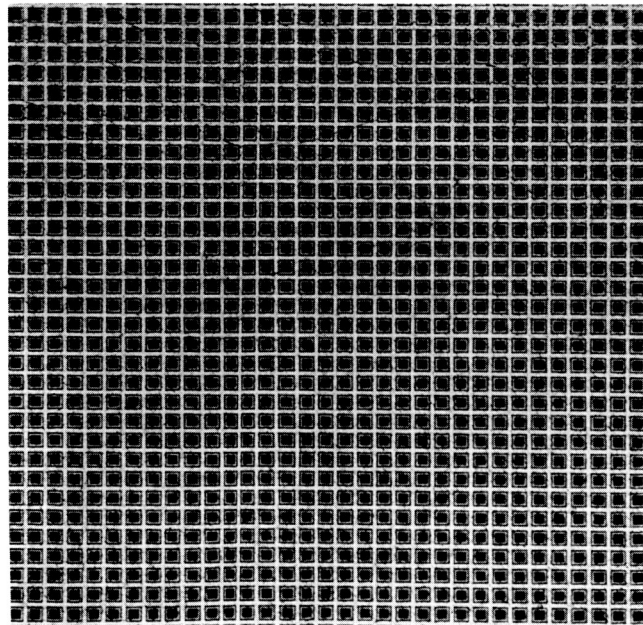
FIGURE 6. SURFACE VIEW OF CENTER OF 500-LINE-PER-INCH ELECTROFORMED SCREEN SHOWING SHAPES OF HOLES



100X

13021

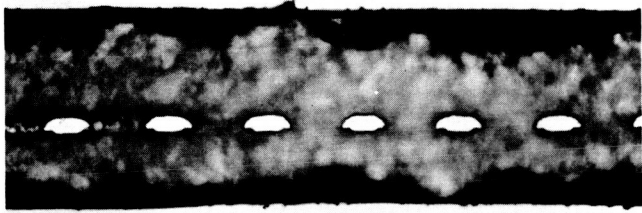
FIGURE 7. SURFACE VIEW OF CENTER OF 250-LINE-PER-INCH ELECTROFORMED SCREEN SHOWING SHAPES OF HOLES



100X

13034

FIGURE 8. SURFACE VIEW NEAR CORNER OF 1000-LINE-PER-INCH ELECTROFORMED SCREEN SHOWING THE MOST SEVERE HOLE CLOSURE



500X

13309

a. 1000-Line-per-Inch Screen;  
As Polished



500X

13308

b. 750-Line-per-Inch Screen;  
As Polished



500X

13307

c. 500-Line-per-Inch Screen;  
As Polished



500X

13306

d. 250-Line-per-Inch Screen;  
As Polished

FIGURE 9. CROSS SECTIONS NEAR CORNER OF ELECTROFORMED SCREEN

The nickel wires (white) are surrounded by copper for support during sectioning and polishing.

The size-tolerance differences are also striking. These differences can be described as "percent variation" from average which is arbitrarily defined as follows:

$$\text{Positive percent variation from average} = \frac{\text{maximum diameter} - \text{average diameter}}{\text{average diameter}} \times 100$$

$$\text{Negative percent variation from average} = \frac{\text{average diameter} - \text{minimum diameter}}{\text{average diameter}} \times 100.$$

Results of such calculations are shown in Table 3.

#### Location of Data

All experimental data on Task A are contained in Battelle Laboratory Record Book No. 21516, pp 24-28.

Dr. Maynard B. Neher helped with the obtaining and interpretation of pore-size and -area measurements on sintered powder plaques. These included the mercury-porosimeter and gas-adsorption measurements.

### TASK B - POROUS MAT MANUFACTURE

#### Objectives

Task B of the contract reads as follows:

##### "Item 1 - Thickness Ranges

Methods to construct porous plaques shall be investigated in the following thickness range:

- a. 0.005 ± 0.001 of an inch
- b. 0.010 ± 0.001 of an inch
- c. 0.021 ± 0.001 of an inch
- d. 0.035 ± 0.001 of an inch

##### "Item 2 - Techniques

Techniques shall be developed to electroform and superimpose electroformed screens.

##### "Item 3 - Methods

Methods to construct the plaques having the following three shapes shall be investigated.

- a. Parallel sides
- b. Keyed opening
- c. Staggered taper."

The objective of Item 1 was to provide electrodes that would allow determination of an optimum electrode thickness as a function of pore size. Nothing seems to be known about the relationship of electrode thickness to pore size because heretofore it has not been possible to control the pore size. That is, sintered powder plaques have a range of random pore sizes, as described under Task A.

The main objective of Item 2 was to develop laboratory methods for electroforming and building porous plaques according to advance specifications. A second objective was to devise manufacturing methods which appeared to be feasible for production use.

The objective of Item 3 was to provide a variety of predetermined pore shapes for experimental study.

### Item 1 - Thickness Ranges

Porous screen electrodes were made in the four required thickness ranges, 5, 10, 25, and 35 mils thick, by stacking electroformed nickel screens. The number of layers of screens needed to obtain any desired thickness was calculated from the thickness desired, and the average thickness of the electroformed screen material. Thicknesses were measured to an accuracy of about 10 microinches, using an auto collimator. Stacked thicknesses of screens were made about 1 mil more than the desired thickness to allow for shrinkage during the bonding and etching steps. A loss in thickness of about 1 mil was found during the etching step. No significant thickness change was noted during the bonding step. Therefore, thickness loss was almost constant and independent of electrode thickness.

### Item 2 - Techniques

#### Electroforming

Commercial Screens. Electroformed nickel screens were purchased from a commercial supplier\*. Screens are electroformed on flat mandrels with a photoresist to mask part of the surface to give the screen pattern. Photoengraving techniques are needed to apply, expose and develop the coating.

Figure 10 is a sketch of cross section of electroforming mandrels. The top section represents squares of photoresist which have metal exposed between the squares. Screens are formed by plating on the exposed metal and peeling the plate from the mandrel. Present commercial quality requirements limit the use of one printed mandrel to about 20 cycles before the photoresist fails in enough areas to be considered unusable.

According to information from Eastman Kodak Co.,\*\* only one electroform can be made on a mandrel with a photoresist stop-off with perfect detail. This is because the edges of the photoresist have a slight overhang and lock the electroformed screen on the mandrel. Removal of the screen chips away part of the resist. However, the loss in detail due to this edge chipping is minor for screen that might be used in battery electrodes.

\*Buckbee Mears Co., St. Paul, Minnesota.

\*\*Bates, T. R., "Photography in Electroforming", presented at the Inco Electroforming Seminar, December 2, 1964, New York City.

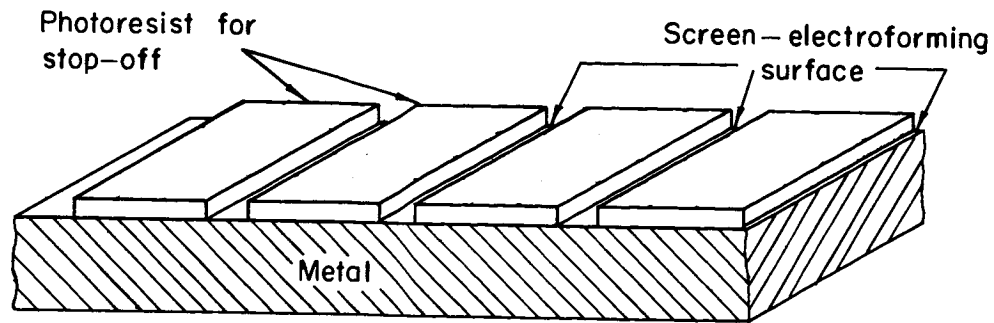


FIGURE 10. SKETCH OF CROSS SECTION OF COMMERCIAL ELECTROFORMING MANDREL

Commercial electroformed screens were ordered by ruling number and percent light transmission. Master rulings used for making negatives are available from 2000 to 5 wires per inch. Control of the percent transmission is obtained by controlling the amount of nickel deposited. Screens were obtained which were plated on the mandrel to 25 percent transmission. These screens were very accurate and could be superimposed with no detectable error at 10X magnification over a 10-inch length. Another set of screens was obtained which had been electroformed to a transmission probably in excess of 50 percent, stripped from the mandrel, and plated on both sides to decrease the transmission to 25 percent. Accuracy of screens plated this way was not as good as those plated to the full amount while on the mandrel. Apparently, stripping the screens (while thin) from the mandrel, stretched the wires. Mismatch of wires was found when screens 2 x 5 inches were stacked. However, only one direction was inaccurate, indicating unidirectional stretching during stripping.

Screen Electroforming Mandrels. Two types of mandrels were made for electroforming nickel screens. Filled flat mandrels were made by etching holes in a flat panel, filling these holes with either plastic or glass, abrading to expose the copper between the filled holes, and electroforming on the exposed screen pattern. The second method was a novel way to electroform a screen by making a mandrel which had silicone rubber projections.

Etching Flat Mandrels. The procedure for making reusable mandrels was successful only for 175- and 250-mesh screens. Mandrels made for electroforming 500-mesh screen were not of good enough quality to be considered successful. The procedure used for etching the copper panels was

- (1) Cleaned plates with Plate Scrub compound
- (2) Washed with water
- (3) Rinsed with 8 percent hydrochloric acid
- (4) Washed with water
- (5) Dried with compressed air blast
- (6) Photoresist (Positop\*, Positop and butyl acetate, equal parts, or KPR\*\*) was flowed on the plate

\*Azoplate Positop by Master Sales & Service Corporation.

\*\*A product of Eastman Kodak Company.

- (7) Plate was spun at 80 rpm, 150 F to spread the photoresist evenly
- (8) Dried at 100 C.

Panels etched by the procedures shown in Table 4 were used to make experimental electroforming mandrels.

The next step in making reusable electroforming mandrels was to fill the etched holes with a nonconductor. Two materials (epoxy and glass) were selected as the most likely nonconductors. Silicone rubber, polyvinyl chloride, wax, and a high-lead-content glass were rejected during screening tests because of poor adherence or resistance to chemical attack in the plating baths. The epoxy material was put in the holes by two steps. A small amount was forced into the holes using a rubber blade. The flexible blade forced the resin to the bottom of the etched holes. A second layer of uncured resin-catalyst mixture was applied and the excess removed with a rigid doctor blade. After curing, the mandrel was abraded with 400-grit paper to ensure exposure of all the copper lands between the holes. Nickel and chromium plates were applied to lock in the plastic and provide a nonbonding surface. Figure 11 is a sketch of a mandrel showing the photoresist applied for etching the holes and the finished mandrel with the nonconductors locked in place.

Glass-filled mandrels were made from the same series of etched copper panels as for the plastic-filled mandrels. Air bubbles were removed from the glass during firing by applying a vacuum of 150 to 200 microns for about 2 minutes after the slip-coated mandrel had been heated for 6 minutes at 1450 F in a nitrogen atmosphere. Nitrogen was used to prevent oxidation of the copper. The coated mandrels were cooled in a nitrogen atmosphere. Polishing of the glass to expose the raised copper cell structure followed by buffing the copper and chromium plating gave a surface suitable for electroforming nickel screens. The glass is preferable to plastic materials because it (1) adheres better, (2) resists chemical attack, and (3) is stronger. However, the glass is harder to polish to expose the copper cell structure. Ten screens were electroformed on a 1 x 2-inch mandrel with no evidence of chemical attack on the glass. Figure 12 shows five layers of this screen superimposed and ready for bonding. Composition of the glass was

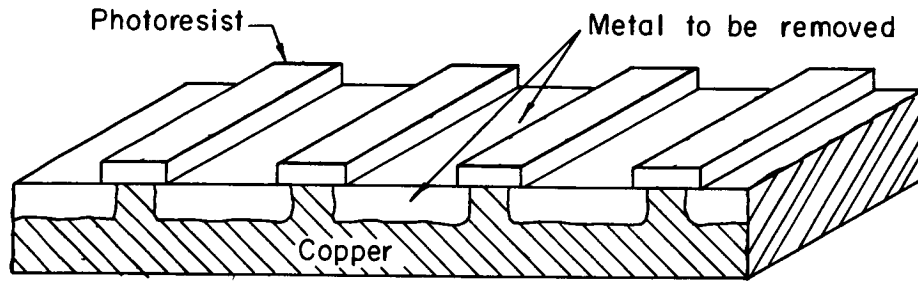
<u>Component</u>	<u>Formula</u>	<u>Weight, grams</u>
Lithium carbonate	$\text{Li}_2\text{CO}_3$	92
Sodium carbonate	$\text{Na}_2\text{CO}_3$	352
Sodium nitrate	$\text{NaNO}_3$	180
Silica	$\text{SiO}_2$	1024
Titanium oxide	$\text{TiO}_2$	120
Copper oxide	$\text{CuO}$	136
Lead silicate	$\text{PbSiO}_3$	1932
Sodium silicofluoride	$\text{Na}_2\text{SiF}_6$	60
Boric acid	$\text{H}_3\text{BO}_3$	64

Larger mandrels with 2 x 4-inch-screen patterns of 175, 250, and 500 mesh were glass coated. During hand polishing of the mandrels with 600-mesh silicon carbide abrasive paper to expose the copper between the etched holes, the glass coating was chipped from the holes on the 250- and 500-mesh mandrels. Only the 175 mesh was of good quality for electroforming mandrels.

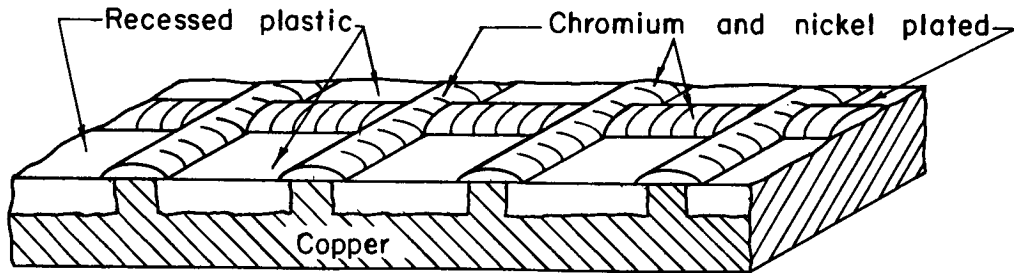


TABLE 4. PHOTOPRINTING AND ETCHING COPPER MANDRELS

Plate	Photo-resist	Screen, lines/inch	Exposure Lux Units	Image Quality	Etching Conditions					Line Width Reduction, percent	Remarks
					Time, min	Temp, C	FeCl <sub>3</sub> , °Bé.	Position of Face	Agitation		
4	Positop	250	30	Fair	5	24	40	Down	None	80-90	Cups on edge undercut
9	"	500	25	Fair	2	24	40	"	"	60-70	Ditto
20	KPR	175	25	Good	5	23	40	"	"	40	Shallow etch
21	"	175	25	Fair	10	23	40	"	"	70	Flow lines
22	"	175	25	Fair	8	23	40	"	Rocking	50-60	Good
23	"	175	25	Fair	8	23	40	"	"	60-80	A few cups undercut at edge
24	Positop	250	40	Fair	4	22	31.8	"	"	40	Ditto
25	"	250	40	Good	4	22	31.8	"	"	60	Good
26	"	250	40	Good	3.5	22	31.8	"	"	50-60	Like Plate 23
27	"	250	40	Good	3	22	31.8	"	"	50-60	Ditto
28	"	500	35	Good	2	22	40	"	"	40	Good
29	"	500	40	Fair	2.25	22	40	"	"	50-60	Like Plate 23
30	"	500	40	Good	2	22	40	"	"	50-60	Ditto
31	"	500	40	Fair	1.75	22	40	"	"	50	Good



Method 3 - Etching Holes



Method 3 - Mandrel Ready for Electroforming Screens

A-49004

FIGURE 11. SKETCH OF CROSS SECTIONS OF SCREEN ELECTROFORMING MANDREL



FIGURE 12. SECTIONAL VIEW OF FIVE SCREENS ELECTROFORMED ON GLASS-FILLED MANDREL IN SUPERIMPOSED POSITION

One mandrel with glass-filled holes was used for electroforming 175-mesh nickel screens with a 2 x 4-inch area. After two screens were made, some of the glass pulled out of the holes. Figure 13 shows a cross section of this mandrel. Apparently the glass cracked during polishing and nickel plated in these cracks, locking the nickel to the glass. Stripping the screen from the mandrel pulled the glass from the holes in the mandrels. Finer abrasives used with less pressure might produce durable mandrels with the smaller hole sizes. No work was done with finer abrasives. Figure 14 shows a cross section of a 500-mesh mandrel coated with glass, before polishing.

Results with glass-filled copper mandrels have been moderately successful. Screens have been electroformed but the mandrel life was too short for practical use. This method could be developed for making long-life reusable mandrels. Reheating to flow the glass after polishing, to heal any cracks that were introduced, might give a long-life mandrel.

Another technique for electroforming screens was devised and one screen was electroformed to demonstrate that a screen can be reproduced by the process. A stainless steel sheet with holes etched through it was used as a master to make an electroforming mandrel. The mandrel had raised silicone rubber projections where the holes had been in the master screen. Figure 15 is a surface view of the mandrel showing the nonconducting, cone-shaped projections.

The procedure used for making the mandrel was

- (1) Fill the holes in the master screen with wax
- (2) Clean one side of the screen free of wax
- (3) Plate about 5 mils of nickel on the master
- (4) Remove the wax and fill the holes with silicone rubber\* with an excess on the nickel-plated side and all excess doctored off the stainless steel side
- (5) Separate the nickel and the stainless steel screens after the silicone rubber hardened.

The resulting mandrel was a screen of electroformed nickel with rubber projections that duplicated the hole size and shape in the stainless steel master.

A nickel screen was electroformed\*\* subsequently on the same mandrel that is shown in Figure 15. The resulting electroformed nickel screen duplicated the hole shape

\*Dow Corning Corporation, 502 Silicone Rubber.

\*\*A nickel sulfamate bath was used.

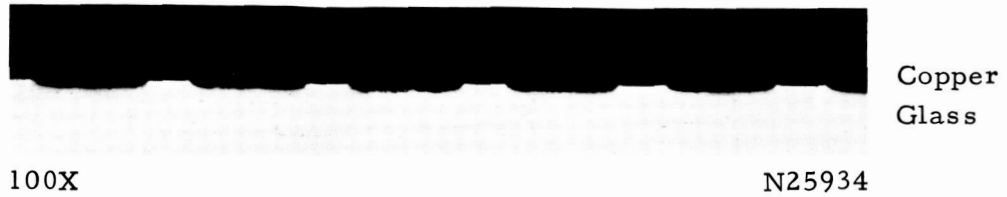


FIGURE 13. CROSS SECTION OF COPPER MANDREL WITH GLASS-FILLED HOLES

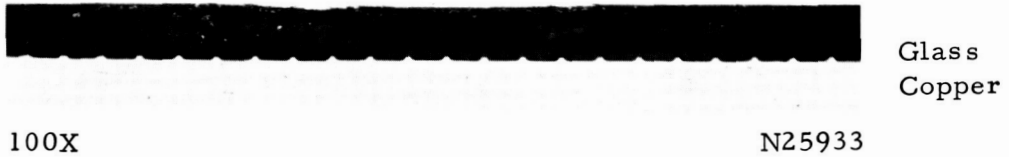


FIGURE 14. CROSS SECTION OF COPPER MANDREL WITH GLASS COATING

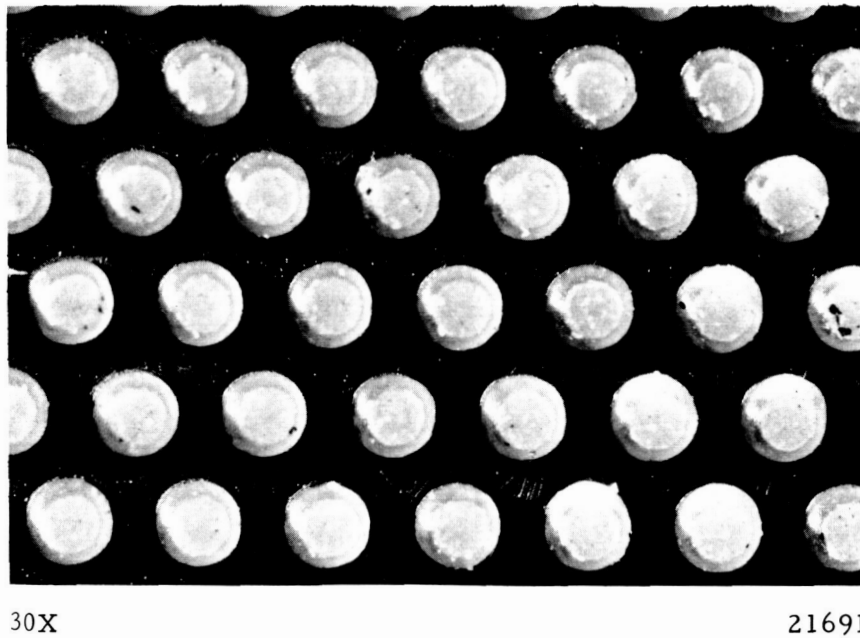


FIGURE 15. VIEW PERPENDICULAR TO SURFACE OF A NICKEL MANDREL (DARK AREA) WITH CONE-SHAPED RUBBER PROTRUSIONS (LIGHT CIRCULAR AREAS)

in the master stainless steel screen, as shown by the cross sections of the stainless steel master and the nickel electroform in Figures 16 and 17, respectively.

The screen size was about 50 mesh, which is coarser than the screens used in battery plaques. However, this master screen was available and was used to check the process for reproducing holes with a preselected contour. Because the rubber cones pulled out of the electroformed nickel screen with no apparent damage, the mandrel could be used again. This duplicating technique could probably be used to electroform screens with smaller holes. Thick structures, made by stacking and bonding thin screens, could be considered as a master form which might be duplicated by electroforming with this technique.

Plating on one side of electroformed screens, according to U. S. Patent 2,879,068, was evaluated for increasing the thickness of screens. The method was developed for increasing the strength of screens by plating on one side of the screen such that much less metal deposited in the holes than in conventional plating. The previous development work was done on screens 5 mils thick with about 50 lines per inch and with a wire size of 10 mils. For this size of screen, plating could be concentrated on one side only.

The same process applied to a 250-line-per-inch electroformed screen did not limit the plate to one side only. Nickel was plated almost uniformly on all sides of the wires. Figure 18 shows a photomicrograph of one wire plated by the special technique. The elliptical area is nickel surrounded by copper for support for microscopic examination. Three layers of nickel were deposited on the wire under different conditions. The difference in the thickness of plate of the three layers was due to a different number of ampere-minutes used. The reason the process did not perform as expected on the fine 250-line-per-inch screen is probably because nickel baths have poor macrothrowing power but good microthrowing power. Throwing power of a plating bath is the relative ability to plate uniformly on all surfaces of a complex-shape cathode. Apparently, screens of 50 lines per inch fall in the poor macrothrowing-power range, whereas the 250-line-per-inch screen is in the microthrowing power range.

Several conditions were identified which gave minor improvements in controlling the efficiency for plating on one side of the screens. These included operating the plating bath with (1) pH, over 4.0; (2) high concentration, 90 g/l of nickel; (3) high temperature, over 120 F; and (4) low current density on the screen with high currents on the secondary cathode.

A screen plated on both sides using anodes on both sides can give a thickness change equal to the wire-width change if plate were to be deposited uniformly. Wire-width measurements in Table 5 were made by microscopic methods. Cross sections of screens showed these measurements to be in error. The widths were less than indicated. Only a flat surface can be measured microscopically without error. Had wire widths been measured on cross sections of wire the last column in Table 5 would have lower numbers. However, the uncorrected data in the last column of Table 5 show that thicknesses increase up to 1.8 times as fast as the widths of the wires. This ratio was much lower than for the process described in U. S. Patent 2,879,068 where ratios of ten were obtained. It was concluded that the patented process had no advantage for the fine-mesh electroformed screens.

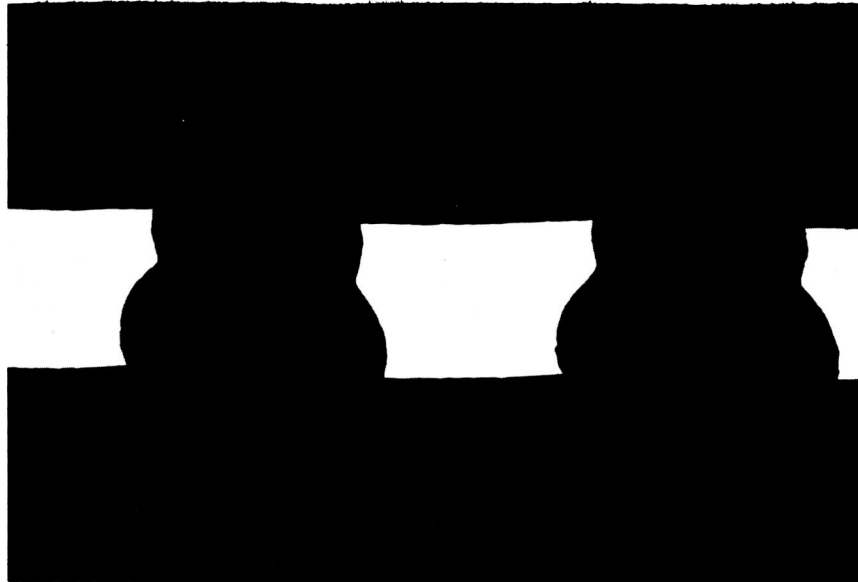


FIGURE 16. CROSS SECTION THROUGH HOLES IN MASTER STAINLESS STEEL SCREEN

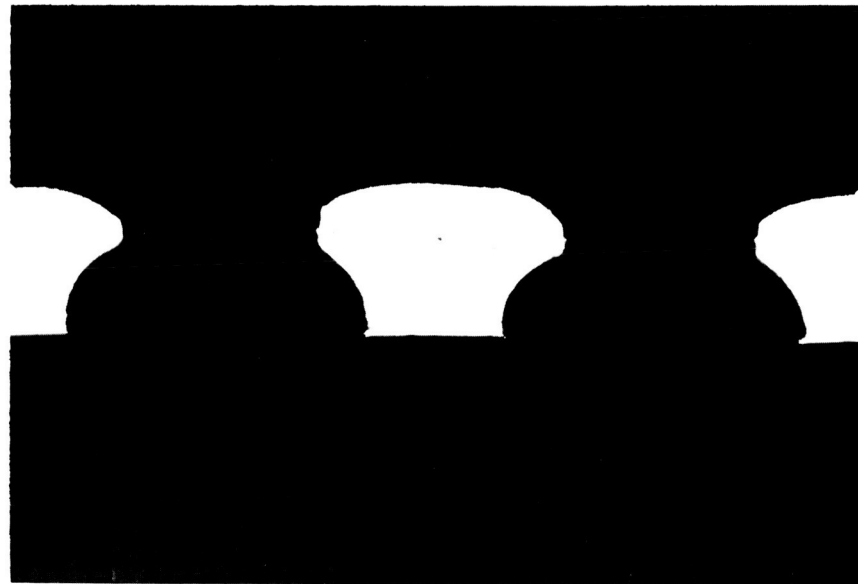


FIGURE 17. CROSS SECTION THROUGH HOLES IN ELECTROFORMED NICKEL SCREEN

Made with the mandrel in Figure 15 to duplicate the shape in Figure 16. The bottom of the picture was the mandrel side.

TABLE 5. PLATING NICKEL ON ELECTROFORMED SCREENS

Experiment	Nickel Plating Bath	Sp. Gr.	Conditions			Plating Current, amp	Screen Cathode Ratio	Change in Dimensions, mils <sup>(a)</sup>			
			Temp, F	pH	Resistivity, ohm/cm			Thickness, $\Delta T$	Wire Width, $\Delta W$	Ratio, $\Delta T/\Delta W$	
8B	Double(b) nickel	1.1	75	5.5	10.5	0.05	0.15	3.0	0.52	0.56	0.93
9B	Ditto	--	75	3.0	--	0.05	0.15	3.0	0.43	0.51	0.85
12B	Chloride(c)	1.26	115	4.0	5.0	0.05	0.15	3.0	0.37	0.29	1.27
13A	"	--	120	5.0	--	0.05	0.15	3.0	0.51	0.48	1.06
13B	"	--	140	5.4	--	0.05	0.15	3.0	0.37	0.36	1.03
7A	Sulfamate(d)	1.26	115	4.7	5.1	0.05	0.15	4.7	0.60	0.57	1.18
14A	"	1.32	140	4.4	--	0.05	0.15	4.4	0.15	0.10	1.50
14B	"	1.36	140	4.4	--	0.05	0.15	4.4	0.18	0.10	1.80
14C	"	1.36	140	4.4	--	0.25	0.5	4.4	0.98	1.01	0.97

(a) Measurements made by a calibrated eyepiece used with a microscope.

(b) Bath contained 70 g/l  $NiCl_2 \cdot 6H_2O$  and 30 g/l  $NH_4Cl$ .

(c) Bath contained 300 g/l  $NiCl_2 \cdot 6H_2O$  and 30 g/l boric acid and 5 cc/l "XXXX" Harshaw antipit.

(d) Bath contained nickel sulfamate, boric acid, and nickel chloride as supplied by Allied Research Products. The concentration was changed by evaporating water from the solution.

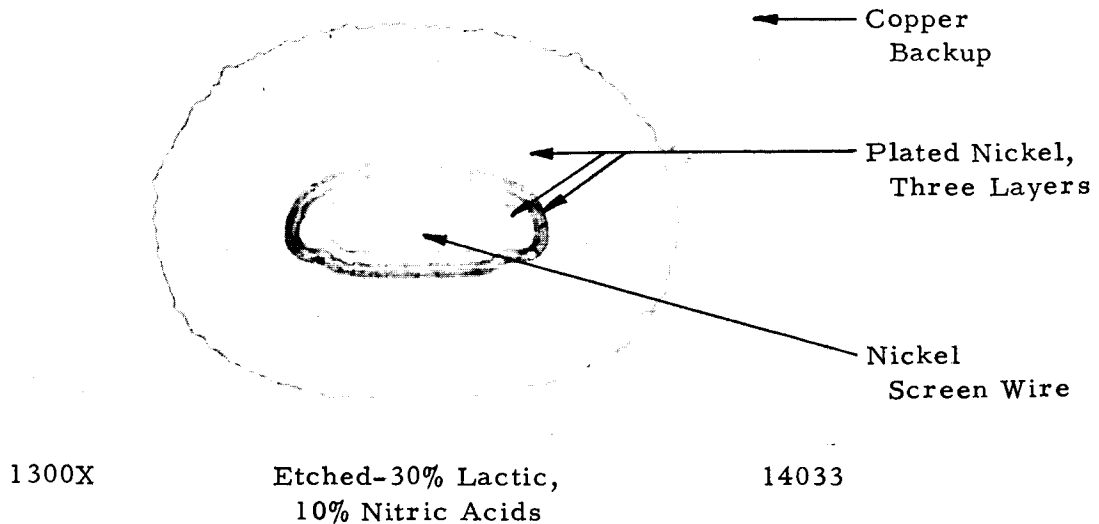


FIGURE 18. CROSS SECTION OF ONE WIRE OF A 250-LINE-PER-INCH SCREEN PLATED WITH THREE LAYERS OF NICKEL PLATE TO INCREASE THE THICKNESS

Superimposing Electroformed Screens. The most important objective of Task B was to construct porous electrodes for evaluation of their electrochemical performance as part of Task F. Toward manufacturing these experimental porous structures, a machine was designed, constructed, and used to stack electroformed nickel screens with superimposed holes. Figures 19 and 20 are drawings of the stacking machine showing the operating principles.

To stack screens, the following steps were used:

- (1) Electroformed nickel screen was cut into about 1-1/2 x 4-1/2-inch pieces. Cutting of the screen was done with plastic covering to prevent damaging of the screen, as by wrinkles. The plastic was cut with the screen. Paper handles, 1-1/2 x 1-1/2 inch, were attached to the ends of the screen pieces with masking tape to aid in handling.
- (2) Average thickness of the screens was calculated from ten thickness measurements.
- (3) One piece of the screen was placed on the slide table and held in place by small magnets. The slide table was moved with the screw adjustment until the wires coincided with the cross hairs in the eyepiece of the microscope.
- (4) The main hold-down lever was depressed to hold the screen while the punch was operated to cut a 1 x 1-cm section and to force the screen section to the bottom of the die. Alignment of the screen in the bottom of the die was rechecked with the microscope.
- (5) The small hold-down was lowered to prevent the punch from lifting the screen section when the punch was withdrawn.
- (6) Steps (3) through (5) were repeated until the calculated number of screens were superimposed.



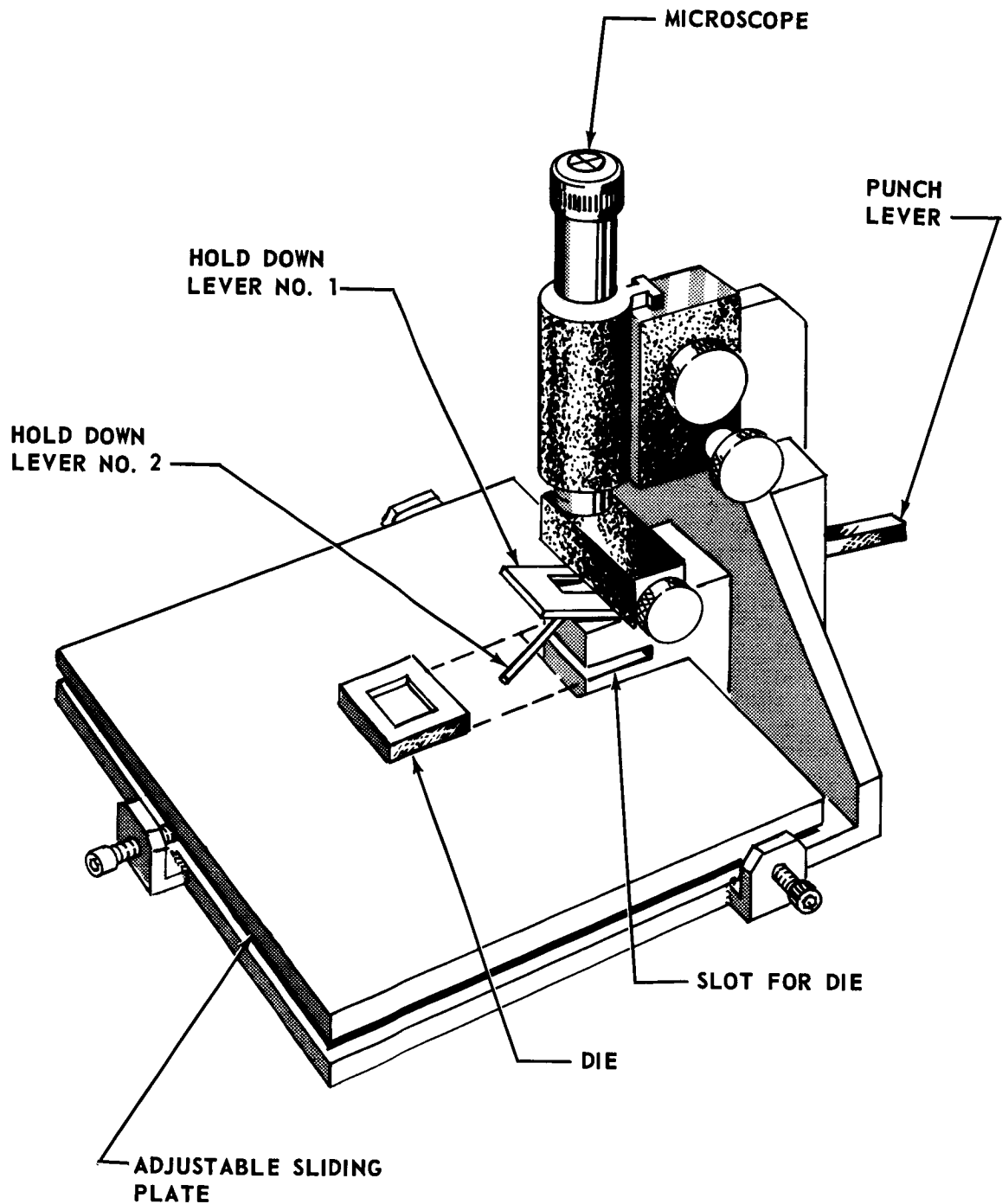


FIGURE 19. PERSPECTIVE VIEW OF MICROSCOPE, ALIGNMENT MECHANISM, AND DIE

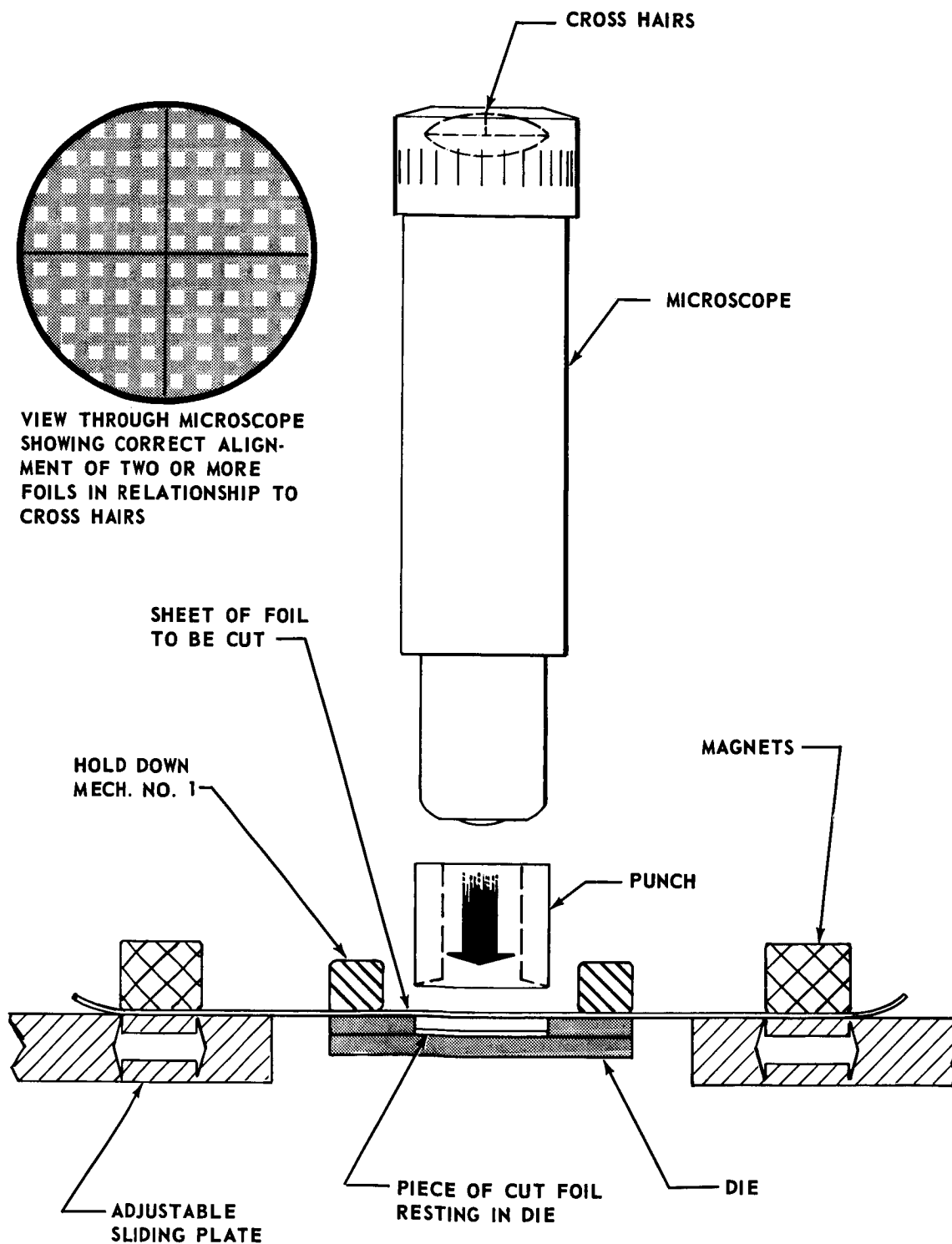


FIGURE 20. SIMPLIFIED SCHEMATIC DRAWING SHOWING FIRST PIECE OF CUT FOIL RESTING IN DIE WITH SECOND CUT READY TO BE MADE IN NICKEL FOIL

A periodic inspection of the stacked screens in the die was made by positioning a light under the machine and looking at the light through the superimposed holes. Dies had a small hole in the center for this purpose.

The critical factor in the stacking machine was the clearance, or "fit", between the punch and die. Good alignment of stacked screens was obtained only when the clearance was essentially zero. To accomplish this fit, dies were made undersize, then broached to size with the same punch that was to be used for cutting the screens. The broaching was done in a small arbor press after removing the punch and die assembly from the machine.

After all the screen layers had been superimposed in the die, the die was removed and the screens heat bonded. Details of the bonding step including antibonding coating used on the die are discussed in Task C. Dies were reused several times by (1) peening along the 1 x 1-cm hole to make the hole smaller, (2) surface grinding, and (3) rebroaching the die.

The precision with which screens were superimposed by using the stacking machine was improved greatly during the program. Near-perfect alignment was obtained toward the end of the stacking campaign. Stacks of screens over 35 mils thick had straight-through holes, and light could be seen through these holes. Figures 21 and 22 are photomicrographs taken perpendicular to the surface of a 35.5-mil-thick screen plaque with both front-surface lighting and back lighting. The square, white areas are the holes with transmitted light. Note that the holes are nearly as large as the openings in the top screen, thus indicating nearly perfect alignment.

These improvements in alignment were obtained by a combination of

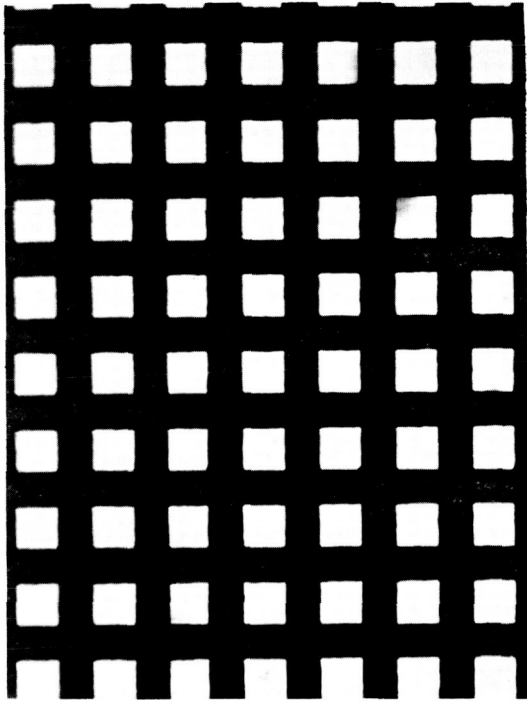
- (1) Better matching of die and punch sizes
- (2) Lighting of the stack from the back to provide constant monitoring of alignment while stacking
- (3) Improved operator skill.

The alignment of these stacked-screen plaques was better than the most optimistic prediction made before this work was started.

The best alignment of holes in stacked screens has been obtained with 250- or 500-mesh screens, each layer about 0.5 to 1.0 mil thick.

Figures 23 through 32 are photomicrographs of three sets of stacked electroformed screens which show how the holes were not exactly superimposed. Figures 23, 24, 27, and 30 show the top surface of screens before the heat-bonding operation. Figures 25, 28, and 31 show this same top surface after the heat-bonding step. Figures 26, 29, and 32 show the bottom surface of the three stacks of screens after bonding.

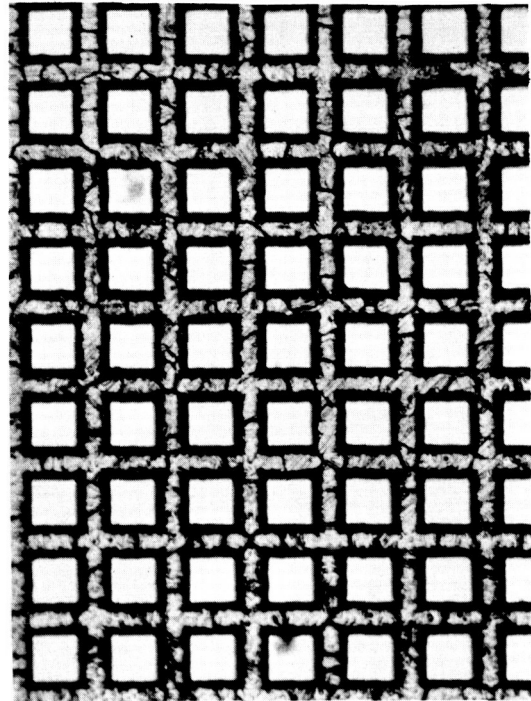
Figures 23 and 24 are of the same specimens photographed under different conditions to show alignment. Figure 23 was taken with the microscope focused on the top layer. Layers underneath the top screen do not show. Figure 24 was taken with the microscope focused on a layer beneath the top layer. Note the alignment is good but not perfect. Figures 23 and 25 are both of 250-mesh screens. The screen in Figure 23 had about 60 percent openings, whereas the screen in Figure 25 had about 25 percent openings.



100X

FIGURE 21. SURFACE VIEW OF 250-MESH SCREENS CONTAINING 32 LAYERS STACKED TO 38.56-MIL THICKNESS BEFORE BONDING

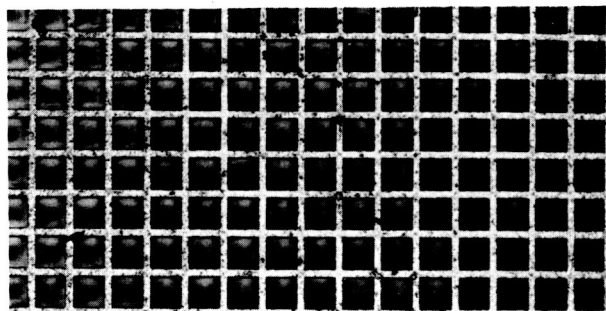
Specimen lighted from the back only. White squares show openings through plaque. Specimen 44.



100X

FIGURE 22. SURFACE VIEW OF 250-MESH SCREENS CONTAINING 32 LAYERS AFTER BONDING TO 35.5-MIL THICKNESS

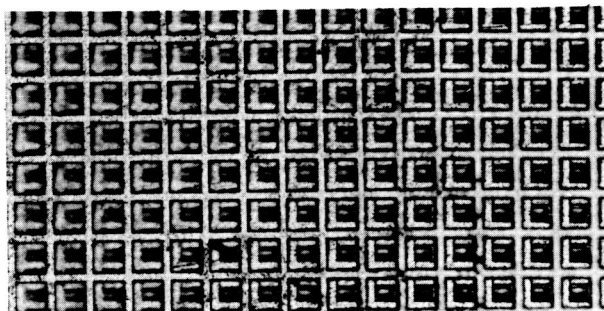
Both front surface and back lighting were used. White squares show openings through plaque. Specimen 44.



100X

19793

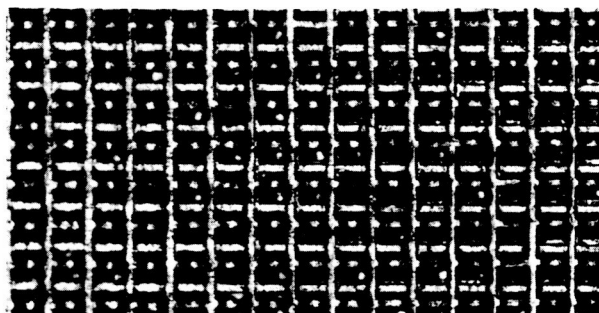
FIGURE 23. TOP SURFACE OF SUPERIMPOSED 250-MESH SCREENS BEFORE BONDING - FOCUSED ON TOP SCREEN



100X

19794

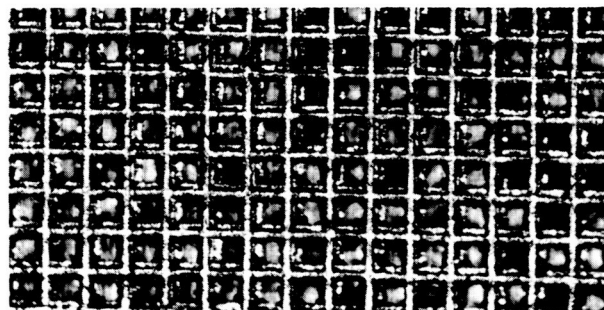
FIGURE 24. TOP SURFACE OF SUPERIMPOSED 250-MESH SCREENS BEFORE BONDING - FOCUSED ON UNDERNEATH LAYER



100X

19795

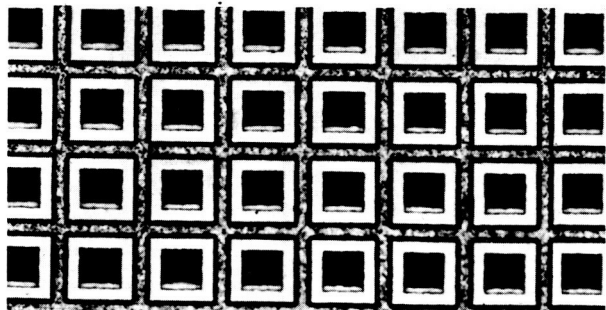
FIGURE 25. TOP SURFACE OF SUPERIMPOSED 250-MESH SCREENS AFTER BONDING



100X

19796

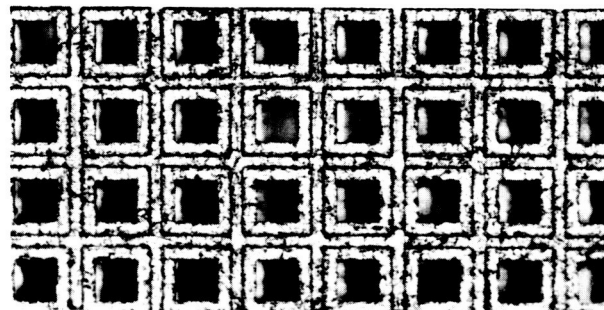
FIGURE 26. BOTTOM SURFACE OF SUPERIMPOSED 250-MESH SCREENS AFTER BONDING



100X

19797

FIGURE 27. TOP SURFACE OF SUPERIMPOSED 250-MESH SCREENS BEFORE BONDING



100X

19798

FIGURE 28. TOP SURFACE OF SUPERIMPOSED 250-MESH SCREENS AFTER BONDING

After the heat-bonding step, all of the nickel screen structures show crystal growth in the metal. This is normal for annealed-nickel electroplated metal.

Screens electroformed at Battelle to 2 x 5-3/4 inches were superimposed by a second technique. Each screen was positioned by hand, using a microscope to check alignment and spot welded in place. Screens were held on clear plastic with pressure-sensitive tape to aid handling. Ten screens were stacked which gave a thickness of 10.5 mils.

Figure 33 is a surface view of the 10 layers. Note that light can be seen through the holes. The spot-welded stack was cut into two 2 x 2-7/8-inch pieces, again stacked and spot welded. The two stacks of screens were spot welded, heat bonded, etched to increase porosity to 60 percent, and used for measurements of physical properties.

A surface view and a cross section of the electrode, 2 x 2-7/8 inches and 21 mils thick, are shown in Figures 34 and 35. Most of the wires are bonded to their neighbors. Pores are shown to be continuous but not straight enough for light transmission. Screens used in this stacking experiment were of poorer quality, as was described in a prior section.

Superimposing Etched Screens. Special nickel screens were obtained from a supplier\* who made them by etching hexagonal holes through a 2-mil nickel sheet. Holes were 125 per inch and were about 6 mil in diameter. Etched holes were nearly round. Five of these sheets were stacked by hand and spot welded. A 6-mil pivot drill was recessed in a sheet of clear plastic and used to locate and hold one corner of the screens. Each screen was pivoted around the drill until the holes were superimposed. The use of the pivot drill simplified the alignment of the screens. Figure 36 shows a surface view of the stacked screens. The white triangular areas are not holes but the remains of the surface of the sheet. These screens provided: (1) larger electrodes, about 5 x 5-1/2 inches, to be made; (2) a check of a different stacking technique; and (3) a chance to evaluate larger pore sizes.

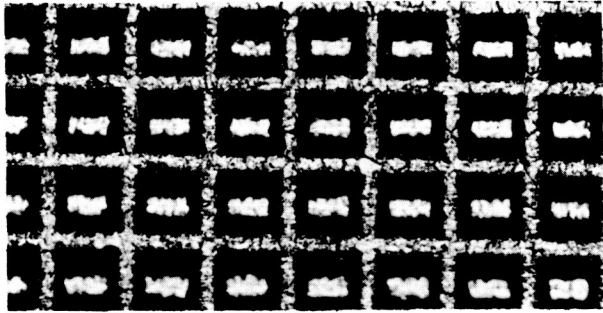
### Item 3 - Method of Controlling Pore Shapes

Included in this section of the report are discussions about the construction of the three shapes of pores required by the contract. Construction of a semirandom pore shape and control of porosity by chemical etching are discussed also.

#### Pore Shapes

Pores with parallel sides were made by stacking electroformed screens with the stacking machine. All the screens had the same size hole. To obtain the keyed opening and the staggered-taper pore, electroformed screens with different hole sizes were used, but all shaped-pore studies were made with 250-mesh screens. Table 6 contains the details of construction of the shaped pores.

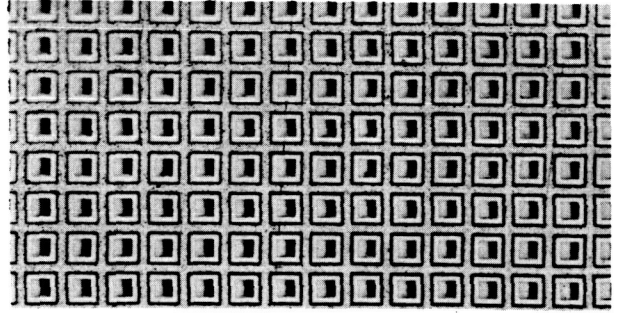
\*Buckbee Mears Company.



100X

19799

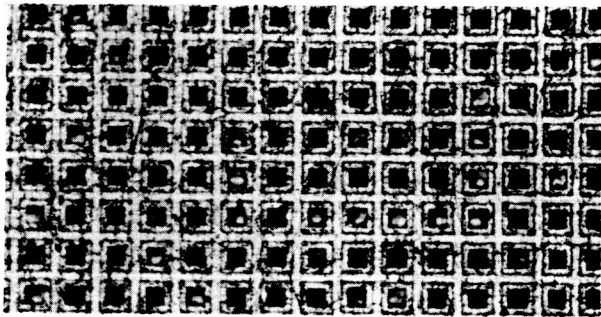
FIGURE 29. BOTTOM SURFACE OF SUPERIMPOSED 250-MESH SCREENS AFTER BONDING



100X

19800

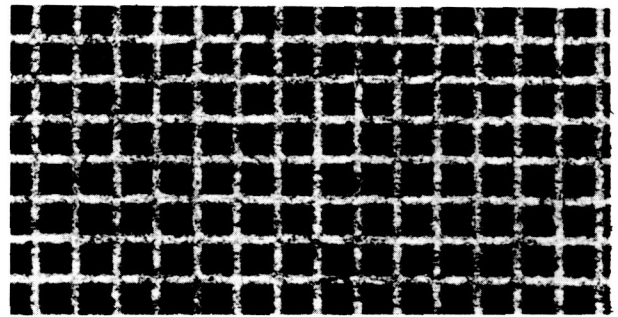
FIGURE 30. TOP SURFACE OF SUPERIMPOSED 500-MESH SCREENS BEFORE BONDING



100X

19801

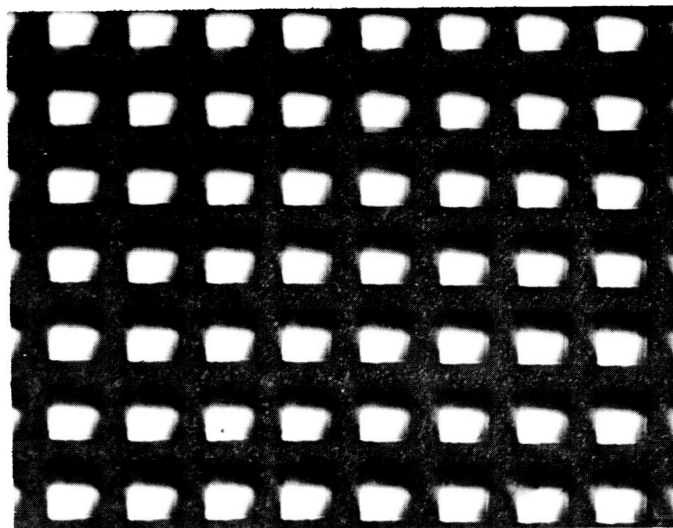
FIGURE 31. TOP SURFACE OF SUPERIMPOSED 500-MESH SCREENS AFTER BONDING



100X

19802

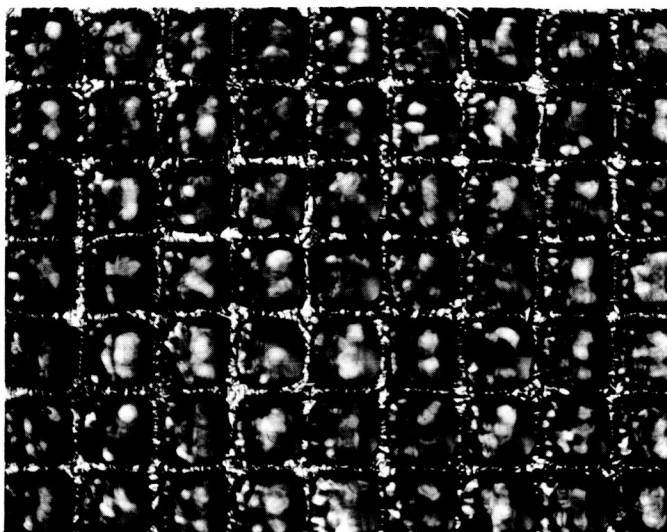
FIGURE 32. BOTTOM SURFACE OF SUPERIMPOSED 500-MESH SCREENS AFTER BONDING



100X

FIGURE 33. SURFACE VIEW OF 250-MESH SCREENS STACKED BY HAND TO 10.5-MIL THICKNESS

White areas are from back lighting.

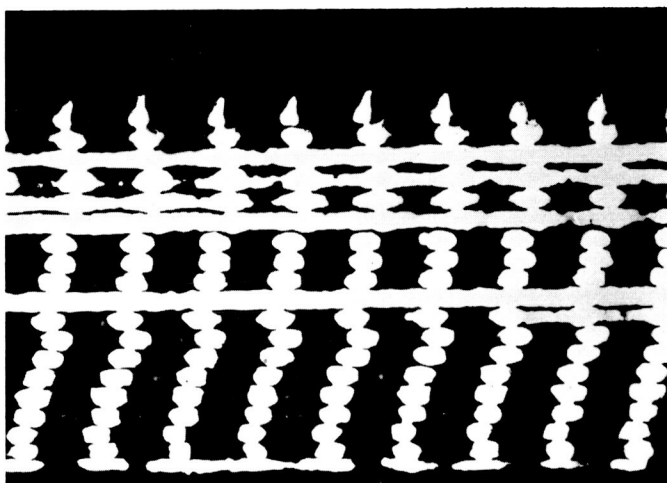


100X

24356

FIGURE 34. SURFACE VIEW OF 250-MESH SCREENS CONTAINING 20 LAYERS STACKED BY HAND TO 35.5-MIL THICKNESS

Screen shown after stacking, bonding, etching, and rebonding.



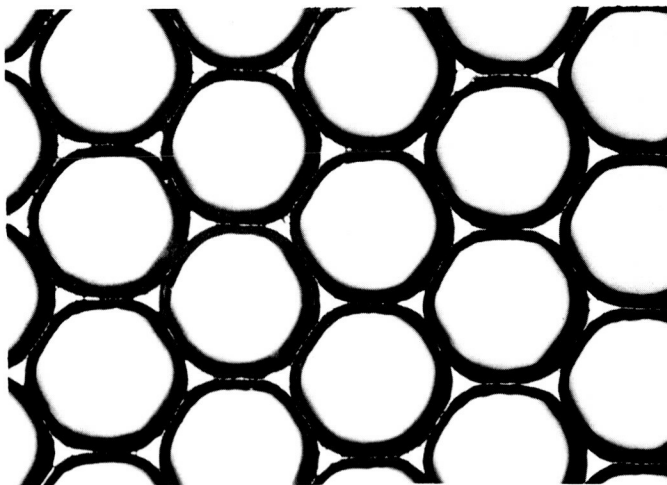
100X

As Polished

24357

FIGURE 35. CROSS SECTION OF 250-MESH SCREENS CONTAINING 20 LAYERS STACKED BY HAND TO 35.5-MIL THICKNESS

Photomicrograph made after stacking, bonding, etching, and rebonding. The white lines are sections through a wire parallel to the surface.



100X

FIGURE 36. SURFACE VIEW OF 125-MESH ETCHED SCREENS AFTER BONDING TO 10-MIL THICKNESS



TABLE 6. CONTROL OF PORE SHAPE IN 250-MESH SCREEN PLAQUES

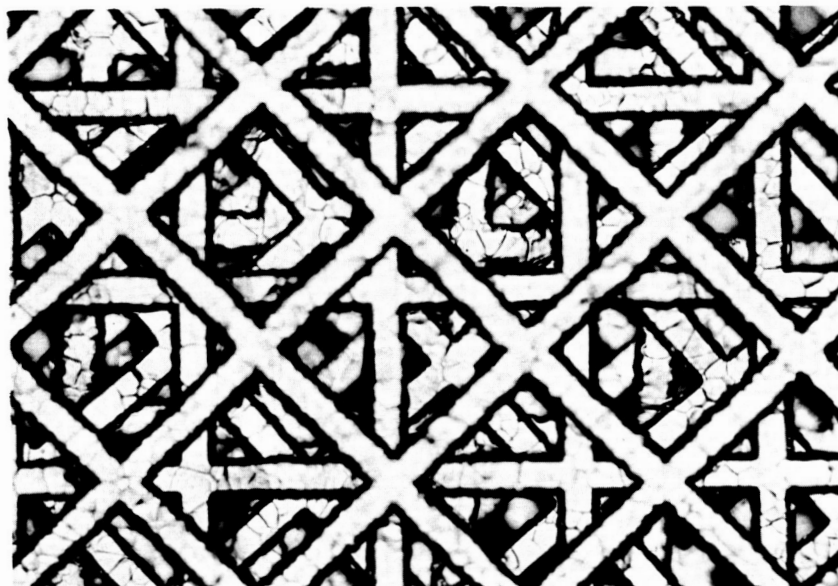
Specimen	Pore Shape	Thickness After Stacking and Bonding, mils	Screen-Stacking Sequence (a) Number of Layers and Percent Openings (b)
38	Keyed	5.6	2-25 : 8-50 : 2-25
37	"	8.7	2-25 : 26-50 : 2-25
45	"	23.5	3-25 : 31-50 : 3-25
49	"	35.5	4-25 : 55-50 : 4-25
48	Staggered taper	5.3	1-25 : 2-50 : 1-35 : 2-50 : 1-25
47	Ditto	11.0	2-25 : 2-50 : 1-35 : 2-50 : 1-35 : 2-50 : 1-35 : 2-50 : 2-25
46	"	20.5	3-25 : 3-50 : 1-35 : 3-50 : 1-35 : 3-50 : 1-35 : 3-50 : 1-35 : 3-50 : 1-35 : 3-50 : 3-25

(a) Number in table refers to number of screens and percent openings in the screens. Example: Specimen 38 had two screens with 25 percent open area, followed by eight screens with 50 percent open area, followed by two screens with 25 percent open area.

(b) Percent open area of screen corresponds to approximately the following hole sizes: 25 percent - 2.0 mils; 35 percent - 2.8 mils; 50 percent - 3.2 mils.

Semirandom pore shapes were made by stacking screens with square holes with approximately 45-degree orientation of wire. Such stacking gives an essentially random shape to pores, but pore sizes cannot be larger than a single square hole of one screen. Pore sizes cannot be smaller than the thickness of a single screen, for screens which have a hole size larger than the thickness of the screen.

The semirandom-orientation screen structure is shown in Figure 37. Screens were stacked by turning alternate layers about 45 degrees. No attempt was made at any other preferred positioning. In Figure 37, the microscope was focused on the third layer from the top. Screens above and below were slightly out of focus. Stacks having the semirandom structure were made 5 mils thick with 250-, 500-, 750-, and 1000-mesh screens and 22 mils thick with 250-mesh screens.



200X

N19054

FIGURE 37. SURFACE VIEW OF STACKED AND BONDED 250-MESH SCREENS - SEMIRANDOM ORIENTATION

#### Control of Porosity

Plaques of stacked and bonded electroformed screens have porosities about half that of commercial sintered powder plaques. The commercial electroformed screens used in this work have wires more oval than rectangular in cross section. These screens, when made thick enough to support themselves, have openings of less than 50 percent. However, because of the shape of the wires, stacked and bonded screens have porosities greater than the percent open area. Most of the commercial screens that were stacked with superimposed holes had openings of 25 to 35 percent and the plaques made from these screens had porosities of about 40 to 50 percent.

A method was devised to etch stacked and bonded screens to increase the porosity to about 60 percent. Plaques were etched by trial and error until the desired porosity

was obtained. After weighing and measuring the experimental plaques, the final procedure used was

- (1) Check weight and dimensions and calculate density and porosity
- (2) Rack the plaque with a spring clip made of nickel wire
- (3) Dip for 30 seconds in 50-50 mixture of concentrated hydrochloric acid and water
- (4) Rinse with water
- (5) Rinse with acetone
- (6) Dry by blowing with air
- (7) Immerse the plaque for 10 to 30 minutes in a solution containing 100 ml ethyl alcohol, 10 ml water, and 10 g iodine crystals
- (8) Rinse with acetone
- (9) Dry by blowing with air
- (10) Check weight loss and calculate new density and porosity
- (11) Recycle through Steps (2) to (9) until the desired porosity is obtained.

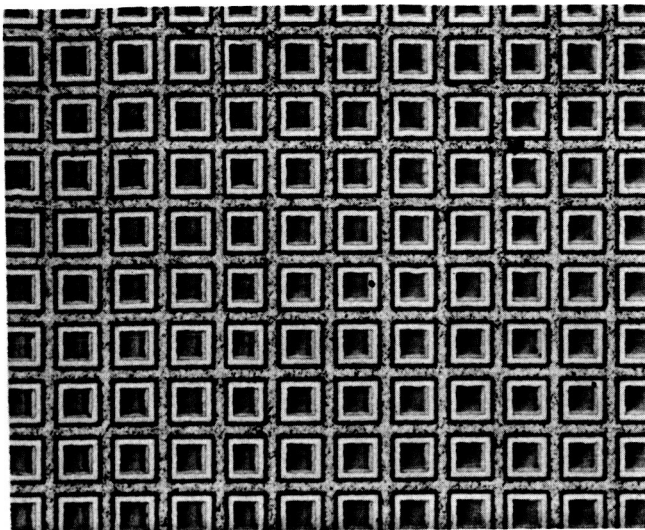
The etching solution, given in Step (7) of the procedure, removed about 1 mg of metal per minute from a 10-mil-thick plaque. The water in the solution increased the etch rate about 10 times over that of a pure alcohol solution of iodine. However, the surface finish was not quite as smooth as the one obtained in a nonaqueous etch. Too much water decreased the solubility of the iodine and promoted intergranular corrosion.

In a few experiments bromine was used in place of the iodine. Higher metal-removal rates were obtained. However, the bromine-containing solution was not stable and the iodine solution is thereby the preferred etching solution.

Figures 38, 39, and 40, respectively, show surface views of stacked screens, heat-bonded screens, and chemically etched screens. The screens as stacked (Figure 38) show a regular pattern caused by the electroforming mandrel. After heat bonding, the screens (Figure 39) had an etch pattern that is referred to as a thermal etch. Some of the mandrel pattern was lost. After etching to increase porosity (Figure 40), all of the mandrel pattern had disappeared and some of the thermal etch lines had been removed. Figures 41 through 44 show cross section of screens electrodes after fabricating was completed and electrochemical evaluations were made.

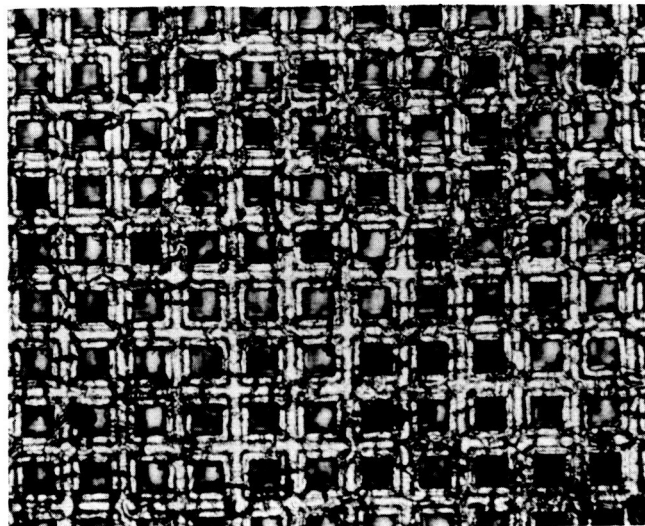
Etching of screen plaques with the iodine-containing solution is considered to be a significant accomplishment for the making of porous electrodes with straight-through holes. Porosities of 76 percent were made by this method. Higher porosities might be possible.

Table 7 contains porosity and thickness data for the screen plaques made for evaluation in Task F. Commercial electroformed screens used in this work have 25 to 60 percent openings. Stacks made with these screens had 30 to 57 percent porosity. Since electrochemical evaluations are more meaningful if all experimental electrodes have the same percent porosity, a study of etching solutions was made. The relationships calculated in Table 8 indicated the wire sizes needed to achieve a given porosity. To experimentally compare the effect of pore size and pore length, high porosity is not needed. To obtain high watt hours per pound, high porosity is needed.



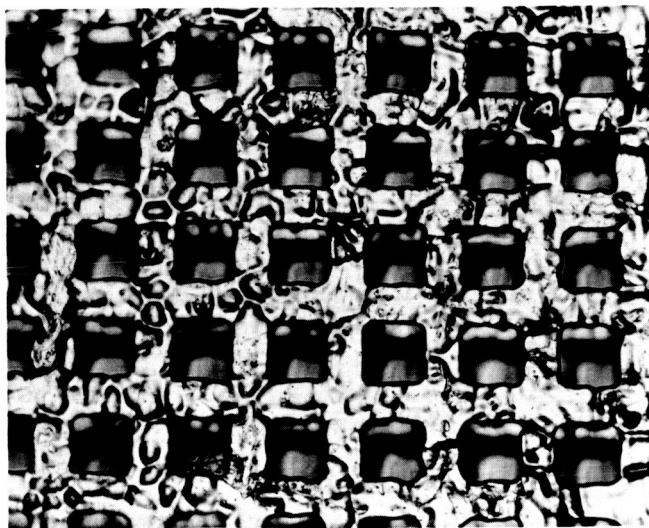
150X

FIGURE 38. SURFACE VIEW OF SUPERIMPOSED 500-MESH SCREENS BEFORE BONDING



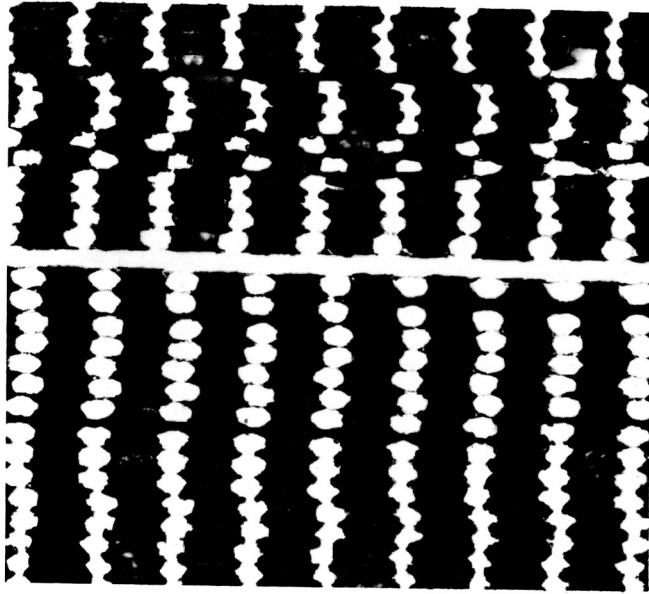
150X

FIGURE 39. SURFACE VIEW OF SUPERIMPOSED 500-MESH SCREENS AFTER BONDING



250X

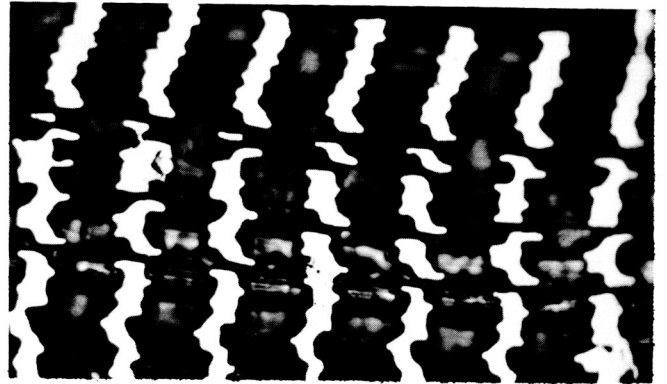
FIGURE 40. SURFACE VIEW OF SUPERIMPOSED 500-MESH SCREENS AFTER BONDING AND ETCHING



100X

25928

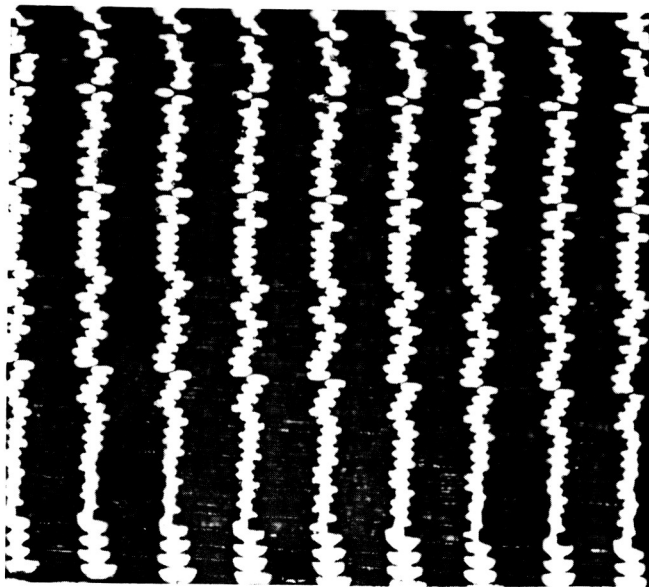
FIGURE 41. CROSS SECTION OF ELECTRODE 44 AFTER FAB-  
RICATION - PARALLEL-SIDED STRUCTURE



250X

25936

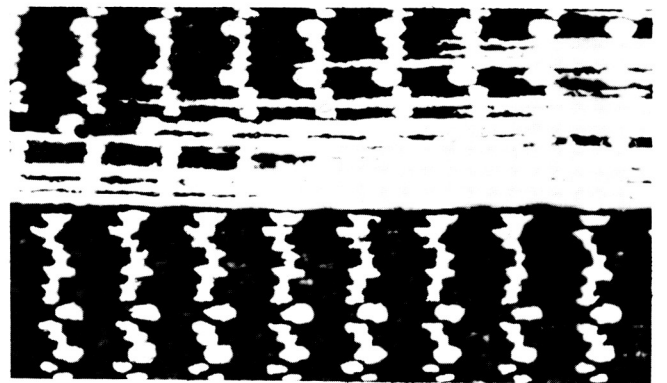
FIGURE 42. CROSS SECTION OF ELECTRODE 35 AFTER FAB-  
RICATION - PARALLEL-SIDED STRUCTURE



100X

25931

FIGURE 43. CROSS SECTION OF ELECTRODE 49 AFTER FAB-  
RICATION - KEYED STRUCTURE



100X

25930

FIGURE 44. CROSS SECTION OF ELECTRODE 47 AFTER FAB-  
RICATION - STAGGERED-TAPER STRUCTURE

TABLE 7. PHYSICAL DIMENSIONS, WEIGHTS, AND POROSITIES OF STACKED SCREEN PLAQUES

Plaque Number	Pore Shape	Pore Size		Pores Per Inch	Number of Screens	Area, cm <sup>2</sup>	After Bonding			After Etching		
		Diameter, mils(a)	Thickness, mils				Weight, mg	Thickness, mils	Weight, mg	Percent Voids	Thickness, mils	Weight, mg
23B	Straight	3.2	17	0.88	5.5	67	39	5.0	40.7	59		
30	"	"	11	0.84	10.5	109	45	9.1	70	59		
31	"	"	22	0.84	21.0	240	47	18	135	60.5		
43	"	"	27	1.0	23		41	22		63		
44	"	"	32	1.0	36		43	35.5	318	60		
24	"	"	40	1.0	35	483	46	33	296	60		
23A	"	1.6	21	0.88	11	103	41	7.1	48.4	66		
35	"	1.6	27	0.72	10	96	40	9.0	77	66		
27	"	1.6	45	1.0	21	280	43	17.4	156	60		
33	"	1.6	87	0.83	32	347	42	28.4	201	62		
26	"	1.0	21	0.81	5.0	61	46	4.2	24.5	59.5		
28	"	1.0	16	1.0	6.8	92	45	6.8	16.5	85(b)		
34	"	0.8	33	0.86	10	113	41	7.6	37	66		
25	"	0.8	10	0.81	3.2	36	38	3.0	33.5	65		
38	Keyed	3.2	12	1.0	5.6	65.5	52	5.2	45.5	61		
37	"	"	30	1.0	8.7	112	57	8.3	61.5	73		
45	"	"	38	1.0	23.5	227	56	23.8	206	63		
49	"	"	63	1.0	35.5	375	53	35.5	332	60		
48	Staggered taper	3.2	7	1.0	5.3	59.5	50	5.0	29.2	76		
47	Ditto	"	15	1.0	11.0	128	48	10.5	94	61		
46	"	"	29	1.0	20.5	230	50	19.7	183	60		
Hex	Hex	6	5	138	10	4962	84	Specimens not etched				
54	Straight	3.2	20	35	21	7979	45	19.5	6554	60		
15A	Semirandom	1.6	26	1.0	5.2	48	61	Not Measured	45.9	65		
17E	"	1.6	111	1.0	22	205	61	Ditto				
15B	"	1.4		1.0	4.0	25	66	"	23.2	71		
16A	"	0.35	50	1.0	3.7	44	48	"	46.2	52		
16B	"	0.24	26	1.0	4.1	55	44	"	46.6	52		

(a) Nominal pore width with 64 percent porosity.

(b) Uniform structure destroyed by overetching.

TABLE 8. RELATIONSHIP OF HOLE SIZE AND POROSITY OF SCREENS

Mesh, lines/inch	Size Center to Center, mils	Hole Width, h, mils	Wire Width, w, mils	Ratio, w/h	Percent Openings <sup>(a)</sup>
1000	1.0	0.95	0.05	0.05	90
1000	1.0	0.90	0.10	0.11	81
1000	1.0	0.85	0.15	0.18	72
1000	1.0	0.80	0.20	0.25	64
1000	1.0	0.70	0.30	0.43	49
750	1.33	1.27	0.07	0.05	90
750	1.33	1.20	0.13	0.11	81
750	1.33	1.14	0.20	0.18	72
750	1.33	0.07	0.27	0.25	64
750	1.33	1.00	0.33	0.43	49
500	2.0	1.9	0.1	0.05	90
500	2.0	1.8	0.2	0.11	81
500	2.0	1.7	0.3	0.18	72
500	2.0	1.6	0.4	0.25	64
500	2.0	1.4	0.6	0.43	49
250	4.0	3.8	0.2	0.05	90
250	4.0	3.6	0.4	0.11	81
250	4.0	3.4	0.6	0.18	72
250	4.0	3.2	0.8	0.25	64
250	4.0	2.8	1.2	0.43	49

(a) Assuming wires have rectangular cross sections.

A preliminary study with aqueous solutions was conducted to chemically etch stacked nickel screens to increase porosity to about 60 percent before selecting the above procedure. Etching solutions were devised that removed metal at different rates, depending on agitation. Such a solution when flowed through stacked screens has the potential of removing metal faster from the projecting side of the wire than from the top and bottom, where the wires are joined. Table 9 shows etching rates of ferric chloride solutions on 1/4-inch nickel rods with and without agitation. The solution of ferric chloride and hydrochloric acid which had the highest ratio (10 to 1) was checked on both a single screen and on stacked and bonded screen. The screen was placed between two filter papers and the solution flowed through the screen and filter papers with a vacuum and filter flask. The filter paper was considered necessary to produce uniform flow rates through each pore.

With a single thickness of an electroformed screen in the as-plated condition, flowing the etch solution (Solution 8, Table 9) through the screen for about 5 minutes reduced the wire width by 1 mil and the thickness by 0.3 mil. This is a ratio of about 3.3 to 1 for the high- to low-agitation areas on the wires.

TABLE 9. NICKEL ETCHING RATES IN FERRIC CHLORIDE SOLUTIONS

Solution	Bath Composition					Weight Loss in 5 Minutes		
	FeCl <sub>3</sub> , g/1	HCl(37%), cc/1	Temperature,		Additives	Weight Loss, mg/in. <sup>2</sup>		Ratio of Weight Loss, agitation/no agitation
			F	pH		Agitation	No Agitation	
1	570	0	74	<0	--	41	17	2.4
2	570	0	74	<0	Dimethylglyoxime	40	16	2.5
3	570	0	74	<0	Thioacetamide	53	20	2.6
4	570	0	74	<0	Thiourea	24	14	1.7
5	140	0	72	1.6	--	58	16	3.6
6	70	0	72	1.7	--	38	7	5.4
7	70	0	75	3 to 4	NaOH	35	8	4.4
8	3	10	80	--	--	10	1	10.0

Stacked-and-bonded screen plaque with semirandom orientation was etched for 1 minute under the same conditions used for the single-layer screen. One minute of treatment time was selected because the expected etching would reduce the wire width from 0.8 to 0.6 mil. However, the screen disintegrated into powder. Examination of the residue showed short lengths of wire. Judging by microscopic examination, the nickel screens recrystallized during bonding so that each wire was a series or chain of crystals, many of which were the full width of the wire. The etching solutions apparently attack the crystal boundaries faster than the crystals and cut through the wires, causing disintegration of the structure. No aqueous solution was found that will attack the crystal boundaries at the same rate (or a lower rate) as it would attack the crystals of nickel.

Alkaline solutions of ferricyanide with sodium cyanide and sodium cyanide and hydrogen peroxide did not seem to attack nickel at any significant rate.

#### Discussion of Manufacturing Porous Screen Electrodes

Stacking of screens into thick electrodes with pores continuous through the structure was a useful tool for fabricating experimental electrodes to be used in identifying efficient pore geometry. A method was conceived whereby screenlike porous electrodes could be made economically with porosities in excess of 90 percent. In this proposed method, corrugated strips of nickel would be electroformed continuously on cylindrical mandrels and assembled into a honeycomb structure.

#### Location of Data

All experimental data on Task B are located in Battelle Laboratory Record Books Numbers 21516, pp 1-92; 21595, pp 1-62; 21867, pp 1-12; and 21652, pp 1-9.

Mr. William F. Scharenberg and Mr. Charlie W. Fick designed the screen-stacking machine. Mr. Richard D. Kreachbaum superimposed and stacked the screens. Mr. Rexford W. Jones did the photoengraving. Mr. Walter A. Hedden applied the ceramic coatings. The help and guidance of the above persons, for the work reported in Task B, is gratefully acknowledged.



TASK C - SINTERED PLAQUE PROCESSING

Objectives

Task C of the contract reads as follows:

"Processing parameters for fastening superimposed screens together shall be determined.

"Item 1 - Temperature

Temperature and pressure for contact bonding.

"Item 2 - Time and Resistivity

Sintering time for high strength and low electrical resistivity.

"Item 3 - Atmosphere

Atmosphere to produce chemically clean surface areas and other special precautions that are required."

The objective of these items of work is to ascertain sintering conditions that are adequate to permit performance of the other tasks. By mutual agreement, between representatives of NASA and of Battelle, it was decided that research to optimize the sintering technique should be postponed until it was deemed necessary for more practical reasons.

Item 1 - Temperature and Pressure

Temperatures ranging from 1950 to 2350 F and pressures of 6, 60, 100, 150, and 175 g/cm<sup>2</sup> were studied in determining the optimum sintering temperature and pressure for bonding nickel screens. The bonding pressure was applied by adding a dead weight made of either steel or Alundum to the stacked nickel screens as shown in Figure 45. Larger stacked screens (up to 4-1/2 x 5 inches) were bonded between two flat Alundum bricks which had been heated and cooled to stabilize the bricks before a surface grinding operation. Temperatures in excess of 2150 F caused excessive grain growth as well as closing in of the pores in the nickel screen. Sintering temperatures less than 2050 F resulted in poor bonding in some areas.

Best results were obtained when the electroformed screens were diffusion bonded at 2150 F at a pressure of 175 g/cm<sup>2</sup>. Loads less than 100 g/cm<sup>2</sup> resulted in nonuniform bonding; dead-weight loads greater than 175 g/cm<sup>2</sup> were not investigated. As may be seen in Figure 43, these sintering conditions produced bonding between most of the superimposed nickel screens with little deformation of the individual nickel wires.

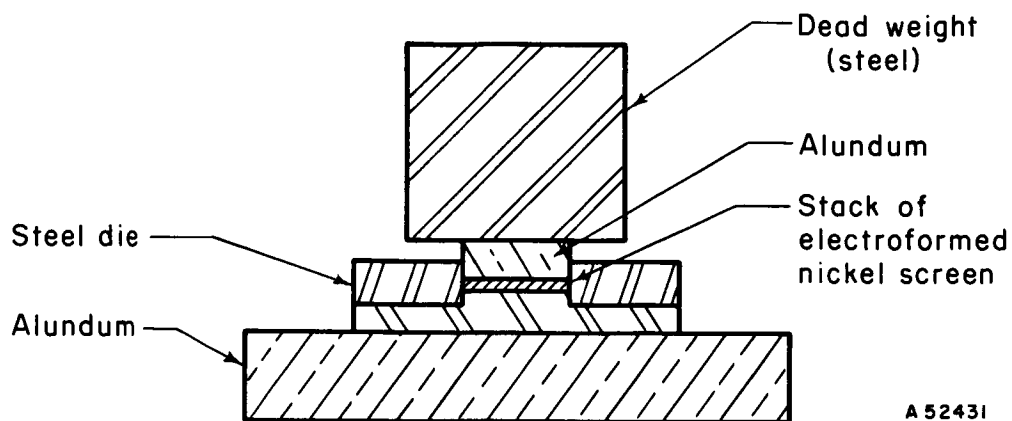


FIGURE 45. DRAWING OF SETUP FOR SINTERING STACKED ELECTROFORMED NICKEL SCREENS

### Item 2 - Time and Resistivity

The sintering conditions required for good bonding between screens were selected based on destructive bend tests and inspection of bonding between screens of metallographic sections of stacked screens. Electrical resistivity was not used as a criterion because unlike sintered powders the electroformed screens supply a continuous electrical path even before bonding and no meaningful correlation can be expected for edge-to-edge measurements. Surface-to-surface resistance measurements were too inaccurate to be useful.

Sintering times of 30, 60, 90, 120, and 150 minutes were studied at 2150 F to determine the minimum period of time required to produce well-bonded screens. Satisfactory results were obtained in 120 minutes. Resistivities are described under Task D.

### Item 3 - Atmosphere and Special Precautions

Commercial tank hydrogen was satisfactory for the reduction of surface oxides on the nickel screens. No other atmospheres were investigated.

Special precautions were required to prevent the electroformed screens from welding to the mild steel die used in alignment of the superimposed nickel screens. Of two oxide die coatings investigated, Nicro Braze Stop-Off\*, a commercial brazing stop-off containing a dispersed oxide in lacquer, prevented welding and it gave a smooth surface finish to the sintered screen. Fine aluminum oxide (-325 mesh) in clear lacquer was also used and was satisfactory as an antibonding coating.

Fingerprints and surface contamination were avoided by handling all screens between plastic and with tweezers.

\*Wall Colmonoy Corporation, 1934 John R. Street, Detroit 3, Michigan.

Location of Data

All experimental data on Task C are located in Battelle Laboratory Record Book No. 21595, pp 1-58. Mr. Hugh R. McCurdy, with the guidance of Mr. H. O. McIntire, worked out the sintering procedures described above.

TASK D - PLAQUE CLASSIFICATIONObjectives

Task D of the contract reads as follows:

"Processed plaques shall be tested to determine the following characteristics:

"Item 1 - Electrical Resistivity

Measurements shall be made in two directions; edge to edge and surface to surface.

"Item 2 - Pore Size Distribution

"Item 3 - Pore Shapes

"Item 4 - Internal Surface Areas

"Item 5 - Density and Porosity

"Item 6 - Measurement of Interconnection Pores

"Item 7 - Tensile Strength

"Item 8 - Flexibility."

The objective of these items of work was to provide technical data with which interested persons might follow and evaluate the work.

Item 1 - Electrical ResistivityEdge to Edge

Edge-to-edge electrical-resistivity measurements were made on commercial sintered powder plaques and bonded superimposed screens, both  $21 \pm 1$  mil thick, according to the procedures in ASTM Standards A-344-60T. The results indicated a screen electrode should have about one-sixth the electrical resistance of a same-sized sintered powder electrode, as follows: powder plaque,  $159 \mu\text{ohm-cm}$ ; superimposed screen,  $26.2 \mu\text{ohm-cm}$ .

### Surface to Surface

Since no ASTM standard has been set up for surface-to-surface electrical-resistivity measurement, a laboratory procedure was devised for making these measurements. The laboratory setup is shown in Figure 46. A range of values for surface-to-surface electrical resistivity was obtained with this equipment: powder plaques, 1,262-2,703  $\mu\text{ohm-cm}$ ; superimposed screens, 84,300-111,000  $\mu\text{ohm-cm}$ . Notice that minimum to maximum values differed by 50 to 100 percent. Moreover, the values were 10 to 1000 times higher than expected on the basis of edge-to-edge resistivity measured another way. Apparently contact resistance, which was included in the measurement, was much greater than the resistance of the nickel structure.

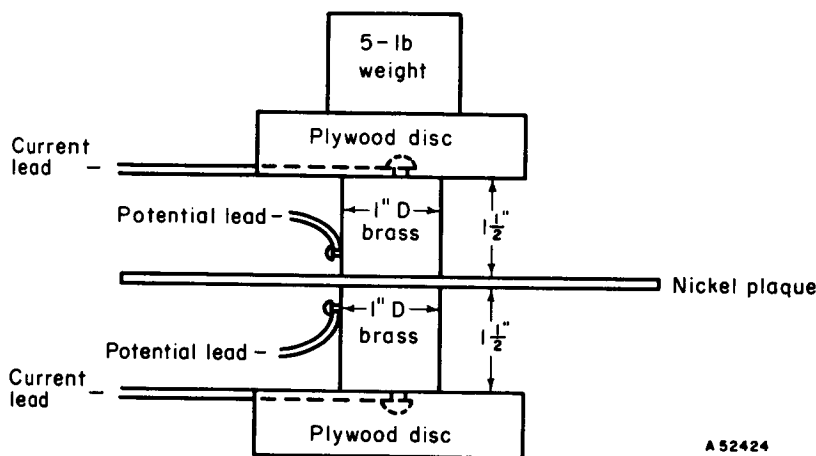


FIGURE 46. APPARATUS USED TO MEASURE SURFACE-TO-SURFACE RESISTIVITY

To check the contact resistance, it was noted that potential leads, when connected to each side of the plaque close to the brass contacts, had less than 0.2-mv reading with 15 amp flowing through the nickel plaque. The vacuum tube voltmeter used had a sensitivity of 0.2 mv but showed no deflection. If a voltage of 0.2 mv had been obtained, the resistivity would have been 500  $\mu\text{ohm-cm}$ , rather than the 84,300 to 11,000 indicated above. Solid nickel at 20 C has a specific resistance of 6.0  $\mu\text{ohm-cm}$ . If the path for current through the bonded screen were about 1.0 percent of the cross-sectional area, the specific resistance would be 690  $\mu\text{ohm-cm}$ . The cross section of the screen, as shown in Figure 32, has about 10 to 20 percent of the cross-sectional area between wires for a current path from surface to surface. Based on a 10 percent estimate the specific resistance should be about 70  $\mu\text{ohm-cm}$ . This number is more reasonable in view of the edge-to-edge resistivity of 26  $\mu\text{ohm-cm}$ . In a similar way, the surface-to-surface resistance of sintered powder plaques would be much lower than the indicated value.

### Item 2 - Pore-Size Distribution

Results on commercial powdered plaques and commercial screens are described under Task A, Items 1 and 2. Porosities for stacks of screens are described in Table 7. The pore-size distribution for a stack of screens is about the same as for a single screen.

### Item 3 - Pore Shapes

Results on commercial powdered plaques and commercial screens are described under Task A. The figures in the Task B section of this report show pictures of the various pore shapes that were made.

### Item 4 - Internal Surface Areas

Internal surface areas were measured by krypton adsorption on the commercial powder plaques described in Task A. The measurement was made by a modification of the conventional B. E. T. technique reported by Nelson and Eggertson\*, employing a flowing gas stream. This method is particularly useful for small surface areas (less than  $1 \text{ m}^2/\text{g}$ ) and is believed to be accurate to better than 20 percent of measured areas for sample sizes having a total area greater than  $100 \text{ cm}^2$ . The commercial powder plaques were found to have an internal area of  $0.088 \text{ m}^2/\text{g}$ . For 5-micron particles, the calculated area was  $0.1 \text{ m}^2/\text{g}$ . The photomicrographs of Figures 2 and 3 indicate the diameters are 5 to 10 microns. For plaques with one-third weight of wire, the expected area would be  $0.07 \text{ m}^2/\text{g}$ . Measurements and calculations agree.

Internal surface areas of superimposed screen plaques were calculated on the basis of geometry of the structures. First an assumption was made that all pores were square and smooth. This assumption permitted calculation of a minimum area. Next, a maximum number was estimated by assuming the surface was made from stacked round wires which increased the area by 1.57. Maximum and minimum areas were calculated based on 60 percent porosity and are listed in Table 10.

TABLE 10. INTERNAL SURFACE AREA OF NICKEL PLAQUES<sup>(a)</sup>

Holes/Inch	Electrode Configuration			Internal Surface Area, $\text{cm}^2/\text{g}$	
				Assuming Smooth Sides	Assuming Round Wire Shape
	Hole Width, mils	Wall Thickness, mils	Hole Shape		
1000	0.8	0.2	Square	360	560
750	1.07	0.26	"	270	425
500	1.6	0.4	"	180	280
250	3.2	0.8	"	90	140
125	6.0	2.0	Round	45	70 <sup>(b)</sup>
Sintered Powder	0.6	0.2 <sup>(c)</sup>	Random	880	--

(a) Based on 60 percent porosity, assuming round wires and surface roughness factor 2 times the plane area.

(b) Area based on 84 percent porosity of an actual hexagonal-hole screen.

(c) Nickel powder assumed to be 5 microns diameter from measurements described in Task A.

\*Nelson, E. M., and Eggertson, F. T., Anal. Chem., 30, 1387-90 (1958).

Although the area indicated in Table 10 for the screen electrodes is consistently less than the measured area of a powder electrode, the result is as expected. Table 11 shows the effect of metal shape on its area per unit of volume. The effect is in the area ratios of 6 to 4 to 2 for spheres to cylinders to flat sheets for a given thickness of metal. This mathematical principle is significant in two ways: (1) porous bodies made with spherical particles will tend to have the largest internal surface area; (2) for a given thickness of metal, the effect of shape on internal surface area will always be less than one order of magnitude.

TABLE 11. RELATIONSHIPS OF AREA TO VOLUME FOR SPHERE, WIRES, AND SHEETS

Shape	Area/Volume	Units of d
Sphere d = diameter	$\frac{\pi d^2}{1/6 \pi d^3}$	$\frac{6}{d}$
Wire d = diameter L = length	$\frac{\pi d \times L}{1/4 \pi d^2 \times L}$	$\frac{4}{d}$
Sheet d = thickness L = length W = width	$\frac{2 \times L \times W}{d \times L \times W}$	$\frac{2}{d}$

#### Item 5 - Density and Porosity

Densities of commercial powdered plaques were measured and the density of the commercial screens were calculated assuming rectangular wires. The density values were used to calculate porosity using the following formula:

$$\text{Percent porosity} = \frac{\text{theoretical density} - \text{observed density}}{\text{theoretical density}} \times 100$$

Results are shown in Table 12.

As a check of the calculated porosity of the sintered powder plaques, the apparent percent volume of the nickel powder was checked from photomicrographs like Figure 3. A fine grid was printed on the pictures and the percentage of intersections that fell on the nickel (white color) phase was 14.3 percent of total number of intersections. Therefore, the approximate volume of voids was 86 percent calculated voids volume which does not include the wire screen in the powder plaque. The wire screen raises the net density and lowers the calculated void volume.

Porosity of experimental electrodes is shown in Table 7.

TABLE 12. DENSITY AND POROSITY OF COMMERCIAL ELECTROFORMED SCREENS AND COMMERCIAL SINTERED POWDER PLAQUES

Screen Size, lines/inch	Density, g/cm <sup>3</sup>	Porosity, % voids
1000	5.33	40
750	3.56	60
500	3.47	61
250	3.60	64
Powdered plaque	1.85	79

#### Item 6 - Measurement of Interconnecting Pores

All pores in the sintered powder plaques were interconnected because all the significant volume can be accounted for. The void volume measured by mercury porosimetry (Figure 1) was 0.425 cm<sup>3</sup>/g. The void volume calculated from geometric dimensions of the plate was 0.413 cm<sup>3</sup>/g and 0.427 cm<sup>3</sup>/g for two determinations, or an average of 0.420 cm<sup>3</sup>/g. The two independent measurements agree. The geometric measurement of gross volume was made by measuring the dimensions of a specimen and correcting micrometer thickness measurements by half of the surface roughness obtained with an electronic surface-roughness gage.

The pores in the stacked screens were not intended to be interconnected but were intended to be continuous through the plaque. Judging by microscopic examination of superimposed and bonded screens with 60 percent porosity, most of the pores were not connected with large openings to their neighbors. This was confirmed during impregnation work when a gas bubble, which formed at ends of a pore and was not dislodged, remained empty. If the pore had been interconnected, some cadmium material may have entered from alternate routes.

#### Item 7 - Tensile Strength

Tensile strengths of sintered powder plaques and superimposed screens were measured with a substandard specimen. Dimensions of the specimen are given in Figure 47. The measured tensile strength values are recorded in Table 13. Note that two end points were determined on the powder plaques. The first was at the first visible cracking of the powder and the second was failure of the supporting screen.

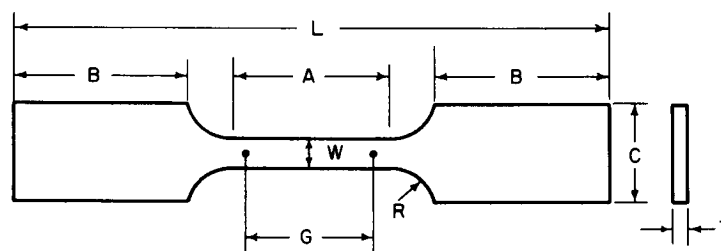
#### Item 8 - Flexibility

Flexibility tests were made on commercial sintered nickel powder plaques and on bonded superimposed nickel screens according to the bend test for ductility described in ASTM Standards A-344-60T. Briefly, the specimens (3 by 15.2 cm) were clamped in

TABLE 13. TENSILE STRENGTH OF COMMERCIAL POWDER PLAQUES AND SUPERIMPOSED NICKEL SCREENS

Material	Tensile Strength, psi	Yield Strength (0.2% Offset), psi	Elongation (1-Inch Gage), %	Remarks
Ni powder plaque	1650	1030	3	Tested to cracking of nickel powder
Ni powder plaque	1700	912	3	
Ni powder plaque	2320	997	15	Tested to failure of wire screen
Ni powder plaque	2850	979	14	
Superimposed Ni Screen	4840	3580	--(a)	Tested to failure

(a) Not determined.



G - 1.000 ± 0.005 in.      L - 4  $\frac{3}{4}$  in.      A 52426  
W - 0.250 ± 0.005 in.      A - 1  $\frac{1}{4}$  in.  
T - thickness of sheet      B - 1  $\frac{1}{2}$  in.  
C -  $\frac{3}{4}$  in.      R -  $\frac{3}{8}$  in.

FIGURE 47. TENSION-TEST SPECIMEN

jaws whose working edges have radii of approximately 0.5 cm over which the test specimen is bent. The specimen is bent through 90 degrees, then bent through 180 degrees in the reverse direction. Again the specimen is bent through 180 degrees in the first direction and continually through 180-degree reversals until a crack appears in the bend or a sudden failure occurs by complete rupture. The results were as follows:

Plaque	Sample Thickness, inch	Number of Bends Required to Cause Cracking	Total Number of Bends Withstood by Specimen
Ni powder	0.019	1	94
Ni powder	0.019	1	105
Ni screen	0.019	5	5
Ni screen	0.019	5	5



The cracking of sintered powder electrode actually occurred during the first bend at less than 180 degrees. Therefore, the sintered screens have considerably more flexibility than the sintered powders. The large number of total bends, in the last column of the above tabulation, is allowed by the large wire supports in the sintered powder electrodes. The useful sintered powder will have spalled away long before flexing has actually broken the 8-mil support wires.

#### Location of Data

All experimental data on Task D are in Battelle Laboratory Record Book No. 21595, pp 1-62.

Mr. Hugh R. McCurdy and Mr. H. O. McIntire worked with Mr. G. R. Schaer in the determination of electrical resistivity, tensile strength, and flexibility values. The characterization of pores and porosities was worked out with the cooperation of Dr. Maynard B. Neher.

### TASK E - IMPREGNATION PROCEDURE

#### Objectives

Task E of the contract reads as follows:

"Electroformed nickel screens shall be impregnated with cadmium oxide. A minimum of two methods of placing the reactant material on the sintered plaque shall be investigated.

- a. Physical Packing
- b. Chemical Impregnation."

The objectives for this task were (1) to show that chemical impregnation procedures used at Battelle are comparable with impregnation procedures actually used in the manufacture of batteries, (2) to ascertain whether simplified impregnation procedures might be used with the new electrode structures prepared as part of Task B, and (3) to impregnate experimental electrodes with enough available cadmium material to have a watt-hour capacity equal to or higher than commercial electrodes.

A comparison of results of impregnation at Battelle with results reported for commercial plaques seemed necessary because commercial impregnation procedures were not known with certainty. There are occasional rumors that manufacturers have proprietary art that is superior in some way to the published procedures. Therefore, a need existed to show that commercial plaque impregnations could be duplicated in the laboratory.

Simplified impregnation procedures are desirable because impregnation seems to be a major item in the high cost of nickel-cadmium batteries. A 6-volt battery rated at about 1 ampere-hour, for example, costs a consumer about \$20. This cost corresponds

to more than 300¢ per watt-hour. The active materials are worth less than 3 cents. A large part of this increased value would seem to be related to the costly impregnation procedures used in the manufacture of batteries. The controlled pore shapes, described in Task B, might lend themselves to a simple physical impregnation, as by rolling. The present work was intended to investigate such possibilities.

### General Conditions

As a general scheme to accomplish the above objectives the following steps were followed:

- Step 1 - Select the impregnation procedure most commonly indicated by the open literature.
- Step 2 - Check weight gains observed in the laboratory against weight gains reported in the literature.
- Step 3 - Check ampere-minutes per in.<sup>3</sup> of plaques observed with laboratory electrodes against values observed for commercial plaques and against values reported in the literature.
- Step 4 - Compare weight gains and ampere-minutes observed with new screen structures and old and new impregnation procedures against values obtained in Steps 2 and 3 above.

### Step 1 - Selection of Procedure

The chemical impregnation procedure described by A. Fleischer\* for the preparation of nickel-cadmium battery plates was selected for two reasons. First of all, the procedure has ample detail for duplication and comparison. Secondly, a review of the literature indicated that Fleischer's procedure is probably used by the battery trade with possible (but unknown) variations.

The procedure consists of the following four steps:

- (1) Vacuum impregnation in saturated nitrate salt solutions at about room temperature
- (2) Precipitation of the hydroxides in the pores by cathodic polarization in hot 25 weight percent potassium hydroxide
- (3) Washing with water
- (4) Air drying.

Repeat Steps (1) through (4) at least four times. The four steps combined are called one impregnation cycle. Each cycle required about 6 hours in the laboratory.

\*Fleischer, A., J. Electrochem. Soc., 94, 293-296 (1948).

Step 2 - Weight Gains

Commercial plaques have been impregnated at Battelle by using the procedure described above. Assuming the density of cadmium hydroxide to be  $4.79 \text{ g/cm}^3$  (Fleischer also assumed this theoretical density), the volume of active material precipitated in the pores was calculated from the weight gain after each impregnation. The percentage of pore volume filled with active material was determined from the active material volume and the calculated pore volume. Battelle observations are given in Table 14. The results obtained compared favorably with those reported by A. Fleischer\*, as shown in Figure 48.

It should be noted that less than 40 percent of the pore volume was filled by four impregnation cycles, because this suggests that more efficient impregnation is possible.

TABLE 14. TOTAL AMOUNT OF CADMIUM HYDROXIDE PRECIPITATED AS A FUNCTION OF THE NUMBER OF IMPREGNATIONS

Sample	Impregnation Number	Cadmium Hydroxide Precipitated		
		Observed, grams	Calculated, $\text{cm}^3$	% Pore Volume Filled
a	1	0.0262	0.00547	12.7
	2	0.0458	0.00957	22.2
	3	0.0600	0.0125	29.0
	4	0.0817	0.0171	39.6
b	1	0.0273	0.00570	13.2
	2	0.0478	0.00998	23.1
	3	0.0616	0.0129	29.9
	4	0.0799	0.0163	37.8

Step 3 - Energy Density Comparison of Electrodes

Table 15 compares Battelle-impregnated electrodes and commercially impregnated electrodes with much larger electrodes reported in the Fleischer report cited earlier. The coulombic densities for the Battelle-impregnated electrodes check closely with those obtained from commercially impregnated electrodes tested at Battelle. Coulombic densities obtained from the literature are lower. However, lower efficiency of utilizing the cadmium is to be expected for thicker electrodes, as will be described in subsequent sections of this report.

\*Fleischer, A., Nickel Cadmium Battery Corp., "Laboratory Investigations and Research Toward the Development of Nickel Cadmium Alkaline Storage Batteries", Quarterly Progress Report (Dec. 31, 1947), p 86.

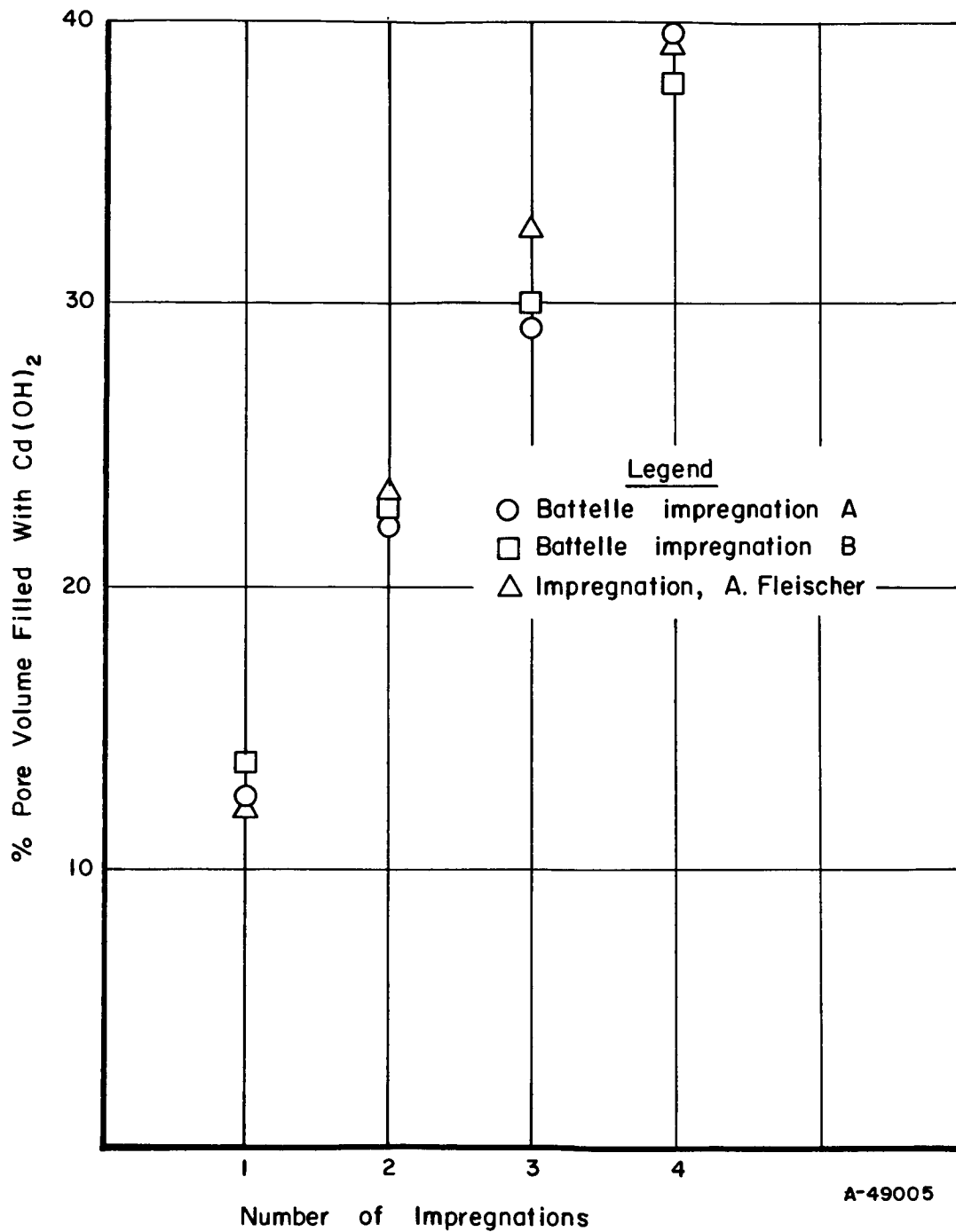


FIGURE 48. PERCENT PORE VOLUME FILLED WITH Cd(OH)<sub>2</sub> AS A FUNCTION OF THE NUMBER OF IMPREGNATIONS

TABLE 15. COULOMBIC DENSITY COMPARISONS

Electrode	Thickness, mils	Area, in. <sup>2</sup>	Volume, in. <sup>3</sup>	Ampere- Minute Capacity		Observed Coulombic Density, amp-min/in. <sup>3</sup>
				Experi- mental	Theoret- ical	
BMI						
Impregnated	21	0.155	0.00326	1.62	2.53	500
Commercial	36	0.155	0.00558	2.95	4.36	530
Literature	83	10.5	0.868	360	--	420
Literature	157	10.5	1.65	485	--	300

Step 4A - Weight Gains and Ampere-Minute Capacity for  
Chemical Impregnation of Screen Electrodes

Fleischer's Method. The first experimental screen structures available for impregnation experiments were the semirandom screens of the type shown in Figure 37. Four such electrodes were impregnated by the same procedure as used on the sintered powder plaques. Weight gains and discharge capacity (percent utilization) are shown in Table 16 for the first discharge cycle. Cycling data are shown in Figure 15.

The data in Table 16 and in Figure 49 illustrate some performance properties that remain unexplained, even after the numerous experiments that followed these first tests with stacked screen electrodes. First of all, notice in Column 11 of Table 16 the wide variation of discharge efficiencies:

<u>Lines/Inch</u>	<u>Discharge Efficiency</u>
250	65
500	40
750	89
1000	77

The wide variations raised questions about reproducibility and about the reliability of conventional impregnation procedures for the screen electrodes. Moreover, the retabulated discharge efficiencies are high, up to 89 percent, for discharge rates of less than 1/2 hour. For comparison, the commercial electrodes in Table 15 have discharge efficiencies of 64 to 68 percent at discharge rates of more than 1 hour. The high efficiency of 89 percent for the 750 lines/inch screen is greater than any seen with the shaped pore electrodes subsequently given in Table 30. The above 77 percent efficiency was achieved again only twice - see Cycles 1 of Tests 103 and 117A in Table 30.

The relative performances shown in Table 16 persisted for several cycles as shown in Figure 49. All the electrodes were charged at 0.5 ma/cm<sup>2</sup> and discharged at

TABLE 16. CHEMICAL IMPREGNATION OF SEMIRANDOM SCREEN STRUCTURES(a)

(1) Electrode	(2) Mesh Size, lines/inch	(3)	(4) Weight Gain Per Cycle, mg			(7) Total	(8) Percent Pore Volume Filled	(9) Discharge Rate, hours	(10) Theoretical Capacity, ma-hours	(11) Discharge Efficiency, percent of theoretical
			1	2	3					
15A	250	3.8	3.4	5.0	3.5	15.7	34	0.33	6.6	65
15B	500	3.5	11.4	2.4	3.8	21.1	58	0.45	8.9	40
16A	750	8.9	3.7	6.4	5.9	17.6	42	0.38	7.4	89
16B	1000	2.6	1.6	2.2	2.5	8.9	33	0.19	3.8	77

(a) Electrode dimensions are given in Table 7.

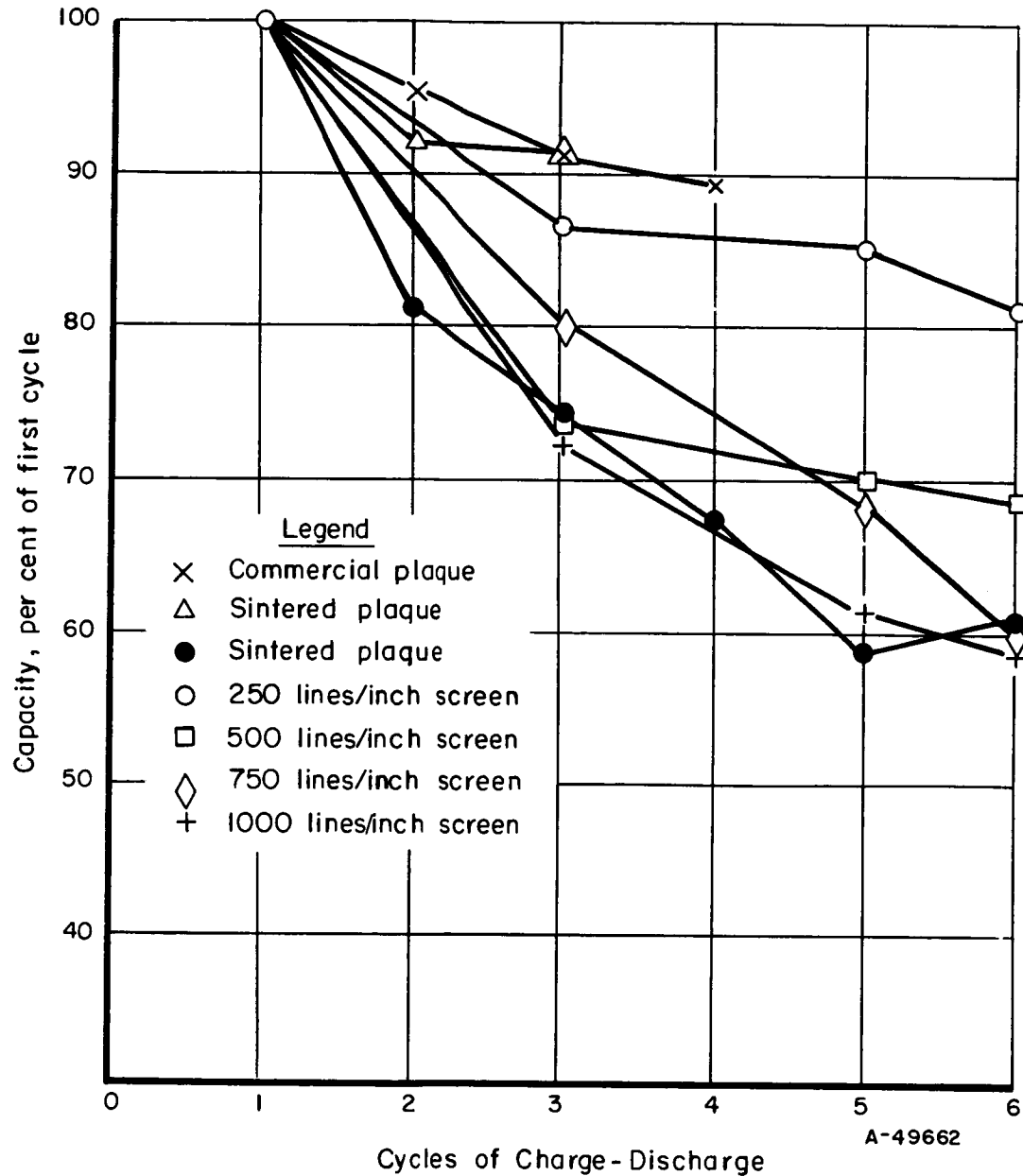


FIGURE 49. CAPACITY OF NEGATIVE PLATES AS A FUNCTION OF CHARGE-DISCHARGE CYCLES

10 ma/cm<sup>2</sup>. These results showed the observed values of Table 16 were real. However, the efficiencies decreased with cycling and these cycling changes presented new and undesired difficulties.

The percent capacity is plotted as a function of cycle number, Figure 49, with the capacity obtained in Cycle 1 considered as 100 percent. The electrodes with the larger pores retain more capacity upon cycling than electrodes with smaller pores. Pore sizes are given in Table 7 of Task B.

The curve for the Battelle impregnated, commercially sintered nickel plaque closely follows the curve for the 1000 lines/inch screen electrode. Both electrodes have average pore diameters of about the same order of magnitude (0.6 mil), and imply such a relationship might be expected.

Capacity losses shown in Figure 49 are attributed to carbonate contamination of the electrolyte and a detailed account will be given in a following section called "Barium Hydroxide".

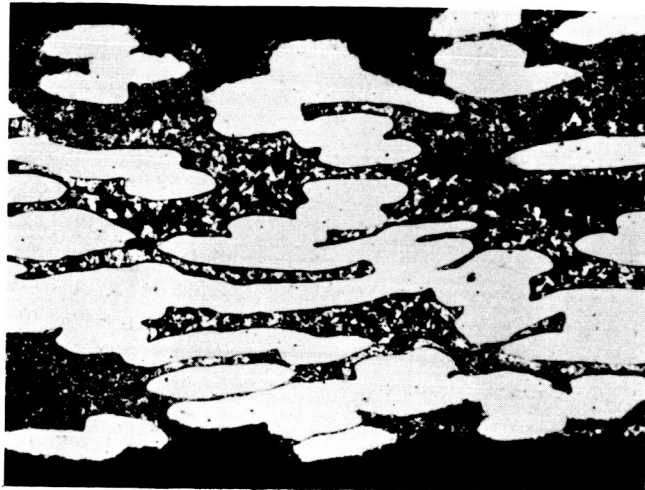
None of these electrodes had a coulombic capacity which was significantly improved over commercial electrodes. Therefore, physical impregnation procedures were considered to try to impregnate enough material into the electrodes to show an improved capacity. Results of physical impregnation work is detailed in the last few sections of this Task.

The four electrodes of Table 16 were sectioned and examined microscopically after the cycling experiments and after charging the electrodes so the cadmium metal could be more easily seen. Figure 50 contains photomicrographs of the four cross sections. The large white areas are sections through wires of the electroformed screens. Because the structure was semirandom and the wires were cut at different angles, the wire sections are not the same size and shape. Figure 37 is a surface view of a similar electrode showing the square hole in each screen layer. Notice in Figure 50 that the small white spots of cadmium metal are larger in the centers than at the surface. The cadmium powder appears similar in size to the physically impregnated cadmium powder shown in Figure 58, shown near the end of this Task.

A comparison of cadmium powder sizes in the four electrodes shown in Figure 50, when compared with discharge efficiencies in Table 16, shows that Electrodes 15A and 16B had larger particles of cadmium in the pores as well as higher discharge efficiencies than Electrode 15B. Electrode 16A had the highest efficiency but is not considered to be comparable because of a mechanical separation near the center of the electrode. The location of the largest particles in the center of the other electrodes suggests further that the large cadmium powder is formed at low current densities whereas small particles are formed at the high current densities at the outer surfaces.

Modified Fleischer Method. The sintered powder plaques and the first experimental screens were impregnated by the same procedures, yet they appeared different. The screens had a dark metallic-looking, spotty coating that the sintered powder plaques did not have. This spotty coating was not brushed off during the usual brushing for both sintered powder and screen plaques. Too high a polarizing current could have reduced the cadmium hydroxide to metal. Lower currents were evaluated for polarizing the electrode during the precipitation of cadmium hydroxide by the reaction of cadmium

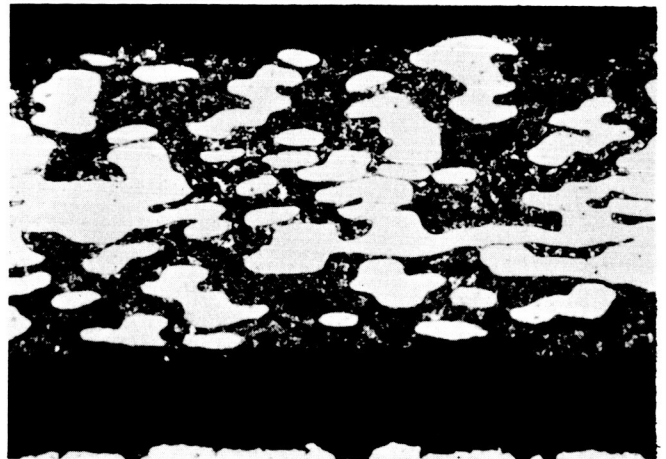




500X

Electrode 15A

N17381



500X

Electrode 15B

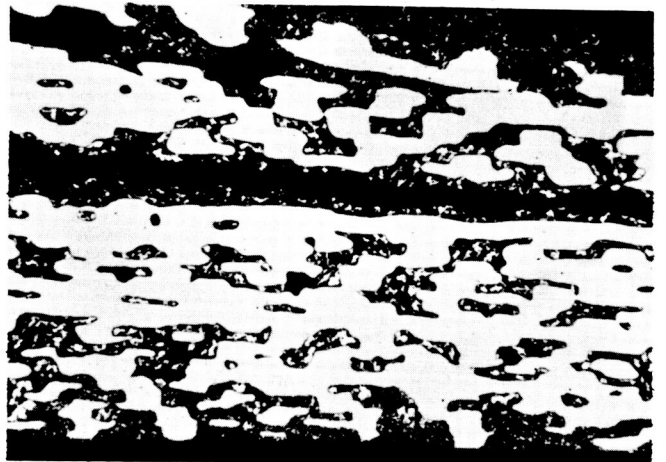
N17382



500X

Electrode 16A

N17383



Electrode 16B

N17384

FIGURE 50. CROSS SECTIONS OF SEMIRANDOM POROUS ELECTRODES 15A, 15B, 16A, AND 16B IN CHARGED CONDITION

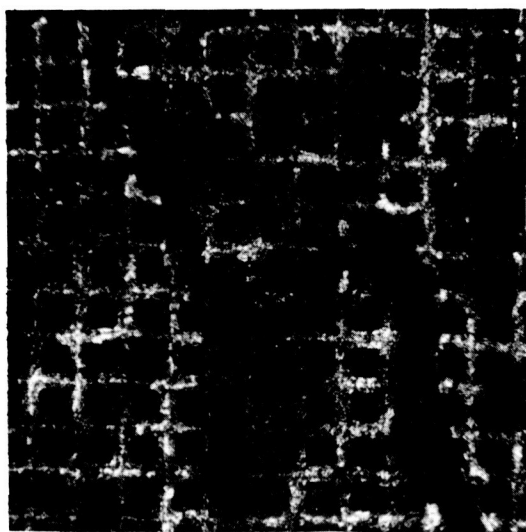
nitrate in the pores with potassium hydroxide. Prior to these experiments all electrodes were polarized for 20 minutes at a current of  $155 \text{ ma/cm}^2$  of surface. Currents were reduced proportionally to the electrode volume. If Fleischer used a 180-mil-thick plaque and the experimental electrode was 3 mils thick, the current used was  $3/180 \times 155$ , or 2.5 ma.

Two screen electrodes, the first trial run of superimposed and bonded electroformed screens, were used in this test. Although the screen alignments were not considered good enough for meaningful electrochemical evaluation, they were good enough for checking impregnation and polarization conditions. The two screens, 500 and 1000 mesh, were chemically impregnated four times and checked for capacity. About 20 percent of the theoretical capacity was available directly after the last polarizing steps, before the electrodes were charged. Obviously the polarization had reduced some of the hydroxide to cadmium. The electrodes subsequently were charged and discharged three times. Efficiencies are shown in Table 17.

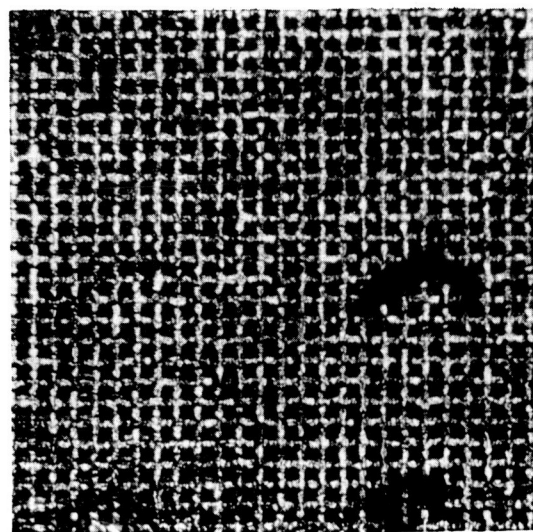
TABLE 17. DISCHARGE EFFICIENCY FOR FOUR-CYCLE IMPREGNATION

Mesh Size of Screen Electrode	Efficiency		
	Cycle 1	Cycle 2	Cycle 3
500	66	56	51
1000	60	54	50

Frequent microscopic examinations at 14 to 120 magnifications were made of screen electrodes during impregnation steps, and after charging or discharging. Chemical impregnation of screen electrodes followed by electrolytic polarization to precipitate  $\text{Cd}(\text{OH})_2$  left a dark-gray material on the surface, often covering many of the pores. Figure 51 shows two photomicrographs of typical surfaces. These areas seemed to be



120X 500 Lines/Inch Electrode Number 23A



80X 750 Lines/Inch Electrode Number 26

FIGURE 51. SURFACE VIEW OF SCREEN ELECTRODES AFTER CONVENTIONAL CHEMICAL IMPREGNATION SHOWING INACTIVE SURFACE DEPOSITS

associated with droplets of cadmium nitrate solution or crystals of salts adhering to the surface prior to the reaction with KOH. Salt crystals were formed in the cadmium nitrate solution during impregnation when the solution was cooled by evaporation of water in the vacuum chamber. The precipitate so formed coated the surface and was reduced by the polarizing current. Once this external material had been formed, no change was seen in it after subsequent charging or discharging steps.

### The Effect of Additives in the Impregnation Solutions

Wetting Agents. During the early attempts to chemically impregnate screen electrodes using the procedure published by Fleischer, visual examination showed that some of the pores were empty while others appeared completely filled with material, at least at the surface. This condition was most noticeable after the first impregnation step. Additional impregnations filled more but not all of the empty pores. Obviously these pores were never filled with cadmium nitrate solution, even though a vacuum was applied during the impregnation. Nonwetting of the nickel by the cadmium nitrate solution was suspected as part of the reason for nonuniform filling of holes.

A wetting agent\* known to be stable and active in concentrated salt solutions was added to lower the surface tension of the cadmium nitrate solution from 80 to 40 dynes per centimeter. Impregnation with this modified solution aided in filling more of the holes during the first impregnation. However, cleaning of the electrodes prior to impregnation in a commercial electrocleaner\*\* followed by an acid dip (3N HCl) to remove any alkali and to condition the nickel to be wet by water followed by vacuum impregnations gave more uniformly filled pores. Therefore, the use of wetting agents was abandoned in favor of careful cleaning of the electrodes before impregnation. Vacuum drying of impregnated electrodes was adopted instead of heating in a hot-air furnace because the vacuum drying was less likely to oxidize or deposit carbon dioxide in the electrode.

Barium Hydroxide. The effect of carbonate contamination on the specific volume of the reaction product of  $\text{Cd}(\text{NO}_3)_2 + (\text{KOH} + \text{K}_2\text{CO}_3)$  is described in the recent literature by E. J. Casey.\*\*\* He showed that increasing the carbonate content of KOH used for precipitation of cadmium hydroxide doubled the precipitate volume when the carbonate increased from 1.5 to 10 weight percent. Because reagent-grade potassium hydroxide normally contains about 1 percent potassium carbonate as an impurity, it was thought that without the 1 percent carbonate impurity, impregnation weight pickup might be increased through the formation of a more dense cadmium hydroxide precipitate. For this reason, barium hydroxide was added to 25 percent potassium hydroxide with a slight excess (about 1 g/l) to precipitate the carbonate impurity. This purified solution was used for impregnation of screen plaques. No significant difference was seen in the weight of material impregnated in porous screen electrodes with this quantitative removal of carbonate.

Impregnation of screen and precipitation of  $\text{Cd}(\text{OH})_2$  in KOH-containing solutions apparently left some carbonate in the electrode. Late in the experimental program,

\*RC-98, Fluorochemical sold by 3M Company.

\*\*Enthone Cleaner Number 160 used as recommended for cleaning nickel.

\*\*\*Casey, E. J., Dubois, A. R., Lake, P. E., and Moroz, W. J., J. Electrochem. Soc., 112, 374-375 (1965).

after all of the impregnation studies had been completed, and when electrodes were charged and discharged in electrolyte containing barium hydroxide, needlelike crystals appeared on the surface. Examination of the surface with needles by X-ray diffraction showed cadmium hydroxide and barium carbonate when the electrode was in a discharged condition. Cadmium, cadmium hydroxide, and barium carbonate were identified when the electrode was in a charged condition. Figure 52 shows some of the needles on the surface of an electrode.

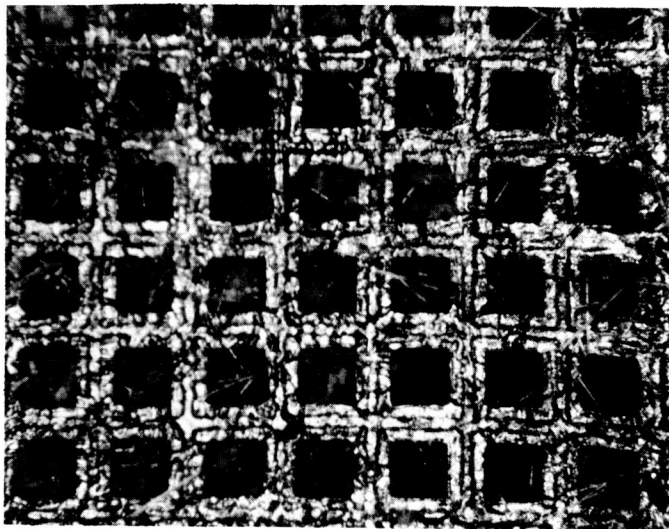


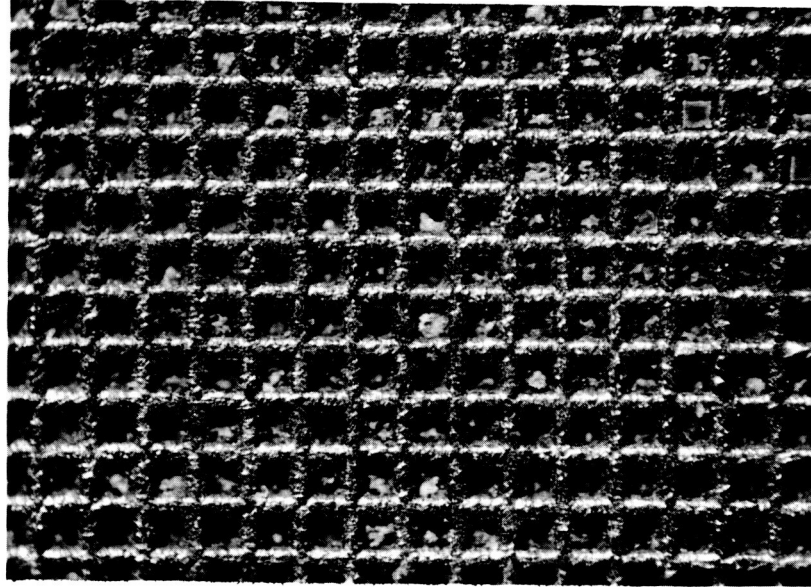
FIGURE 52. PHOTOMICROGRAPH OF ELECTRODE 31 AFTER IMPREGNATION AND CHARGING AND DISCHARGING SHOWING NEEDLES ON SURFACE

120X

During electrolytic cycling of screen electrodes in a carbonate-containing electrolyte, the following changes were observed in the pores: (1) During the first charging a shrinkage of the active material into the pore was seen with a change from white to light gray. (2) Discharging changed the color from light gray to dark gray. (3) Shrinkage of the active material into the pores was observed to take place when the electrodes lost capacity.

Passivation of Nickel. Screen electrodes frequently had no cadmium material contacting the surface layers of nickel screens after several charge-discharge cycles. Exposed nickel on the surface changed from a white color to a yellow. Judging by the color change, the nickel at the surface had oxidized and was no longer active. Two electrodes were compared under similar conditions. Both were cleaned to remove oxides from the surface and one was cadmium plated. Two impregnation cycles in aqueous  $\text{CdNO}_3$  solution were used to impregnate both electrodes. Figures 53 and 54 are photomicrographs of these two electrodes, after several charge-discharge cycles of the unplated and cadmium plated electrodes respectively.

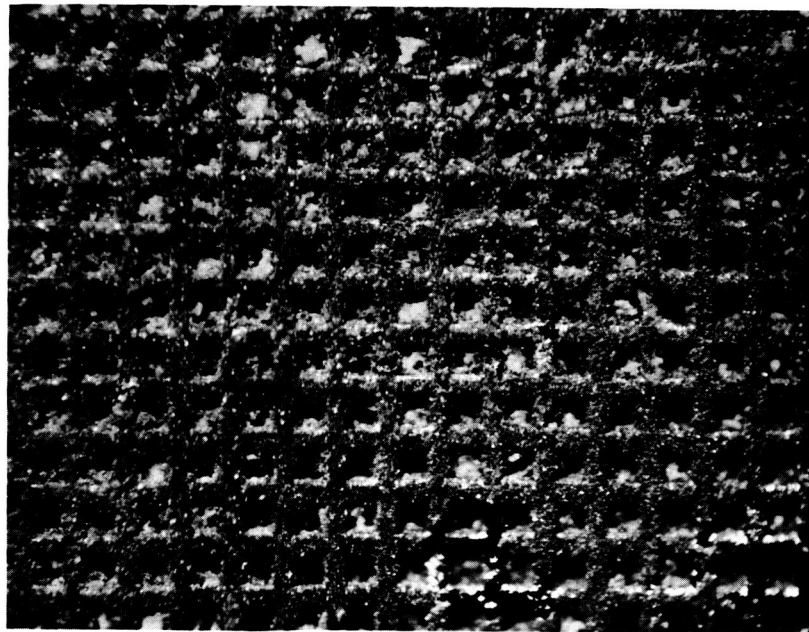
The surface of the electrode in Figure 53 was lustrous and a light yellow color typical of a light tarnish on nickel. The surface on the electrode in Figure 54 was coated with a dark crystalline material which was light gray when charged and dark gray when discharged. Two spots on the electrode area seen in Figure 54 have exposed nickel. These spots appeared after the fourth discharge.



60X

N22315

FIGURE 53. SURFACE VIEW OF SCREEN ELECTRODE NUMBER 37 AFTER SEVERAL CHARGE-DISCHARGE CYCLES SHOWING BARE NICKEL EXPOSED ON OUTSIDE SCREEN



60X

N22314

Bare Spot

Bare spot

FIGURE 54. SURFACE VIEW OF CADMIUM-PLATED SCREEN ELECTRODE NUMBER 24 AFTER SEVERAL CHARGE-DISCHARGE CYCLES SHOWING COVERAGE OF SCREEN WITH CADMIUM MATERIAL

Note two bare nickel spots along bottom edge.

To confirm the passivity of the nickel surface, an electrode similar to the one shown in Figure 53 was reimpregnated and charged. None of the white  $\text{Cd}(\text{OH})_2$  which coated the surface during impregnation appeared to be reduced in place, on the nickel surface, but disappeared, probably to inside the pores because there was no residue in the beaker.

Multiple Impregnations. In view of the nonuniform impregnation described above, the procedures for cleaning electrodes were selected so that material could be put in all the pores. At the same time, it had been noted that four cycles did not impregnate the screen electrodes with enough material to show an improvement in coulombic capacity over commercial electrodes. The low porosity, 60 percent, of the screens required that more material would be needed because 60 percent porous electrodes have twice as much metal in them as 80 percent porous electrodes. It was recognized also that up to eight chemical impregnation cycles might be required to compensate for porosity values. Table 18 shows results with stacked screens selected from those described in Table 7 after eight impregnation cycles. After the weight measurements of the eighth impregnation, the electrodes were charged at a current density of  $4.8 \text{ ma/cm}^2$  and then discharged at  $9.6 \text{ ma/cm}^2$ . Perhaps a significant result to glean from Table 18 is the apparent fact that pores might be filled up to about 70 percent of their void space without affecting efficiency. Comparison of Specimens 31 and 34 with Specimen 24, for example, shows relatively high efficiency can be obtained with pores highly filled.

To see whether the overall low efficiencies of Table 18 might be associated with the more than four standard chemical impregnations, commercial electrodes were evaluated with extra chemical impregnations.

#### Effect of Multiple Chemical Impregnations of Sintered Powder Plaques on Energy Output

Commercial-battery plaques were used to determine the effect of additional chemical impregnations on discharge capacity. The plaques used initially had 44.7 percent of their pore volumes filled with cadmium hydroxide by the manufacturer. They are believed to have had four impregnation cycles prior to assembly in the battery. These plaques were then given 0, 1, 2, and 3 additional chemical impregnation cycles. The charging current density used was  $4.8 \text{ ma/cm}^2$  and the input time was adjusted to give the theoretical capacity of the plaques. All plaques were then discharged at a current density of  $9.6 \text{ ma/cm}^2$  until a potential decrease of 0.1 volt from open-circuit voltage was reached. After an electrochemical evaluation of energy output, each sample was given one additional chemical impregnation and retested. The percentage of the pore volumes filled with cadmium hydroxide was calculated from the weight gains after each additional impregnation. The experimental results are given in Table 19.

Comparison of efficiencies for commercial electrodes in Table 19 with the efficiencies for screen electrodes in Table 18 shows the greater efficiencies for the commercial electrodes. Table 19 also suggests a trend of increasing efficiency with increased impregnation. However, if exception is made to the two blanks, Samples S-4 and S-5, there seems to be little effect of increased percent of pore volume filled upon the discharge efficiency. The practical importance of this finding is that cadmium electrodes could be more completely filled with no adverse effect on electrode efficiency, at least up to 55 percent of pore volume compared with commercial practice of about 40 percent.

TABLE 18. DISCHARGE DATA FOR SCREEN ELECTRODES CHEMICALLY IMPREGNATED EIGHT TIMES

Specimen	Screen Mesh, lines/inch	Thickness, mils	Porosity, percent	Weight of Impregnated Cadmium, mg	Pore Volume Filled, percent	Discharge, ma-hr	Discharge Efficiency, percent
23B	250	5.0	59	15.8	65.3	3.2	42.8
30	250	9.1	59	26.6	69.7	6.1	48.3
31	250	18.0	60.5	59.4	69.5	15.6	55.1
24	250	33.0	60	109.5	59.0	30.9	59.3
27	500	17.4	60	61.4	63.0	16.0	55.0
34	1000	7.6	65.5	28.1	68.3	6.7	59.9

TABLE 19. ENERGY OUTPUT AS A FUNCTION OF PERCENTAGE OF PORE VOLUME FILLED WITH  $\text{Cd}(\text{OH})_2$  FOR COMMERCIAL ELECTRODES

Specimen	Number of Additional Impregnations	Estimated Total Impregnations	Pore Volume Filled, percent	Efficiency, percent	Watt-Hours/Pound
S-4	0	4	44.7	73.2	69.5
S-5	0	4	44.7	74.4	70.8
S-3	1	5	50.0	80.3	80.4
S-1	2	6	50.6	88.5	89.1
S-2	3	7	54.8	81.2	85.0
S-4	1	5	49.8	77.7	79.5
S-3	2	6	54.2	78.3	82.5
S-1	3	7	54.3	82.4	84.6
S-2	4	8	55.0	77.7	81.3

The greater efficiency with powder plaques is attributed to the effect of geometry on the impregnation process rather than the effect of geometry on the discharge process. This interpretation follows because elemental cadmium build-up can be associated with discharge inefficiency, as described in the next section. The standard chemical impregnation process of sintered powder plaques yields cadmium hydroxide, which is the objective. The same impregnation process of stacked screens yields cadmium metal. Thus, referring again to Table 18, the screens with the longer pores or with the smaller diameter pores show the greater discharge efficiencies because they were impregnated with less inactive cadmium metal. This statement implies that more inactive cadmium was deposited in large and easily accessible pores where current densities were higher, during the polarization step of conventional impregnation.

#### Energy-Output Efficiencies

The discharge efficiencies in Table 18 are less than 60 percent for screen electrodes but in Table 19 are greater than 70 percent for sintered powder electrodes. The data seemed to show that impregnation was yielding cadmium metal in the screens but cadmium hydroxide in the powdered plaques. A part of the cadmium metal so deposited within the screens is not available for discharge. With these observations and ideas in mind, a material balance was determined for the above discharged screens.

Assuming  $\text{NaCN}$  dissolves  $\text{Cd}(\text{OH})_2$  without any attack on the nickel plaque or on the contained cadmium metal, it should be possible to determine the percentage of each contained material in the plaque. The distinction between metal and hydroxide is important because one can account for efficiency changes either by assuming cadmium metal build-up during discharge or by assuming cadmium hydroxide build-up during charge. Table 20 shows results with two of the plaques from Table 18.



TABLE 20. MATERIAL BALANCE OF DISCHARGED-SCREEN ELECTRODES

How Obtained	Item		Screens, lines/inch:		
			250	1000	
			Specimen:	23B	34
Observed	1	Final Plate Weight After Discharge, mg	58.7	82.4	
Observed	2	Initial Plaque Weight, mg	40.7	50.3	
1 - 2 =	3	Final Weight of Contained Materials, mg	18.0	32.1	
Observed	4	Experimental Ma-Min Discharge Capacity	194	402	
Calculated from 4 =	5	Weight of Cd(OH) <sub>2</sub> Formed on Discharge, mg	8.72	18.25	
3 - 5 =	6	Calculated Cadmium Weight Remaining After Discharge, mg	9.18	13.85	
Observed	7	Weight of Material Stripped by NaCN [Probably Cd(OH) <sub>2</sub> ], mg	12.2	21.5	
7 - 5 =	8	Excess Weight Loss by NaCN Strip	3.38	3.25	
3 - 7 =	9	Weight of Material Remaining (Probably Cadmium Metal), mg	5.8	10.6	

In Table 20, Item 2 is the weight of starting electrodes before the eight impregnation steps. Item 4 is the ma-min discharge capacity observed and used for calculating the discharge efficiencies in Table 18. Item 1 is the dry weight after the discharge in Item 4. Item 3 is the numerical difference between Items 1 and 2, so that Item 3 contains cadmium and cadmium hydroxide, the proportions of which are unknown.

From Item 4, one can calculate the minimum amount of cadmium hydroxide using Faraday's law, as was done for Item 5. The difference between Items 3 and 5 is, therefore, the weight of unidentified material, either Cd or Cd(OH)<sub>2</sub>, as given by Item 6. Item 7 shows the observed weight losses by a sodium cyanide leach. Notice that the weight losses of Item 7 are a little larger than the expected weight losses based on Item 5, as shown in Item 8. The important point is that Item 9, which is presumed to be cadmium metal, accounts for the majority of unidentified weight of Item 6. This is the important point because Item 9 implies that a substantial amount of cadmium metal remains in the electrodes after complete discharge.

Further work confirmed cadmium build-up as the cause of the observed low discharge efficiencies with Specimen 23B. After the NaCN strip, Item 7 of Table 21, the electrode was discharged without prior charging. The material undissolved by the NaCN yielded an additional 77 ma-min of discharge capacity. Based on the 5.8 mg of Cd metal, Item 9, discharge efficiency was about 46 percent, in good agreement with the original efficiency of about 43 percent. It is apparent that the Cd(OH)<sub>2</sub> stripped by the NaCN solution was "insulating" the cadmium metal thus preventing further discharge capacity.

TABLE 21. ACTIVATION OF A FUSED-SALT IMPREGNATION FOR ELECTRODE 38

Cycle	Charging Time at 9.65 ma, minutes, seconds	Volts at End of Charging	Discharging Time at 19.3 ma, minutes, seconds	Efficiencies		
				Input to -1.26 Volts vs SCE, percent of theoretical	Output, percent of actual input	Output, percent of theoretical
1	12, 0	1.31	4, 5	8.5	67.2	23.0
2	9, 0	1.26	4, 20	25.4	96.2	24.4
3	8, 30	1.26	4, 20	24.8	101.9	24.4
4	9, 26	1.26	4, 30	26.6	95.5	25.3
5	18, 0	1.34	7, 6	27.0	78.9	39.9
6	14, 11	1.26	6, 56	40.0	97.8	39.0
7	40	1.375	11, 52	39.9	--	66.7(a)
8	23	1.26	11, 23	65.0	98.9	64.0
9	40	1.40	12, 37	63.8	--	71.1(a)
10	40	1.41	12, 38	68.0	--	71.1(a)
11	40	1.42	12, 28	68.2	--	70.0(a)
12	40	1.43	12, 11	67.5	--	68.5(a)
13	15 hours (0.50 ma)	1.325	11, 46	--	--	66.0(a)
14	40 minutes	1.45	11, 11	65.0	--	62.7(a)
15	40	1.46	11, 5	60.6	--	62.4(a)
16	40	1.46	10, 58	57.5	--	61.8(a)

(a) Actual input equals theoretical input.

The eight impregnation steps had filled much more of the pore volume than could be done by four cycles. However, capacity per pound was still less than for commercial electrodes. Research efforts were then directed toward improving the utilization efficiency of the cadmium compound as impregnated into the pores.

#### Polarizing With Controlled Potential

In carrying out the above experiments, a four-step chemical impregnation of Screen Electrode 30 was done without using a polarizing current and in a 70 to 80 F, 25 percent KOH solution. The percent of pore volume filled was 35.9. By comparison, Screen Electrode 31 had 41.8 percent of the pore volume filled with 8 ma of polarizing current used in a 180-190 F, 25 percent KOH solution. Electrode 30 (no current) had an open circuit voltage of about -0.6 volt vs saturated calomel electrode, which is similar to that of nickel. By contrast, Electrode 31 (polarized) had a voltage of -1.125 vs SCE, or a normal cadmium voltage. No material was exuded from Electrode 30. Fleischer reported that if current was not used, "loss of metal hydroxide will occur by exudation". Possibly the thin screen electrode (9.1 mils) would not show this action as easily as Fleischer's >150-mil-thick electrode.

Impregnation of electrodes without producing metallic cadmium was encouraging because the work with physical impregnation and with eight chemical impregnations had shown that cadmium metal produced by high-current-density deposition could be unavailable for electrochemical discharging.

Very low polarizing currents were evaluated in 70 to 80 F, 25 percent KOH while electrode potentials were measured vs SCE. Currents from 0.6 to 0.8 ma for the 1 x 1-cm electrode were used. Voltages started at about zero, rose slowly to more negative values, showed a voltage plateau at about -0.6 to -0.8 volt then rose to -1.0 volt where the current was turned off. This technique prevented formation of cadmium metal. However, only about 30 percent of the pore volume was filled by four chemical impregnations. Apparently, the reason much higher impregnation percentages were obtained

before was that in each polarizing step most of the  $\text{Cd}(\text{OH})_2$  was reduced to metal which occupied much less volume and did not significantly plug the pores.

### Fused-Salt Impregnation

Impregnation with molten  $\text{Cd}(\text{NO}_3)_2 \cdot 4\text{H}_2\text{O}$  was used for filling screen electrode pores with the low-current-density limited potential polarization. The same limiting percent of pores filled was seen with the fused salts as with the aqueous solution. About 20 to 28 percent was the maximum filled with one cycle. However, with the fused salts, only two cycles were needed for electrodes with pores from 0.8 to 3.2 mils wide to achieve about 40 percent of voids filled.

Figure 55 is a surface view of an impregnated screen plaque. Additional impregnation steps did not increase the plaque weight when conventional vacuum impregnation was used; namely about 40 percent of voids filled. Moreover, the impregnated product was an impervious and hard product that required activation, as illustrated by the results shown in Table 21 for Electrode 38.

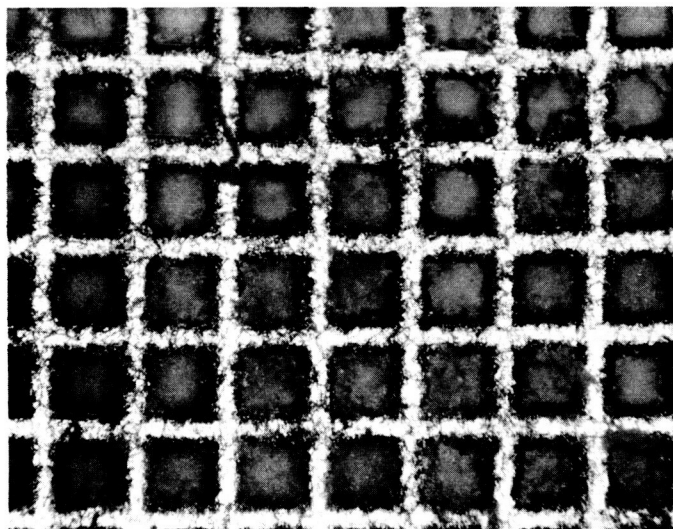


FIGURE 55. SURFACE VIEW OF SCREEN ELECTRODE 45 WITH 3.2-MIL HOLES AFTER IMPREGNATION WITH 22 PERCENT OF PORE VOLUME FILLED, TEST 106

120X

Electrode 38 is a 250-line/inch stack with a keyed opening whose physical dimensions are given in Table 7 and constructed as described in Table 6. It was impregnated for three cycles from aqueous solution followed by four cycles from the fused cadmium hydrate using the procedure as described in the preceding paragraph. After seven impregnation cycles, the pores were only 40.3 percent filled, as follows:

<u>Cycle</u>	<u>Impregnation Solution</u>	<u>Voids Filled, %</u>	<u>Cumulative Pore Volume Filled, %</u>
1	Aqueous	4.4	4.4
2	"	4.9	9.3
3	"	5.7	15.0
4	Fused nitrate	10.9	25.9
5	Ditto	5.7	31.6
6	"	5.6	37.2
7	"	3.1	40.3

When through, the appearance of Electrode 38 was similar to that shown in Figure 55 for Electrode 45.

The above impregnation results are significant because they show clearly that impregnation of stacked screens is quite different from impregnation of sintered powders. For example, the first three cycles tabulated above averaged about 5 percent per cycle with 15 percent of voids filled after three cycles. By way of contrast, the first three cycles in Figure 48 averaged about 10 percent per cycle with 30 percent of voids filled after three cycles.

The last four cycles in the above tabulation show fused-salt impregnation to be more effective than the aqueous impregnation procedure. But after seven cycles, the electrode is seen to be only about 40 percent filled and additional cycles after Number 4 filled smaller percentages with each cycle.

Even worse, the cadmium hydroxide resulting from the above seven impregnations cycles required the activation shown in the last columns of Table 21. Notice how efficiency, on a theoretical basis, continuously increased up to Cycles 9 and 10. Beyond Cycle 10, efficiency decreased with further cycles. These changes obviously complicate the experimental program but they also illustrate why much of the literature on nickel-cadmium batteries is difficult to intracompare.

Several additional points of practical importance may be deduced from Table 21. First, notice how Cycle 1 has a low efficiency, only 23 percent of the output predicted on the basis of the 15.6 mg of  $\text{Cd}(\text{OH})_2$  in the electrode. The input efficiency to hydrogen evolution was only 8.5 percent. These low efficiencies on first cycle show that the voids were 40.3 percent filled with a cadmium hydroxide that was not easily reduced to metal. The low electrochemical efficiencies combined with the low efficiency of impregnation are clear reasons why modified impregnation procedures had to be developed and used.

Second, notice in Cycles 2, 3, 4, 6, and 8 of Table 21 that when charging was limited to the first point of hydrogen evolution, then output was about equal to input. When charging was continued beyond hydrogen evolution, then additional output capacity was obtained. (Cycle 14 was a single exception following an overnight charging.)

Figure 56 is a plot of the efficiencies from Table 21 to illustrate how input and output coulombs are related to each other and related to the state of activation of the impregnated  $\text{Cd}(\text{OH})_2$ . Notice again how Cycles 2, 3, 4, 6, and 8 had slightly higher input efficiencies than output efficiencies. All the other cycles (excepting Cycle 14 again) had higher output efficiencies than input efficiencies. All the other cycles (but including Cycle 14) had charging beyond the point of hydrogen evolution. The significance of these facts is twofold. First of all, some reduction of  $\text{Cd}(\text{OH})_2$  must continue after the start of hydrogen evolution. Second, any input up to hydrogen evolution is fully recovered on discharge. This latter finding implies that the "depth of discharge" parameter, mentioned in the contract for Item F, will have significance only when cycling is involved or when input exceeds the hydrogen evolution reaction.

Another item of importance to be deduced from Figure 56 is associated with the relatively large activations occurring on Cycles 1, 5, and 7. These are the cycles shown in Table 21 to have been charged to greater than -1.3 versus SCE. The cycles following 1, 5, and 7, namely Cycles 2, 3, and 4 after 1, Cycle 6 after 5, and Cycle 8 after 7, were limited in charging to -1.26 versus SCE. These intervening cycles provided no additional activation of the cadmium hydroxide. This result suggests that cycling of a sealed battery will not increase the active capacity at the negative electrode

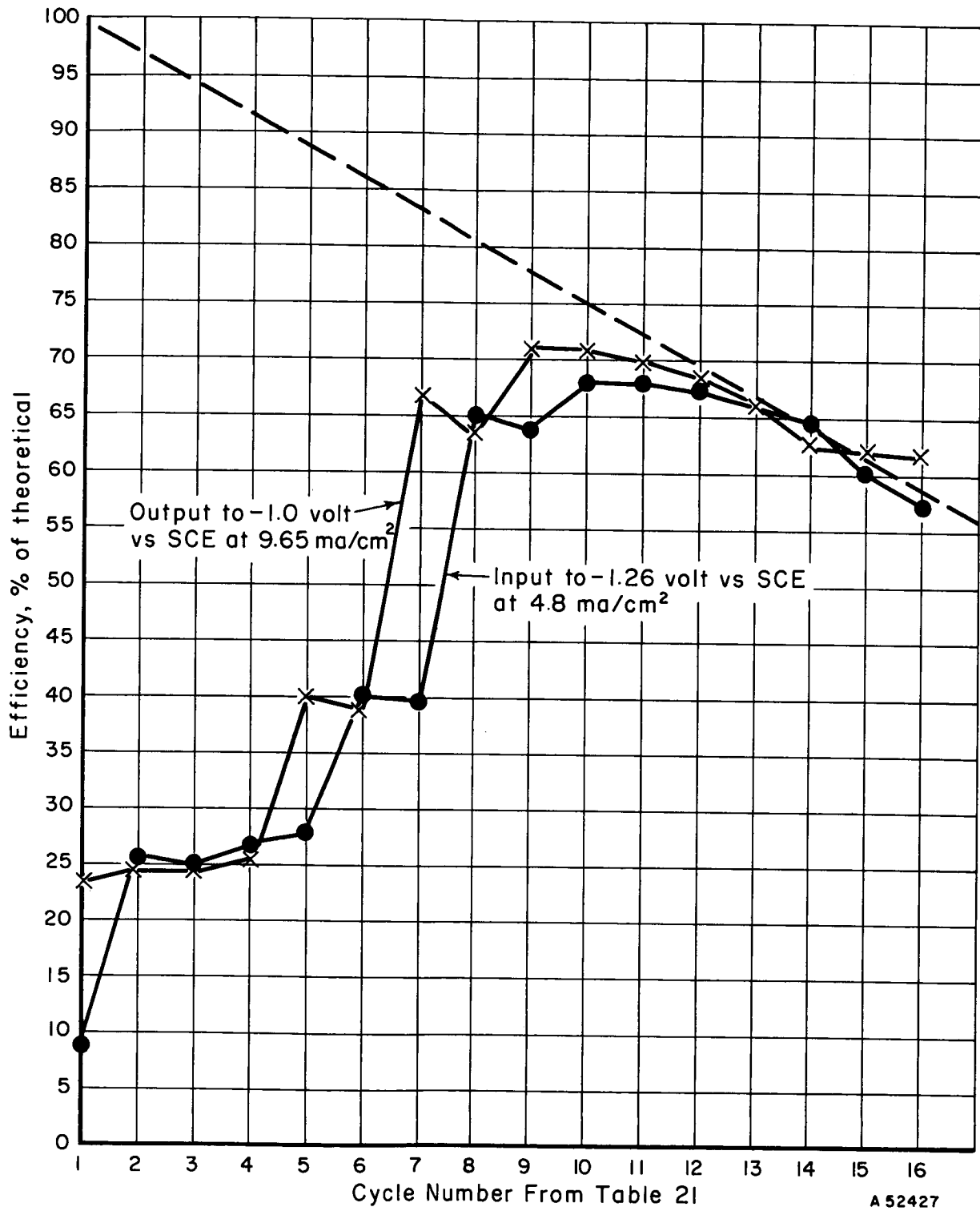


FIGURE 56. RELATIONSHIP OF INPUT AND OUTPUT CAPACITIES AS THE CADMIUM HYDROXIDE IS ACTIVATED

because the point of hydrogen evolution is seldom reached in the unbalanced electrode combination.

Finally, the overnight charging at low current density, Cycle 13 in Table 21 and in Figure 56, had no apparent advantage. This is important because there are suggestions in the literature\* that a slow trickle charging will reactivate an electrode. If true, these suggestions must have referred to the positive electrode rather than negative cadmium electrode.

The dotted line at the top of Figure 56 is a highly speculative extrapolation of the last 4 or 5 cycles back to the 100 percent efficiency at Cycle 1. This questionable procedure suggests a loss of 2 to 3 percent in both charging and discharging efficiency with each cycle to maximum depth each way. The extrapolation seems to be consistent with cycle life data described by Francis\*\* for sealed nickel-cadmium batteries. Thus, the cycle life data reported by Francis show the "cycle to failure" falling approximately exponentially with "depth of discharge, percent of capacity". Extrapolation of that published data to 100 percent of battery capacity would indicate failures at about 40 cycles. Further extrapolation to 100 percent of the negative electrode capacity (as is the case for Figure 56) indicates failure at about 14 cycles. Since "failure" was defined by Francis to be the cycle where one-half the batteries had lost their ability to deliver the required current for the entire 35-minute discharge time, the losses of efficiency in Figure 56 would lead to "failure" as just defined. The theoretical discharge time for Figure 56 was about 18 minutes at 19.3 milliamperes. There is, thus, qualitative and suggestive agreement between the results in Figure 56 and the results reported by Francis for commercial sealed batteries. At least the comparison helps to emphasize the severe test to which the experimental electrodes were subjected.

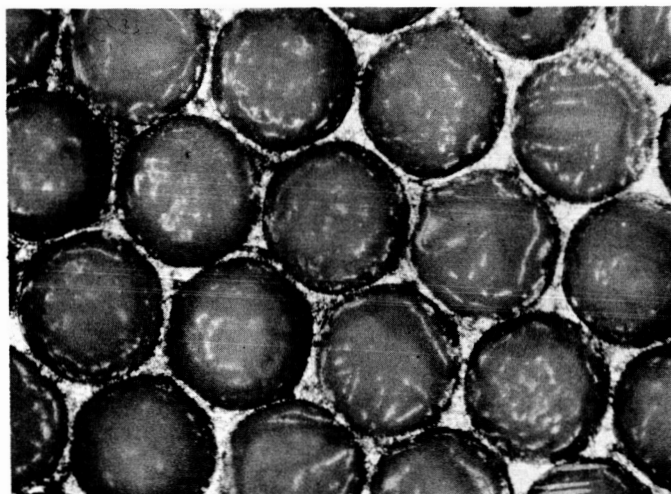
In view of the above results, a modified procedure was developed which did allow more efficient impregnation with a porous form. Crystals of cadmium nitrate and dry electrode were placed in a glass tube and a vacuum of 27 inches of mercury was maintained for about 15 to 20 minutes. The tube then was heated to melt the crystals while maintaining the vacuum for at least another 15 minutes. Bubbles escaped from the electrode during this time and this step was continued until bubbling essentially stopped. Then air was allowed to enter the glass tube. The screen electrode was soaked in the molten salts under atmospheric pressure for another 15 minutes before removing the electrode from the glass tube. After the first impregnation step, the electrode was placed on a filter paper kept hot on an electric hotplate. Both sides were blotted to remove part of the molten salts from the electrode. The remaining cadmium nitrate located in the middle of the pores was precipitated as the hydroxide in hot potassium hydroxide solution. The hydroxide was held in a test tube with a stopper to minimize pickup of CO<sub>2</sub> from the atmosphere. A second cycle filled the pore to the surface of the electrode. At least 2 hours' reaction time, at 160 to 180 F in 25 percent potassium hydroxide, was needed to convert the cadmium hydroxide from a hard precipitate to a soft white powder. Electrodes which contained the powder form of cadmium hydroxide had a negative potential (about -0.6 to -0.8 volt vs SCE), before charging, the same as electrodes impregnated by the cathodic polarization technique. Electrodes which did not receive either cathodic polarization or the 2-hour reaction time in potassium hydroxide had a potential about 3/4 volt less negative, versus a cadmium potential, or -0.2 volt vs SCE. Finally, the molten cadmium nitrate left in the tube was cooled and

\*Koren, H. W., and Baumstork, G., Sonotone Corp., "Electric Storage Battery", U. S. Patent 2,696,515 (Dec. 7, 1954).

\*\*Francis, Howard T., Space Battery Hand Book, Armour Research Foundation of Illinois Institute of Technology, p 36, April 15, 1963.

seeded to crystallize the salt before the next impregnation step. If the molten cadmium nitrate were left in the tube as a supersaturated solution, during the next impregnation step, the electrode would be wet and the surface tension of the liquid would prevent extraction of the air in the pores of the electrode.

Electrodes 10 mils thick with 6-mil holes were impregnated to 38 percent by this fused salt method with two cycles. After four cycles the percent pore volume filled approached 50 percent. Figure 57 shows a surface view of a screen electrode after two impregnation cycles, using the modified technique just described. All the data in Task F and in Table 30 used the fused salt impregnation procedure just described because filling of voids was effective and the material impregnated had a reasonable activity with first cycle.



100X

FIGURE 57. SURFACE VIEW OF SCREEN ELECTRODE WITH 6-MIL HOLES AFTER IMPREGNATION WITH 38 PERCENT OF PORE VOLUME FILLED

#### Step 4B - Weight Gains and Amp-Minute Capacity for Physical Impregnation of Screen Electrodes

##### Physical Packing Materials

The plaque structure with straight-through holes made with stacked screens is more amenable to physical packing methods than is the structure of sintered nickel powder with random pores. Cadmium powders, cadmium oxide, and cadmium hydroxide were checked for bulk densities to determine whether enough of these materials could be packed in the pores to give sufficient capacity. Screen plaques were physically impregnated with cadmium oxide or cadmium metal powder but not cadmium hydroxide. The semirandom pore shape was used because plaques with superimposed holes were not available for this part of the experimental program. However, if the random pore shape can be impregnated, the straight-through pores should be at least as easy to impregnate.

Cadmium Oxide. Reagent-grade cadmium oxide powder was slurried in water and filtered, and a bulk-density measurement was made of the filter cake. On a  $\text{Cd}(\text{OH})_2$  basis, the cake had a 48 percent density. Thus, if 83 percent of the pore volume of a plaque could be filled with this product, the impregnated plaque would have the capacity equivalent to that obtained with four cycles of the chemical-impregnation method.

One check was made with a semirandom-pore shape-stacked screen electrode with CdO forced into the pores as a slurry. On a  $\text{Cd}(\text{OH})_2$  basis, 37 percent of the pore volume was filled. Alternate charge and discharge of this electrode showed 53 percent of the cadmium material was electrically available. These results are encouraging for a first trial but the lead was not pursued with further work.

Cadmium Hydroxide. A freshly prepared cadmium hydroxide filter cake had the equivalent of 9 and 19 percent theoretical density for as-filtered and for filtered-and-compressed conditions, respectively. Physically filling the pores of a plaque with cadmium hydroxide is considered impractical because it is unlikely that enough active material could ever be packed into the pores to give capacity equal to that obtained with the chemical impregnation.

#### Physical Impregnation of Screen Electrodes With Cadmium Metal

Experimental screen electrodes were physically impregnated with cadmium by plating directly onto electrodes from a cadmium hydroxide slurry in 30 percent KOH solution. A current density of about  $24 \text{ ma/cm}^2$  was used until a spongy coating of cadmium was visible. Usually this required about 2 hours at ambient room temperature. Excess material was physically rubbed into the pores after plating. One such impregnation step gave a weight gain equivalent to having the pores 40 percent filled with  $\text{Cd}(\text{OH})_2$ . Four impregnation steps by the standard chemical impregnation procedures are required to yield the same percentage of filled pores.

Figure 58 shows a cross section of screens stacked by the spot-welding technique described in Task B. The white pattern in the figure is electroformed nickel screen. The darkest areas are unfilled voids. The lighter gray areas are the electrodeposited material that resulted from the physical impregnation procedure.

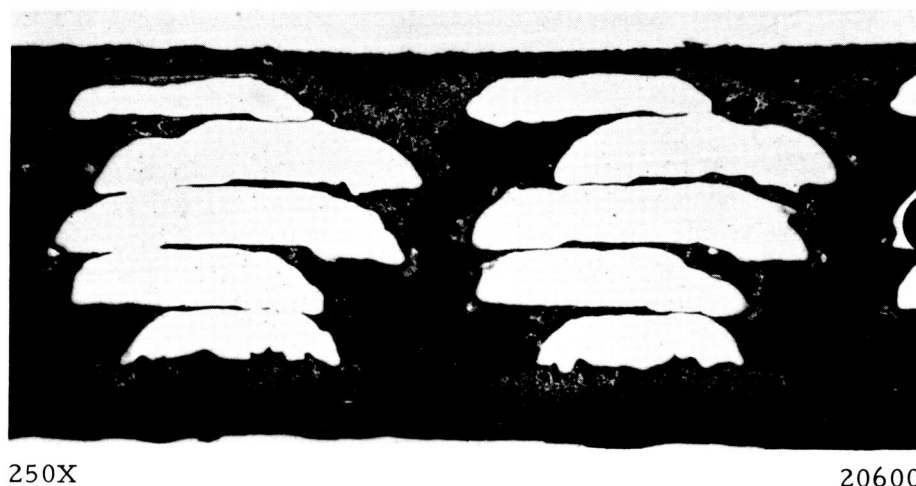


FIGURE 58. CROSS SECTION OF A PHYSICALLY IMPREGNATED STACKED-SCREEN ELECTRODE

Prior to photographing Figure 58, the excess material on the top side of the electrode was rubbed into the pores. The bottom side of the electrode was untouched in order to indicate the thickness of the cadmium plated. The figure shows that cadmium fills the top entrance to the pore, but also that cadmium was plated directly on the wires



within the pores. Since the quantity of cadmium plated on the surface was small compared with the pore volume, only a portion of the pore volume was filled. However, with sufficient cadmium plating on the surface and within the pores, the entire pore volume could be filled by this physical impregnation method because the pores are continuously straight through. This impregnation method would be unsuitable for the random-pore structure of powdered, sintered plaques, but might be desirable for straight-through pores because of its simplicity.

### Electrochemical Evaluation of Physical Impregnation

Following the encouraging weight gains obtained by the impregnation method just described, the next step was to evaluate the impregnated material to learn whether it was active. Early stacked screens, which were too thin for useful tests in Task F, were used for this evaluation of the new impregnations. Descriptive data are given in Table 22 and the following conditions were held constant for each experiment:

- (a) All electrodes were impregnated by plating from a slurry, as described in the previous section.
- (b) After impregnation, drying, and weighing, each electrode was charged at 2.4 ma/cm<sup>2</sup> to the hydrogen-evolution potential (Cycle 1 of the 250-mesh screen is a single exception as described later).
- (c) Discharge was at constant current at 9.6 ma/cm<sup>2</sup> to a voltage loss of about 0.1 volt from initial closed-circuit voltage.

TABLE 22. DESCRIPTIVE AND EXPERIMENTAL DATA FOR PHYSICALLY IMPREGNATED SCREEN ELECTRODES

	Screen Mesh, lines/inch		
	250	500	1000
Cycle 1 Efficiency, percent	56.5 (73) <sup>(a)</sup>	70.5	63.2
Cycle 2 Efficiency, percent	60.10	57.3	53.0
Cycle 3 Efficiency, percent	50.7	50.0	45.8
Thickness, mils	2.0	2.1	3.0
Porosity, percent	42.1	39.8	34.0
Pore Volume Filled With Cd, percent	27.1	20.7	19.7
Maximum Pore Volume Filled With ● Cd(OH) <sub>2</sub> , percent	63.8	48.7	46.3

(a) Estimated value.

The Cycle 1 discharge efficiency in the 250-mesh screen was made immediately after weighing the impregnated plaque without precharging. The apparent low efficiency value is evidence that the weighed material was partially oxidized. Therefore, all other discharge tests started after a charging step. The parenthetical value of 73 percent efficiency in Table 22 for Cycle 1 on the 250-mesh screen was estimated by ratioing Cycle 2 efficiency in the same proportion observed for Cycle 2 to Cycle 1 for the 500- and 1000-mesh screens. The significant points to be noted in connection with Table 22 are these:

- (1) All the observed efficiencies are low relative to what was expected on the basis of Table 30 which appears later in Task F. Therefore, standard chemical impregnation was tried in the same thin plaques,

as described in a prior section. The results in Table 22 show that metallic cadmium is not always actively accessible whereas Table 21 showed the same problem of activity would be encountered with cadmium hydroxide.

- (2) Discharge efficiency decreased with each cycle. This effect suggested the need for new electrodes for each experiment. Therefore, means to clean impregnated electrodes were sought so that the same electrodes might be used several times, as described in the next section.

#### Removal of Cd/Cd(OH)<sub>2</sub> From Screen Electrodes

Notice in Table 21 that capacity losses occurred during deep cycling of the electrode. This cycling effect means that duplicate data may require using duplicate electrodes.

Solutions were evaluated for stripping cadmium and cadmium hydroxide from the screen electrodes without significantly attacking the nickel structure. Chromic acid solution, 200 g/l CrO<sub>3</sub>, containing 10 cc H<sub>2</sub>SO<sub>4</sub>/l, removed cadmium from the negative electrode with no significant attack on the nickel structure. Chromic acid will dissolve both cadmium metal and cadmium hydroxide, so that the charge condition of the electrode is not important. Therefore, the active materials in a stacked-screen electrode can be stripped and the electrode can be reimpregnated for reuse.

#### Discussion of Physical Impregnation

Physical impregnation of screen electrodes was successful for impregnating more than the conventional equivalents of cadmium per unit of volume. However, the coulombic capacity seemed to be low. Efficiencies were 56.5 to 70.5 percent for the first cycle and dropped to about 50 percent by the third cycle. Two factors, not considered at the time, make the physical impregnation results more attractive now. The first was the high deposition current densities that formed the small cadmium powders discussed in connection with Figure 50. The second factor was carbonate pickup. Mechanically forcing the electrodeposited cadmium metal powder into the pores was done with the electrode still wet with 30 percent KOH. This technique was used because no washing would be required, saving considerable handling. However, these conditions were ideal for allowing pickup of carbonate from the atmosphere. The large amount of carbonate in the electrode pore could have caused the rapid loss of capacity during the three charge-discharge cycles.

Assuming that high efficiencies could be obtained by forming larger particles of cadmium powder at lower current densities and could be maintained during cycling in a carbonate-free electrolyte, the physical impregnation system could be a successful method.

#### Comparison of Energy Densities

Table 23 compares a commercial sintered nickel electrode with an experimental stacked screen electrode. The screen electrode had 6-mil pores and was 84 percent porous. The commercial electrode had random, interconnected pores and was about

78 percent porous. Equivalent densities were obtained on both electrodes when each was discharged at a 1/2-hour rate. Energy densities obtained in Table 15 were for a 1-1/2-hour discharge rate and are therefore greater than those reported in Table 23 within the 1/2-hour rate. Note the effect of discharge rate on the coulombic density of the commercial electrodes in Tables 15 (530 amp-min/in.<sup>3</sup>) and 23 (380 amp-min/in.<sup>3</sup>). The effect of rate will be discussed further in Task F. One important point here is that energy densities with the new fused-salt procedure compare favorably with the commercial procedure reported under Step 3.

TABLE 23. ENERGY DENSITY COMPARISON OF AN EXPERIMENTAL SCREEN ELECTRODE WITH A COMMERCIAL SINTERED NICKEL ELECTRODE

Electrode	Thickness, mils	Internal Surface Area, cm <sup>2</sup>	Geometric Area, in. <sup>2</sup>	Volume, in. <sup>3</sup>	Experimental Capacity, amp-min	Coulombic Density, $\frac{\text{amp-min}}{\text{in.}^3}$	Energy Density, $\frac{\text{watt-hr}}{\text{lb}}$
Commercial	36	150	0.155	0.00558	2.136	380	62
Experimental	10	2.5	0.155	0.00155	0.630	410	62

Thus, a procedure was devised for a two-step chemical impregnation of large-pore screen plaques which compares favorably with the four-step chemical impregnation described in the literature. A second important point is that two electrodes having widely different internal surface areas gave identical energy densities per unit of weight. This result implies that the fused-salt impregnation is satisfactory. Thus all results reported in Task F were obtained using the fused-salt impregnation method just described.

#### Location of Data

All experimental data in Task E is recorded in Battelle Laboratory Record Books Nos. 21516, 21685, and 21981, or on recorder charts filed with the detailed records of the project.

### TASK F - ELECTROCHEMICAL EVALUATION

#### Objectives

Task F of the contract reads as follows:

"Charge and discharge data shall be obtained on single- and multiple-screen electrodes to obtain the following:

"Item 1 - Energy Output

Energy output per weight and per unit volume of electrode as a function of current density, depth of discharge, pore size, pore shape and electrode thickness.

"Item 2 - Energy Input

Energy input required to charge electrodes as a function of their charging current density, depth of discharge, pore size, pore shape and electrode thickness."

The objective of Item 1 is to show the conditions for increased energy densities on a weight and volume basis.

The objective of Item 2 is to show the conditions for minimizing energy input.

Summary of Electrochemical Evaluations

Referring to the specific contract objectives, the results of this Task allow the following to be said about energy outputs and inputs as a function of current density, depth of discharge, pore size, pore shape, and electrode thickness:

- Increasing current density on any given electrode decreases both the input and output efficiencies.
- Current density and electrode thickness are related in that rate, or the time to charge or deliver capacity, must be considered for comparing electrodes with different thicknesses.
- Pore size and electrode thickness are related in that efficiency of charging and discharging increases as the ratio of thickness to pore size decreases. Thus thin electrodes with large pores are preferred over thick electrodes with small pores when compared at the same hourly rate of discharge.
- Depth of discharge seems to be less important than amount of over-charge, so far as cadmium utilization is concerned. When charging was equal to or less than that required to evolve hydrogen, then cycle losses of capacity were small and electrode efficiencies tended to stabilize at relatively low constant values with further cycling.
- Pore shapes, other than straight through, add to electrode weights with no apparent electrochemical advantage during the first few cycles.
- The work of the entire task showed that both output and input energies are changed or controlled by the same electrode variables. Energy densities will be improved by attaining high plaque porosities with thin electrodes having large and straight-through pores.

Preliminary work with commercial electrodes showed cadmium electrodes were the single biggest component of total cell weights. Cycling changes were observed that are only partially explained because reproducibility of data was achieved only part of the time.

Item 1 - Energy OutputRelationship of Commercial Batteries to Commercial Cells

To give perspective to future experimental results, it was necessary to relate plaque data to single-cell data and to battery data. This was necessary because new electrodes were evaluated under special laboratory conditions but their use must be projected for assembled cells and batteries.

The general scheme was to show relative scale-up factors in going from experimental plaques to single electrodes, then from single electrodes to sealed cells, and, finally, from sealed cells to a battery. The needed scale-up factors could not be found in a review of the open literature.

A sealed commercial battery with flat plates was purchased. It had a nominal capacity of about 1 ampere-hour and contained five cells per battery. Physical dimensions were measured on the battery and on individual cells taken from the battery. Results are shown in Table 24. In Table 24, height includes the distance from the bottom of the battery to the top of the terminals. Width was measured parallel to the flat plates. Thickness was measured perpendicular to the flat plates. Measurements on other cells from the battery showed less than 1 percent variation from the values given in Table 24.

TABLE 24. PHYSICAL DIMENSIONS OF A COMMERCIAL NICKEL-CADMIUM BATTERY TO BE USED FOR COMPARISON PURPOSES

<u>5-Cell Battery</u>	
Height, inches	3.08
Width, inches	1.81
Thickness, inches	2.08
Total Volume, cubic inches	11.6
Total Weight, grams	403.2
Weight of Case Materials, grams	155.6
Volume of Case Materials, cubic inches	2.22
<u>Individual Cells</u>	
Height, inches	2.98
Width, inches	1.65
Thickness, inches	9.335
Total Volume, cubic inches	1.65
Total Weight, grams	49.3

The results in Table 24 indicate scale-up factors of about 38 weight percent and 19 volume percent in going from an individual cell to a battery. This particular battery had a metallic case with plastic-encased cells. This arrangement yields a relatively large weight scale-up in going from cells to batteries. Some commercial batteries have plastic cases with metal-encased cells. This alternative arrangement

gives a smaller weight percentage scale-up as low as 14 weight percent on another commercial model. Scale-up percentages will depend also on the size of the battery. An important point, however, is that at least one metallic-case arrangement is required to contain the pressures that build up in sealed batteries during charging.

As a first approximation, scale-up factors of 20 volume percent and 30 weight percent would seem quite reasonable to estimate battery data from cell data.

#### Relationship of Cell Components to Commercial Cells

The objective of this part of the work is to provide physical and electrochemical data that can be used for evaluating future work. The first step is to provide weight and size data on the various components of a sealed cell. The second step is to provide electrochemical data for a complete cell, both sealed and with flooded electrodes. The third step is to combine the data into conversion factors that will permit new data to be used for predicting the performance of sealed cells or complete batteries.

#### Weight and Size Breakdown

A single cell was dismantled and dimensions were obtained on its various parts. Each cell had the overall dimensions described in Table 24. Each cell had three negative cadmium electrodes and two positive nickel electrodes. Cells were completely discharged to zero terminal voltage before dismantling. Weight and dimensions are given in Table 25.

Each negative electrode in the cell was 4.47 cm high, 3.76 cm wide, and 0.08 cm thick, exclusive of electrical connection tabs. The positive electrodes had the same area but were 0.09 cm thick.

In Table 25, Items 1, 2, 3, 4, 5, and 6 were weighed wet as dismantled from the cells. They were then washed and dried to constant weights to give the data showing in the table. Any losses of weight brought about by washing were added to electrolyte weights, assuming 30 weight percent potassium hydroxide. The sealant, Item 2, included rubber grommets and a safety valve.

Item 7 was determined by chemical analysis, as described later. Item 8 was estimated from electrochemical data given in Table 28 (given later).

Items 9 and 10 were obtained by the difference between weights of total plaques (Items 5 and 6) and weights of active material (Items 7 and 8). That is,  $(9) = (5) - (7)$  and  $(10) = (6) - (8)$ .

Item 11 is the sum of collected free electrolyte plus weight changes in other components.

The free electrolyte accounted for only 0.30 gram, as most of the electrolyte was contained within the plates and the separator. A breakdown of electrolyte weights in the dismantled cell is as follows:

	<u>Grams</u>
Free electrolyte	0.30
From separator	2.31
From 3 negative plates	1.62
From 2 positive plates	1.07
Total electrolyte weight	<u>5.30</u>

Item 12 is the difference between internal case volume and the volume of the electrode assembly, as measured by the volume of liquid required to completely fill a cell.

Duplicate weight measurements on two cells showed the data in Table 25 are accurate to  $\pm 0.15$  gram or  $\pm 5$  percent, whichever is the smaller error. Volume measurements are also accurate to  $\pm 5$  percent.

TABLE 25. PHYSICAL DIMENSIONS FOR SEPARATE COMPONENTS OF A COMMERCIAL NICKEL-CADMIUM CELL

Item	Cell Parts	Weight, g	% of Total	Volume, in. <sup>3</sup>	% of Total
1	Case material	11.67	23.6	0.538	32.61
2	Sealant	1.12	2.28	0.018	1.09
3	Terminals	5.84	11.9	0.050	3.03
4	Separator	0.66	1.34	0.065	3.94
5	Negative plates	14.5	29.5	0.237	14.4
6	Positive plates	9.96	20.3	0.181	10.9
7	Cadmium hydroxide Cd(OH) <sub>2</sub>	6.75	13.7	0.085	5.15
8	Nickel hydroxide Ni(OH) <sub>2</sub>	4.11	8.35	0.064	3.88
9	Nickel plaques, negative, including grids	7.75	15.7	0.054	3.28
	(a) Iron grids	2.03	4.13	0.015	0.91
10	Nickel plaques, positive, including grids	5.85	11.9	0.041	2.48
	(a) Iron grids	1.35	2.75	0.010	0.61
11	Electrolyte	5.30	10.8	0.250	15.2
12	Free space (gas space)	--	--	0.281	17.0
	Totals, measured	49.3		1.65	

The most significant conclusion, for the research objective of reducing cell weights and sizes, is that the negative plates (Item 5) are the largest single component of weight. That is, Item 5 contains the greatest percentage of total weight and would remain so even in large batteries. Therefore, any decrease in the weight of plaques (Item 9) and increase in the weight of active material (Item 7) should significantly decrease the weight of a battery.

#### Reproducibility and Effect of Flooding

A single commercial cell was charged at 60 milliamperes for 17 hours and discharged at 640 milliamperes to 0.5-volt cut-off for a number of cycles until reproducible ampere-hours were obtained on discharge. The above charging rate was used because it was recommended by the manufacturer. The charging coulombic capacity was 1.02 ampere-hours. The above discharge rate was used because it corresponded to a nominal 1-hour rate, based on the manufacturer's specifications. The first two cycles, shown in both parts of Table 26, represent the first two reproducible cycles. The results show an actual capacity of 0.95 ampere-hour instead of the 0.64 ampere-hour predicted from the manufacturer's brochure for a 1.0-volt cut-off.

TABLE 26. EFFECT OF FLOODING IN A COMMERCIAL NICKEL-CADMIUM CELL

<u>Input</u>		<u>Ampere-Hours</u>
Per Cell, Sealed, Cycle 1		1.02
Per Cell, Sealed, Cycle 2		1.02
Per Cell, Flooded, Cycle 3		1.02
Per Cell, Flooded, Cycle 4		1.20
Per Cell, Flooded, Cycle 5		1.20
	<u>Discharge Rate,</u>	
<u>Maximum Output</u>	<u>hours</u>	<u>Ampere-Hours</u>
Per Cell, Sealed, Cycle 1	1.5	0.939
Per Cell, Sealed, Cycle 2	1.5	0.917
Per Cell, Flooded, Cycle 3	1.5	0.944
Per Cell, Flooded, Cycle 4	1.5	0.915
Per Cell, Flooded, Cycle 5	1.5	0.963

After Cycle 2, the cell was dismantled and the electrodes were submerged in 30 weight percent potassium hydroxide. The objective was to determine whether the same results would be obtained with flooded electrolyte as was obtained with the sealed cell. There were three negative plates with two positive plates between them. Flooding the electrodes in this manner caused them to flare out from the connecting terminals so that the electrode spacings became relatively large. Results are given in Table 26, as Cycles 3 to 5. The discharge curves of Cycles 2 and 3 are shown in Figure 59 to compare flooded and sealed conditions. The voltage data in Figure 59 show the electrolyte resistance is negligible. The time data show that the ampere-hour capacity is practically identical in the sealed and flooded conditions. In addition, Cycles 3, 4, and 5



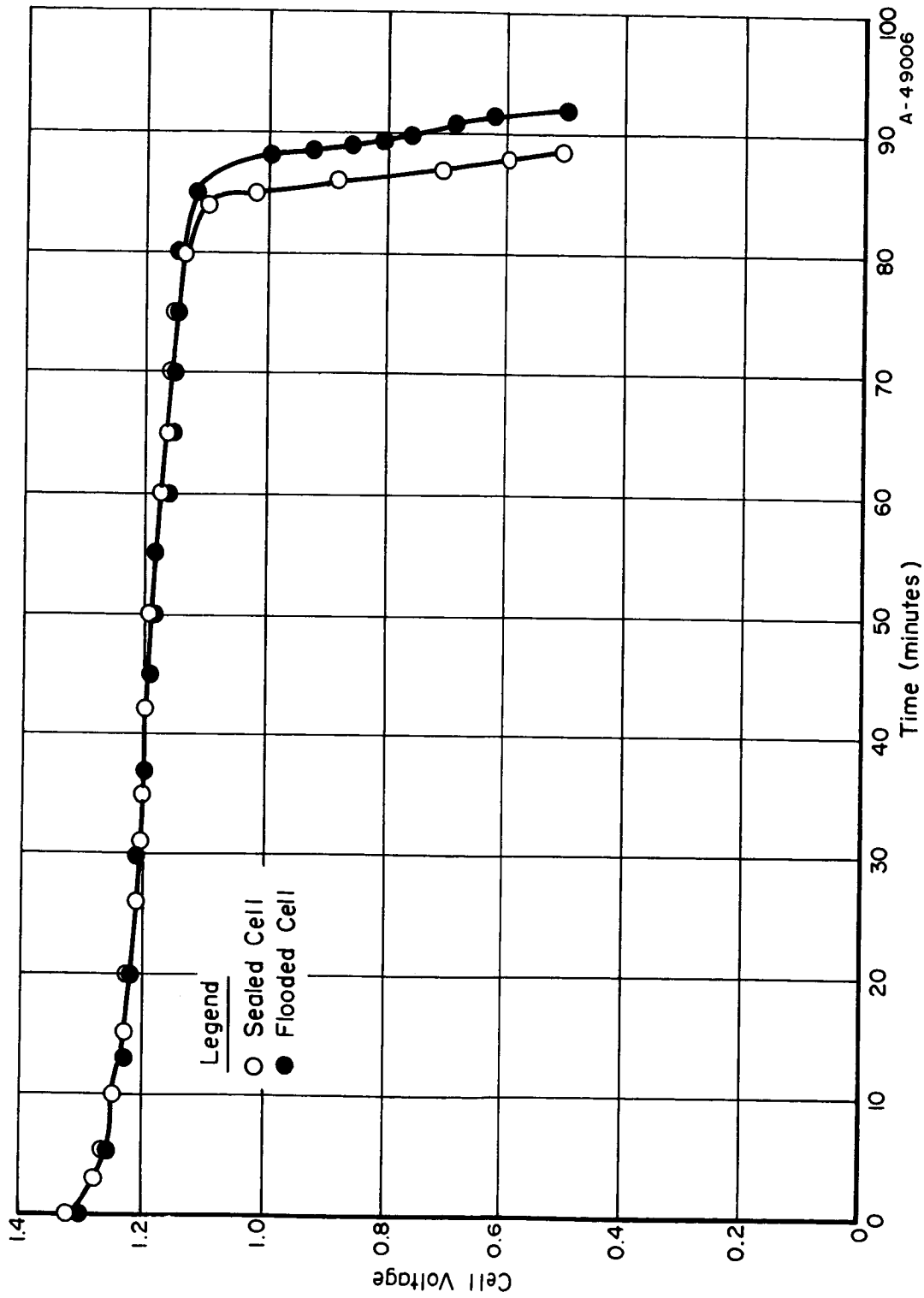


FIGURE 59. DISCHARGE DATA FOR COMMERCIAL NICKEL-CADMIUM ELECTRODES AT 0.640-AMP CONSTANT CURRENT IN A SEALED CELL AND UNDER FLOODED CONDITIONS

of Table 26 show that the same outputs are obtained with flooded electrodes as were obtained with the sealed cell.

Because the charging coulombs were so close to output coulombs, it appeared the electrodes might not be receiving full charge. Therefore, Cycle 4 was performed to increase the charging coulombs to 1.2 ampere-hours. Output for Cycle 4 actually showed fewer coulombs with the extra charging coulombs. Cycle 5 was, therefore, a repeat of Cycle 4 conditions. The result of Cycle 5 confirms the conclusions: (a) ampere-hour capacity is the same whether the electrode is flooded or sealed in a cell, and (b) the positive electrode had received full charge on all the cycles shown in Table 26.

A duplicate sealed cell was charged and discharged a number of times to determine the accuracy of results in Table 26. Measured values of 0.993 and 0.988 ampere-hour showed that cells from the battery may be considered to be identical.

The first five cycles with complete cells combined with Cycle 6 in the positive electrode, Table 28, show that the output capacity of the positive plate is unchanged by deep cycling. That is, the ampere-hour capacity of the positive plate remains reproducible after six full charge-and-discharge cycles at constant rates. However, Cycles 9P, 10P, and 11P show that the measured capacity is a function of rate of discharge. Therefore, the ampere-hour capacity from a sealed cell must be measured at constant rates to obtain reproducible results.

Integration of the area under the curves in Figure 59 shows about 1.15 watt-hours. Combining the energy output with the weights given in Table 24 gives the following values:

$$(\text{watt-hr/lb cell})_{\text{comm.}} = 10.6$$

$$(\text{watt-hr/lb battery})_{\text{comm.}} = 6.46$$

The above battery value is significantly lower than values reported in the literature for nickel-cadmium batteries. Some of the values reported are

Reference	(watt-hr/lb battery) <sub>comm.</sub>
Duddy, J. C., and Salkind, A. J., The Electric Storage Battery Company, "High Energy: Weight Ratio, Nickel-Cadmium Cells", J. Electrochem. Soc., <u>108</u> (8), 717-719 (August 1961).	10
Howard, Paul L., Yardney Electric Corporation, "Wet-Cell Batteries for Power", Product Engineering, <u>31</u> , 75-82 (February 15, 1960).	12
Grimes, C. G., and Herbert, W. S., The Electric Storage Battery Company, "The Choice of Battery Systems", SAE Preprint No. 269D presented at the 1961 SAE International Congress and Exposition of Automotive Engineering, Detroit, Michigan (January 9-13, 1961).	11.5

Reference	(watt-hr/lb battery)comm.
Francis, Howard T., Armour Research Foundation of Illinois Institute of Technology, <u>Space Battery Handbook</u> , prepared under NASA Contract NASw-401 (April 15, 1963).	12
Shair, R. C., Rampel, G., and Kantner, E., Gulton Industries, Inc., "Hermetically-Sealed Nickel-Cadmium Storage Batteries", IRE Transactions on Military Electronics, <u>MIL-6</u> (1), 67-71 (January 1962).	12

The most obvious explanation for the smaller value found at Battelle is associated with the smaller cells and higher rates used at Battelle. The literature values are for batteries on the order of 100-ampere-hour capacity discharged at 5- or 10-hour rates. The Battelle values are for 1-ampere-hour cells discharged at a 1.5-hour rate. The larger batteries have a larger percentage of electrode weight and smaller percentages of cases and adjunct parts. The weights of electrodes, electrolyte, and separators in the cells, checked at Battelle, for example, are only 39 percent of the total battery weight. In a large battery, these vital parts would exceed 60 percent of the total weight. Moreover, a lower discharge rate can be expected to increase watt-hr/lb by 5 to 10 percent. The effect of rate is discussed later.

Energy-Conversion Factors. The simplest procedure for estimating cell or battery performances from the performance of separate parts is to use units of lb/watt-hr and in.<sup>3</sup>/watt-hr for each part. Such units are additive whereas the more common reciprocal units of watt-hr/lb and watt-hr/in.<sup>3</sup> are not additive.

By definition,

$$(\text{lb/watt-hr})_{\text{Total}} = \text{Sum } (\text{lb/watt-hr})_{\text{Each Part}}$$

$$(\text{in.}^3/\text{watt-hr})_{\text{Total}} = \text{Sum } (\text{in.}^3/\text{watt-hr})_{\text{Each Part}}$$

Using 1.15 watt-hours measured from Figure 59 and the weights and volumes of each component in Table 25 of this report, the values shown in Table 27 were calculated for a cell. Using the watt-hours from five cells and the weight and sizes of battery-case materials in Table 24, a total battery value was calculated.

This method of presentation has the advantage that it shows quickly the relative importance of each item on the overall weight and volume. Suppose, for example, the lb/watt-hr and in.<sup>3</sup>/watt-hr of the negative electrode, Item 5 in Table 25, were each decreased 50 percent. The following changes would be predicted:

	Present Value, lb/watt-hr	Predicted New Value, lb/watt-hr	Percent Decrease	Present Value, in. <sup>3</sup> /watt-hr	Predicted New Value, in. <sup>3</sup> /watt-hr	Percent Decrease
Negative plates	0.0277	0.0138	50	0.206	0.103	50
Total cell	0.0939	0.0800	17.4	1.399	1.296	7.4
Total battery	0.1536	0.1397	9.5	1.981	1.878	5.2

TABLE 27. APPROXIMATE WEIGHT AND VOLUME FACTORS FOR ESTIMATING PERFORMANCES FROM INDIVIDUAL COMPONENTS

Item	Cell Part	Weight, lb/watt-hr	Volume, in. <sup>3</sup> /watt-hr
1	Case material	0.0223	0.468
2	Sealant	0.0021	0.016
3	Terminals	0.0112	0.043
4	Separator	0.0013	0.056
5	Negative plates	0.0277	0.206
6	Positive plates	0.0191	0.157
11	Electrolyte	0.0102	0.208
12	Free space	--	0.245
	Total Cell	<u>0.0939</u>	<u>1.399</u>
13	Battery case	0.0597	0.386
14	Battery free space	--	0.196
	Total Battery	<u>0.1536</u>	<u>1.981</u>

This method of calculation has another advantage in that manufacturers, or other workers in the field, can use new data with their own data expressed in the same units. Thus, a different case arrangement might change Items 1, 2, 12, and 13, in Table 27 without changing the other factors.

The method has a disadvantage because it implies that each component can change independently. In actuality, an improvement in any one component can change the observed values for other components. Improved electrodes might be packed in the same containers, for example, thereby changing values for case materials, sealant, terminals, separators, electrolyte, and free space because the watt-hr were changed. This is a complication that need not be dealt with on the present project to show improvements in negative electrodes.

#### Commercial Single Positive Electrodes

Following the above results with sealed and flooded cells, single-electrode measurements were commenced. Details of the experimental procedures with single electrodes are given in a later section, "Experimental Method for Single Electrodes".

The majority of work was concerned with measurements on single negative electrodes. But in order to relate future results to their effect on total cell or battery performances, data had first to be obtained on single positive electrodes under identical conditions.

Effect of Rate of Discharge. Cycles 9P, 10P, and 11P (Table 28) show the rate dependence of the positive electrode. Less capacity is obtained at higher discharge rates, which is to be expected, since the electrode efficiency is a function of current density. Thus, the maximum capacity should be expected from Cycle 10P, which had the lowest

TABLE 28. ELECTROCHEMICAL HISTORY OF A SINGLE POSITIVE ELECTRODE FROM A COMMERCIAL NICKEL-CADMIUM BATTERY

Input		Ampere-Hours
Per Positive, Flooded, Cycle 6P		0.60
Per Positive, Flooded, Cycle 7P		0.60
Per Positive, Flooded, Cycle 8P		0.60
Per Positive, Flooded, Cycle 9P		0.80
Per Positive, Flooded, Cycle 10P		1.60
Per Positive, Flooded, Cycle 11P		0.84
	Discharge Rate, hours	Ampere-Hours
	Maximum Output	
Per Positive, Flooded, Cycle 6P	1.5	0.477
Per Positive, Flooded, Cycle 7P	5	0.485
Per Positive, Flooded, Cycle 8P	11.5	0.479
Per Positive, Flooded, Cycle 9P	24	0.594
Per Positive, Flooded, Cycle 10P	45	0.581
Per Positive, Flooded, Cycle 11P	1.5	0.528

rate of discharge. However, the values obtained from 9P and 10P are similar within experimental error, and the highest capacity value will be used as theoretical in this report. Ritterman and Seiger report that a 50-hour rate is required to achieve theoretical capacity at a positive electrode.\*

A second result to be deduced from Table 28 is that of the current densities that correspond to the more conventional units of hours for discharge rate. Current density was assumed to be the variable that determines the majority of an electrode polarization. A constant current density was sometimes used when electrode thickness was varied, to provide comparisons.

The electrodes in Table 28 and in Figures 60 and 61 were  $4.47 \times 3.76 \times 0.090$  cm. The total area was, therefore,  $33.6 \text{ cm}^2$  for both sides. The current for a 1.5-hour rate of discharge was 320 milliamperes, giving  $9.54 \text{ ma/cm}^2$  as the current density equivalent to the 1.5-hour rate of discharge.

However, the commercial electrodes had a small perimeter of supporting grid on which sintered powder was missing. And since future experimental electrodes will be  $1 \times 1$ -cm plaques without an inert perimeter, this small area difference was accounted for as follows: the area of sintered plaque was  $4.27 \times 3.47$  cm, or  $29.6 \text{ cm}^2$  on both sides. A 320-milliamper discharge would then correspond to  $10.8 \text{ ma/cm}^2$  for the 1.5-hour rate.

Figure 62 summarizes the average half-cell potentials for positive electrodes, where the  $10.8 \text{ ma/cm}^2$  point corresponds to the 1.5-hour rate of discharge. Other hourly rates of discharge are inversely proportional to current density. For example,  $16.2 \text{ ma/cm}^2$  corresponds to a 1.0-hour rate of discharge and  $5.4 \text{ ma/cm}^2$  corresponds to a 3.0-hour rate, for a 21-mil-thick electrode.

\*Ritterman, P., and Seiger, H. N., Gulton Industries, Inc., "Investigation of Battery Active Nickel Oxides", Quarterly Progress Report (September 11, 1964).

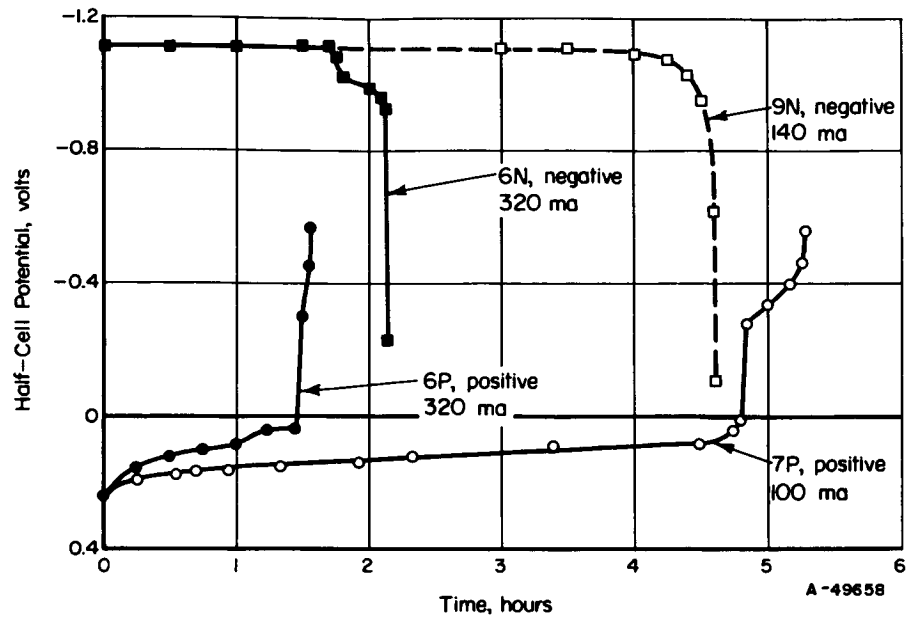


FIGURE 60. HALF-CELL DISCHARGE DATA FROM COMMERCIAL NICKEL-CADMIUM ELECTRODES

Potentials are in reference to the saturated calomel electrode.

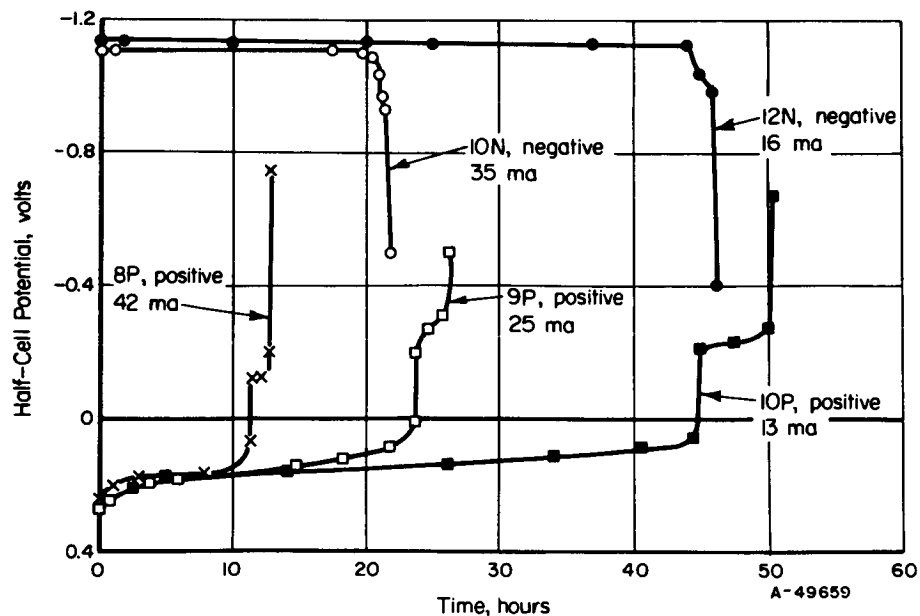


FIGURE 61. HALF-CELL DISCHARGE DATA FROM COMMERCIAL NICKEL-CADMIUM ELECTRODES

Potentials are in reference to the saturated calomel electrode.

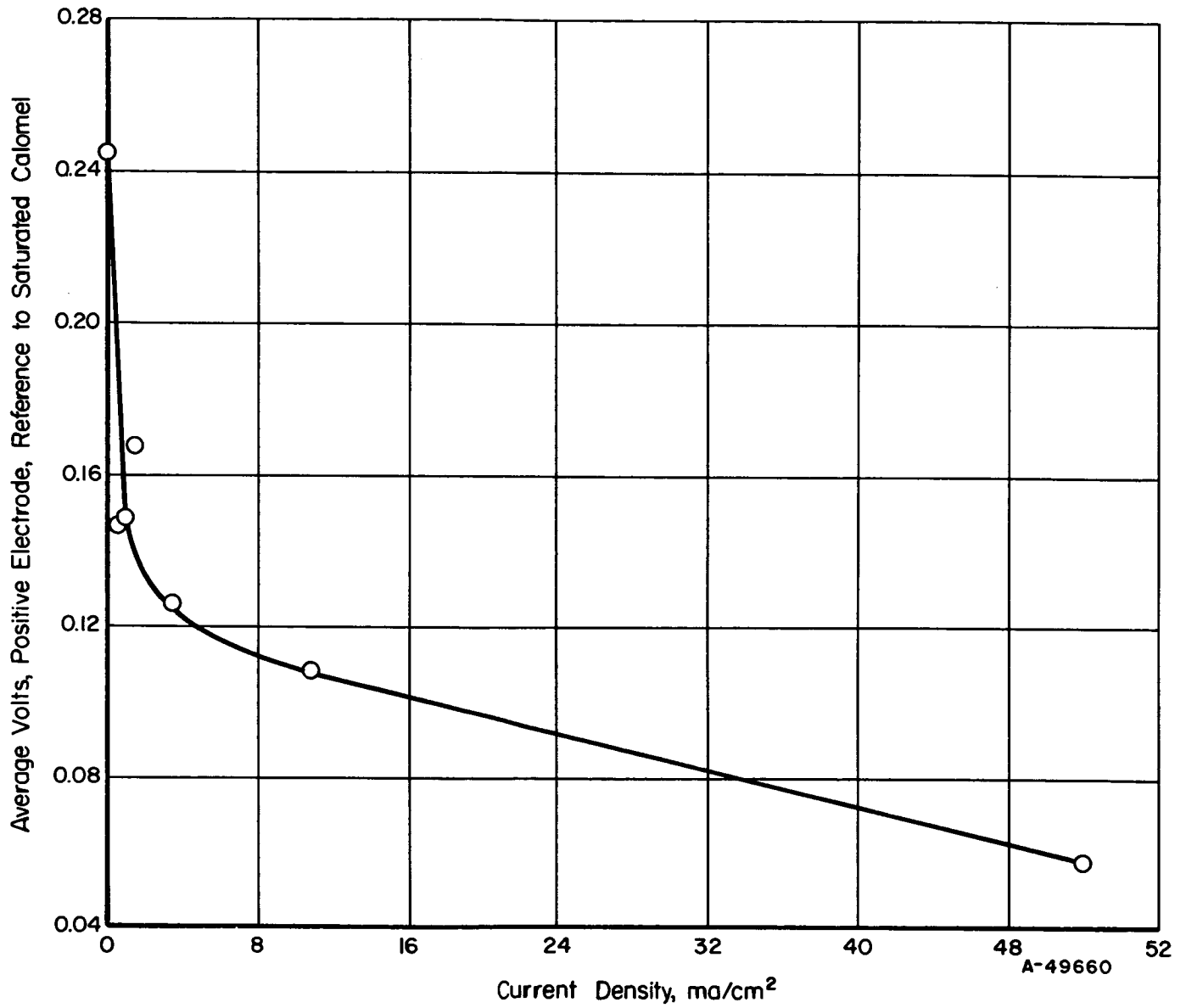


FIGURE 62. AVERAGE VOLTAGE OF POSITIVE HALF-CELL VS CURRENT DENSITY

The voltages in Figure 62 are the midpoint voltages between beginning and the end of discharge at each current density from the voltage-time curves given in Figures 60 and 61. Subsequently, the voltage values in Figure 62 may be added to observed values for single negative electrodes to provide a cell voltage for calculation of watts.

Oxygen Effect. Note that the discharge curves for the single positive electrode, 6P through 10P as shown in Figures 60 and 61, are composed of a primary and secondary discharge reaction. S. Uno Falk reports that the secondary discharge stage of the positive electrode is probably caused by oxygen adsorbed by  $\text{Ni}(\text{OH})_2$ .\* Thus, to obtain true capacity from the positive electrode, a voltage cut-off of zero volt with respect to the saturated calomel reference electrode has been used to eliminate the oxygen effect.

### Commercial Single Negative Electrodes

New experimental electrode structures were evaluated as single negative electrodes. A first step, therefore, was to provide analogous data for commercial single negative electrodes as a reference for evaluating new data. This section of the report describes (1) methods and results with single negative electrodes and (2) how laboratory data might be used to predict performances of sealed cells and batteries.

Chemical Analysis. As a means for calculating theoretical values and efficiency of utilization of active materials, commercial negative electrodes were chemically analyzed.

A negative plate from the cell described in Table 25 was subjected to chemical analysis to determine its percentage composition and ampere-hour capacity. One negative plate was weighed wet with the tab removed. The recorded weight was 5.093 grams. The entire sample was dissolved in nitric acid. It was then fumed in sulfuric acid in order to permit plating of nickel. Nickel was plated and weighed as a metal. Cadmium was separated as the sulfide, then converted to the sulfate and weighed. Iron was separated by an ammonium hydroxide precipitation and determined volumetrically. The following percentage composition was reported: nickel 34.3%, cadmium 33.9%, and iron 13.3%. The remaining 18.5% was electrolyte.

Based on the electrode weight of 5.093 grams, the following weights of metal were reported: nickel 1.747 grams, cadmium 1.727 grams, and iron 0.677 gram. The remainder of the weight, 0.942 gram, was electrolyte and represents a larger quantity than that reported earlier, in the preceding section "Weight and Size Breakdown", because the electrode was flooded with electrolyte before chemical analysis. The flooded electrode contained 0.942 gram of electrolyte while the sealed-battery electrode had 0.54 gram of electrolyte. Therefore, about 43 percent of the void volume in the sealed-battery electrode was free volume, probably filled with oxygen. Since the active material after impregnation is reported as cadmium hydroxide, the weight of cadmium, 1.727 grams, was converted by calculation to the equivalent weight of cadmium hydroxide, 2.250 grams. Thus, the weight percentage of total solids, neglecting electrolyte weight, was 37.4 nickel, 48.1 cadmium hydroxide, and 14.5 iron.

The dimensions of the analyzed plate were 4.47 x 3.76 x 0.080 cm. Therefore, area = 16.8 cm<sup>2</sup> and volume = 1.344 cm<sup>3</sup>. Since the weight of iron was 0.677 g, the

\*Falk, S. Uno, J. Electrochem. Soc., 107, 662-663 (1960).



volume of the supporting iron grid was  $0.086 \text{ cm}^3$ . The  $1.747 \text{ g}$  of nickel, therefore, occupied  $1.258 \text{ cm}^3$ , giving an apparent density of  $1.39 \text{ g/cm}^3$ , and a calculated porosity of 84.1 percent voids. The overall calculated density of the plate was  $1.82 \text{ g/cm}^3$ . Assuming a density of  $8.90 \text{ g/cm}^3$  for nickel and  $7.86 \text{ g/cm}^3$  for iron, the theoretical density of the mixed metals is  $8.60 \text{ g/cm}^3$ , giving an overall calculated porosity of 78.0 percent voids. This calculated porosity for a plate from a battery agrees well with 79 percent voids reported in Table 12 for a commercial unimpregnated sintered powder plaque.

The  $1.727 \text{ g}$  of reported cadmium corresponds to  $2.25 \text{ g}$  of cadmium hydroxide whose theoretical density is  $4.79 \text{ g/cm}^3$ . The theoretical volume of the cadmium hydroxide is, therefore,  $0.470 \text{ cm}^3$ . The volume of voids is 78.0 percent of  $1.344 \text{ cm}^3$ , or  $1.050 \text{ cm}^3$ . The voids were 44.7 percent filled, according to this calculation, which is slightly higher than the 39 percent of pore volume filled with four impregnation cycles, as reported in Table 14.

Cadmium hydroxide, as noted above, was present in the quantity of 2.25 grams. Since 0.366 ampere-hour is obtained from 1 gram of cadmium hydroxide, the theoretical capacity for the negative electrode is 0.823 ampere-hour.

A subsequent analysis on a second negative plate checked within 2 percent of the above analytical results. All the calculations are considered, therefore, to be accurate within 2 or 3 percent.

An additional sample of a commercial negative plate was analyzed spectroscopically in order to determine whether additives, which would reduce capacity losses due to cycling, were present. In addition to the cadmium, nickel, and iron previously reported there was evidence of the following:

Silicon	0.01%
Manganese	0.05%
Magnesium	0.05%
Copper	0.02%
Calcium	0.01%
Aluminum	0.01%

Indium, which is reported in the section of this report on cycle effects as a possible additive which reduces capacity losses, was not detected in the above analysis. The detection limit of the method used in the spectroscopic analysis is 0.01%. Thus, the conclusion is that no additive was used in the fabrication of the commercial negative electrode under consideration.

Experimental Method for Single Electrodes. Standard electrodes  $1 \times 1 \times 0.08 \text{ cm}$  were cut from battery plaques taken from commercial cells. These electrodes were charged and discharged separately against platinum counterelectrodes in beakers flooded with 30 percent KOH electrolyte.

Charging and discharging were carried out at constant current densities. The constant current was maintained by using a large voltage-dropping resistor in series with the cell across an 18-volt rectifier. With this arrangement, voltage changes in the cell are negligible compared to the voltage across the dropping resistor, thereby assuring constant current. For some experiments constant current was provided with the Sargent Model IV Coulometric Current Source.

Half-cell potentials were determined by means of a saturated calomel reference electrode. A Luggin capillary attached to the reference electrode was used to minimize the voltage drop due to the ohmic resistance of the electrolyte. Voltage measurements are believed to be accurate within  $\pm 10$  mv. The voltage-time curves were recorded using a Sargent Recorder Model MR. The experimental screen electrodes were  $1 \times 1$  cm. Electrode thickness, which is a contract variable, is specified with the experimental data. Experimental screen electrodes are being tested in the same way.

The ampere-hour capacity was determined using a voltage cutoff of  $-1.0$  volt for the negative electrode and zero volt for the positive electrode, both with respect to the saturated calomel reference electrode. The watt-hour capacity equals the product of the ampere-hour capacity and the average voltages. The electrode weight is defined as the dry weight after washing in the completely discharged condition. This weight corresponds also to the weight of an electrode after the completion of its formation cycling.

Effect of Rate of Discharge. Cycles 10N, 11N, 12N, and 13N, Table 29, show the rate dependence of the negative electrode on ampere-hour output. Less capacity is obtained at higher discharge rates. The maximum capacity should be expected from Cycle 12N, the 45-hour rate. However, possibly due to experimental error, maximum capacity was obtained from Cycle 10N, the 21-hour rate.

No data seem to be reported in the literature on how low a rate is required to achieve theoretical capacity of a negative electrode. However, chemical analysis of a negative electrode showed enough cadmium to provide 0.823 ampere-hour. Therefore, this value will be used as the theoretical capacity for a single negative electrode in this report. The maximum output of 0.744 ampere-hour, Cycle 10N, is 90.3 percent of the theoretical capacity. The minimum output of 0.568 ampere-hour is only 69.0 percent of the theoretical capacity. There is, therefore, considerable room for improving the efficiency of utilization of active material in negative electrodes.

The observed voltage-time curves for some of the cycles listed in Table 29 were plotted in Figures 60 and 61. The most striking feature of those voltage-time curves is that the single-negative-electrode voltage was essentially independent of the rate of discharge. The single-positive-electrode voltage, by contrast, depended greatly on rate of discharge, as shown in Figure 62. The constant negative-electrode voltage with changing rate of discharge is important because it implies that large pores might be used for the cadmium electrode without any increase in polarization.

Another value to be deduced from Table 29 is a conversion factor between current density and hourly rate of discharge. The negative electrodes in Table 29 have the same area dimensions as the positive electrodes described in Table 28, namely,  $29.6 \text{ cm}^2$  of porous powder area on both sides. The negative electrodes of Table 29 were discharged at 320 milliamperes, as were the positive electrodes in Table 28, but required 2 hours for complete discharge because of excess negative active material relative to the active material in a positive electrode. However, in a sealed cell or battery, the hourly rate is always determined by the limiting positive capacity. Therefore, for both positive and negative electrodes,  $10.8 \text{ ma/cm}^2$  corresponds to a 1.5-hour rate of discharge;  $16.2 \text{ ma/cm}^2$  corresponds to a 1.0-hour rate of discharge; and  $5.4 \text{ ma/cm}^2$  corresponds to a 3.0-hour rate of discharge, as described earlier, for the 21-mil-thick single positive electrode.

TABLE 29. ELECTROCHEMICAL HISTORY OF A SINGLE NEGATIVE ELECTRODE FROM A COMMERCIAL NICKEL-CADMIUM BATTERY

<u>Input</u>		<u>Ampere-Hours</u>
Per Negative, Flooded, Cycle 6N		0.75 <sup>(a)</sup>
Per Negative, Flooded, Cycle 7N		0.75 <sup>(a)</sup>
Per Negative, Flooded, Cycle 8N		0.75 <sup>(a)</sup>
Per Negative, Flooded, Cycle 9N		0.84
Per Negative, Flooded, Cycle 10N		0.84
Per Negative, Flooded, Cycle 11N		0.84
Per Negative, Flooded, Cycle 12N		0.84
Per Negative, Flooded, Cycle 13N		0.84
	<u>Negative Electrode Discharge Rate, hours</u>	<u>Ampere-Hours</u>
	<u>Maximum Output</u>	
Per Negative, Flooded, Cycle 6N	2	0.582
Per Negative, Flooded, Cycle 7N	2	0.603
Per Negative, Flooded, Cycle 8N	2	0.568
Per Negative, Flooded, Cycle 9N	4.5	0.618
Per Negative, Flooded, Cycle 10N	21	0.744
Per Negative, Flooded, Cycle 11N	2	0.656
Per Negative, Flooded, Cycle 12N	45	0.719
Per Negative, Flooded, Cycle 13N	2	0.640
Theoretical Negative Capacity Based on Chemical analysis		0.823

(a) 91 percent of theoretical capacity.

Hydrogen Effect. The discharge curves for the single negative electrode show in some cases, Cycles 6N, 10N, and 12N, Figures 25 and 26, a secondary-stage reaction similar to that mentioned previously with the single positive electrode. S. Uno Falk reports that hydrogen may be adsorbed by porous metals, thus giving some extra capacity on discharge.\*

This excess capacity has been eliminated from capacity measurements by using a cutoff voltage of -1.0 volt with respect to the saturated calomel reference electrode. This cutoff voltage is justified since, when no hydrogen is present, the capacity observed at a cutoff of -1.0 volt differs within a few percent of that observed at zero volt.

Current derived from adsorbed hydrogen appears only occasionally. When such current does appear, it occurs only after the majority of cadmium metal is oxidized and at a more positive voltage. Consequently, a negative cadmium electrode might be saturated with adsorbed hydrogen and that hydrogen might remain unoxidized through many cycles in a sealed cell. This follows because the cadmium is never fully oxidized in an "unbalanced" sealed cell. The hydrogen, once oxidized, does not reappear on subsequent cycles unless charging is carried to the point of considerable hydrogen evolution.

\*Falk, S. Uno, J. Electrochem. Soc., 107, 663 (1960).

Thus the charging history determines whether a hydrogen current will appear at the end of the cadmium discharge.

Cycling Effect. Although tested identically, negative plates gave different capacities with each cycle. Compare output Cycles 6N, 7N, 8N, 11N, and 13N, for example. This variability with deep cycling of negative electrodes is quite different from the reproducibility described in the section discussing the positive electrode. This change of capacity with deep cycling of negative electrodes has been recognized by other workers\* and adds a serious complication to the experimental work. At worst, the result means that duplicate data can be achieved only by using duplicate electrodes. At best, the result shows this project was properly directed toward a study of the single negative electrode which has a serious and fundamental weakness.

Literature concerning the change of capacity of the negative electrode with deep cycling discloses possible causes of the effect and illustrates methods of retarding or possibly eliminating such losses. For example, the literature has many references to the use of expanders to prevent contraction of the active material in negative plates of both acid and alkaline batteries. Three basic types of expanders which have been used in the preparation of negative plates are lampblack, barium sulfate, and lignin.\*\* However, later work with sintered nickel electrodes has shown that the addition of indium or cellulosic materials to the negative plate retards capacity losses due to cycling.\*

Furthermore, A. Fleischer reports that the capacity loss in the negative plate is a complex function of the discharge rate, the charging rate, and the open-circuit stand in the as-discharged state.\*\*\* It has been reported that cycle losses were eliminated to a large extent by increasing the charging-current density to 22 ma/cm<sup>2</sup> or higher as compared with conventional current densities of about 1 ma/cm<sup>2</sup>.

The data in Figure 49, Task E, showed the capacity loss with each cycle plotted as a percentage of the capacities obtained on the first cycle. The sintered plaque, Battelle impregnated, which was subjected to the normal charging-current density recommended by most manufacturers, shows the greatest capacity decreases of almost 20 percent of the first-cycle capacity. The sintered plaque, Battelle impregnated, which was charged at twice this current density, shows a decrease of less than 10 percent after the first cycle. This is in agreement with the literature just cited. However, the commercial sintered nickel plaque, even though subjected to twice the normal cycling-current densities, showed the least loss in the first cycle.

Because of the importance of capacity changes in the negative plate, a preliminary study was undertaken to determine the effect of active-material aggregation in the sintered nickel plate. It is reported that the capacity losses in the negative electrode are associated with the increase of the crystal size of active deposits, cadmium metal, and cadmium hydroxide on the electrode.\*\*\*\* However, according to X-ray studies, the capacity decrease on cycling is reported to be due not simply to crystal growth, defect of crystal lattice, or compound change. It is furthermore concluded that the capacity loss is mainly due to the aggregation of microparticles of cadmium.\*\*\*\*\*

\*Fleischer, A., Eleventh Annual Battery Research and Development Conference, pp 83-86 (May, 1957).

\*\*Vinal, Storage Batteries, pp 24-27.

\*\*\*Fleischer, A., Tenth Annual Battery Research and Development Conference, pp 37-41 (1956).

\*\*\*\*Yamashita, D., and Yamamoto, Y., Kogyo Kagaku Zasshi, 67 (4), 536-9 (1964), Japan.

\*\*\*\*\*Sugita, K., Denki Kagaku, 29 (3), 176-9 (1961), Japan.

Photomicrographs were taken of cross sections of several negative plates before and after cycling. Figures 63 and 64 show the same cross section of a commercial electrode in a charged condition prior to cycling. White lines were added to Figure 64 to show the outlines of several large pores in the electrode. These large pores are filled with cadmium metal, which appear as small white spots.

Figures 65 and 66 are photomicrographs of cross sections of commercial and Battelle-impregnated plaques after five charge-discharge cycles. The discharges were taken to 100 percent of capacity. Note that the photomicrographs show areas void of cadmium. These areas correspond to the large pores in the original nickel structure. Thus, during deep cycling of a negative electrode, the active material (cadmium) shifted position and collected in the smaller pores. This movement coincided with loss in capacity of the electrode with no loss in electrode weight. Packing of the cadmium in the smaller pores would reduce its availability for electrolytic reaction.

So far as can be determined from review of the literature, the movements of negative material from large pores to small pores during cycling seems to be a new discovery. The result implies that uniform large pores may be preferred for best operation in a sealed battery because there would be no small pores to be packed. Indeed, it was shown in Table 23 that a stacked screen electrode with uniform 6-mil pores gave more coulombs per unit of electrode volume than a commercial electrode with random pores averaging 0.63 mil in diameter. Also, results described later in Figures 67 and 68 suggest that larger pores are capable of giving improved performances.

N/P Ratios. The ratio of negative material to positive material (N/P ratio) is a significant parameter for determining sizes and weights of electrodes. Sealed nickel-cadmium batteries require an excess of negative plate capacity to avoid evolution of hydrogen. Hydrogen gas is not easily oxidized and any accumulation of the gas would tend to permanently pressurize the cell, perhaps bursting it. Excess negative material avoids the hydrogen evolution problem but adds dead weight to a battery. Therefore, the N/P ratio must be minimized to decrease the weight of batteries. The N/P ratio is used frequently in battery literature with two different bases: (1) by weight and (2) by electrochemical capacity.

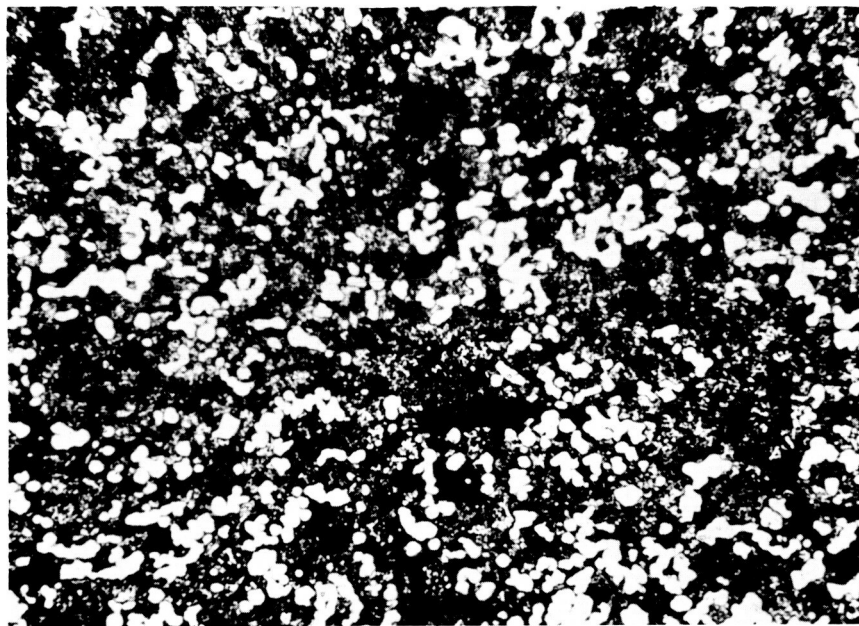
The ratio is more commonly used to designate the ratio of the weight of cadmium hydroxide to weight of nickel hydroxide per unit volume of plaque. Fleischer\* reports that an N/P weight ratio of 1.75 is considered normal after four chemical impregnation cycles of both electrodes. Sonotone Corporation considers an N/P weight ratio of 1.7 as normal in its production processing.\*\* However, in subsequent work, Fleischer lists variations of the N/P weight ratio, after four impregnation cycles, of from 1.381 to 1.539, with an average weight ratio of 1.449.\*\*\*

The commercial plaques under consideration as comparison standards show an N/P weight ratio of 1.64, based on figures obtained from Table 25, by dividing Item 7 by Item 8. The weight ratios are generally of interest in connection with the impregnation process.

\*Fleischer, A., J. Electrochem. Soc., 94, 296 (1948).

\*\*Alliegro, F., and Mundel, A., Proceedings of the 15th Annual Power Sources Conference (May 9-11, 1961), p 67.

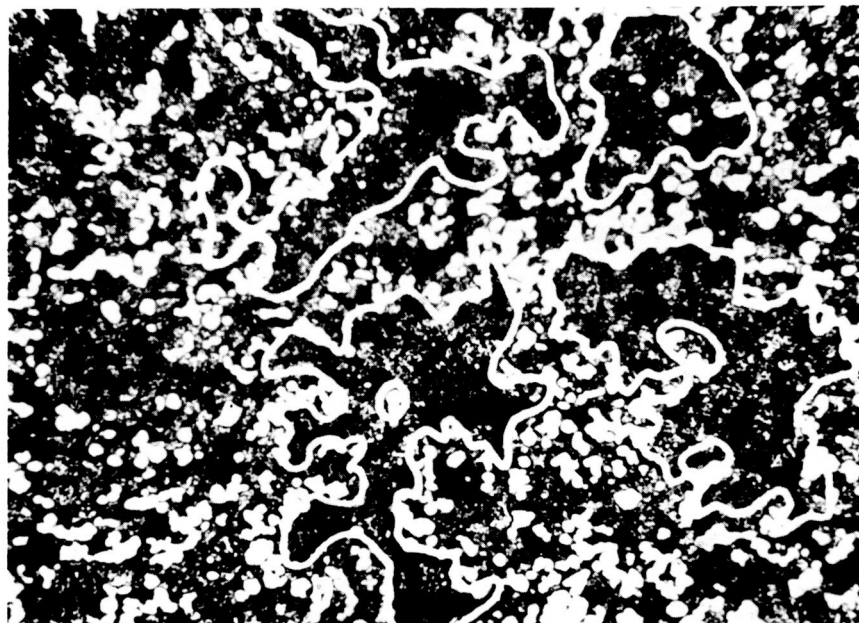
\*\*\*Fleischer, A., Nickel Cadmium Battery Corporation, "Investigations on the Improvement in the Performance Characteristics of the Nickel Cadmium Battery", First Quarterly Progress Report (August 14, 1956), p 37.



500X

17244

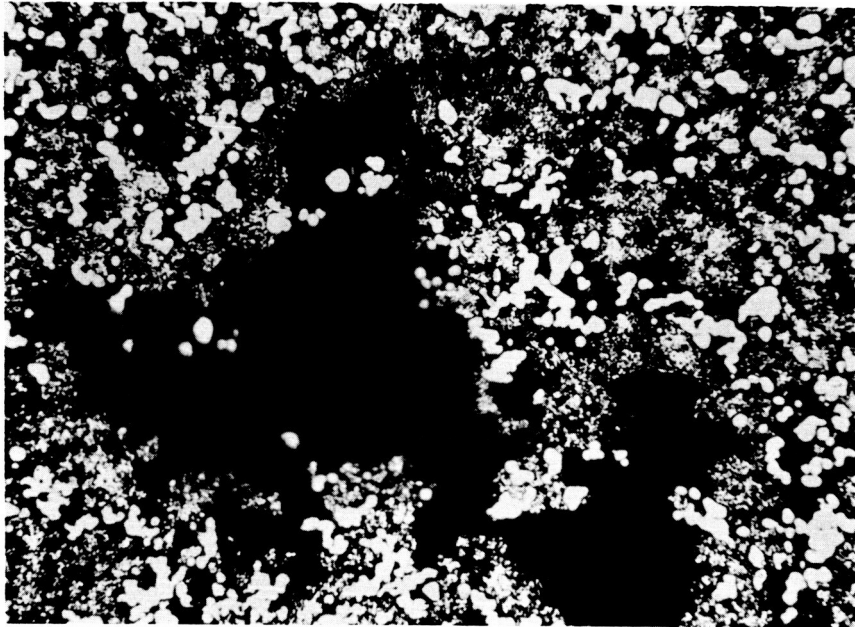
FIGURE 63. CROSS SECTION OF A COMMERCIAL IMPREGNATED BATTERY PLATE BEFORE CYCLING (WITHOUT OVERLAY)



500X

17244

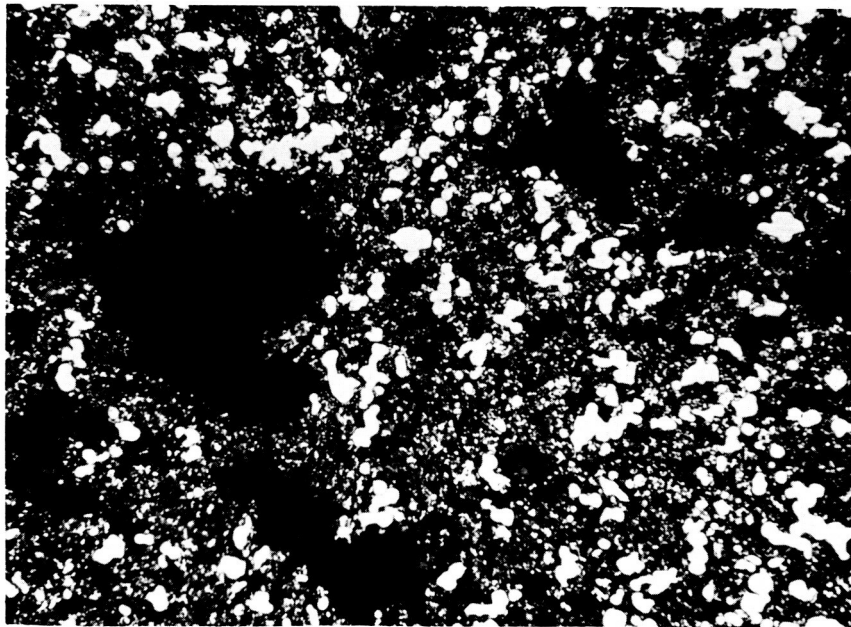
FIGURE 64. CROSS SECTION OF A COMMERCIAL IMPREGNATED BATTERY PLATE BEFORE CYCLING (WITH OVERLAY)



500X

17245

FIGURE 65. CROSS SECTION OF A COMMERCIAL IMPREGNATED BATTERY PLATE AFTER FIVE CHARGE-DISCHARGE CYCLES OF 100 PERCENT DEPTH



500X

17246

FIGURE 66. CROSS SECTION OF BATTELLE IMPREGNATED COMMERCIAL SINTERED NICKEL PLATE AFTER FIVE CHARGE-DISCHARGE CYCLES OF 100 PERCENT DEPTH

A more practical N/P ratio is a capacity ratio, in which N is the ampere-hours per unit volume of negative plate and P is the ampere-hours per unit volume of positive plate. An ideal capacity ratio would be N/P = 1.0, which would correspond to a weight ratio of N/P = 0.79. However, extra negative capacity is needed:

- (a) To compensate for oxygen pressure within a sealed cell
- (b) To avoid less than 100 percent negative charging efficiency toward the end of charge or during overcharge
- (c) To compensate for loss of negative capacity by the cycling effect.

The excess negative material required to compensate for oxygen evolution at end of charge is given by\*

$$\text{ampere-hours} = 4.39 \times 10^{-3} \frac{\text{amp-hr}}{\text{atm} \times \text{cm}^3} \times P \times V \quad ,$$

where

P is the maximum operating pressure in the sealed cell

V is the free volume within the cell.

Assuming P is 5 atmospheres, the minimum negative plate reserve for the commercial cell of Table 25 is 0.101 amp-hr. Since the positive plates described in Table 25 had an observed capacity of 1.19 amp-hr, the negative plates must have a minimum of 1.29 amp-hr to allow for the oxygen evolution. The theoretical minimum capacity ratio is, therefore, N/P = 1.08.

The results in Table 28 show that not all of the impregnated cadmium hydroxide was effectively available. Efficiency varied from 90 percent to 69 percent, depending on the rate of discharge and cycle. Results on charging reported later in Figure 69 also show that 10 to 30 percent of the negative material may be untouched with normal charging procedures. Therefore, the capacity ratio should be increased at least another 10 percent, to N/P = 1.19, to prevent hydrogen evolution during charging. The loss of negative-discharge capacity with cycling, described above, should occur also with charging efficiency as shown in Figure 67 for discharging and Figure 71 for charging. Increasing the capacity ratio another 30 percent leads to an estimated desired value of N/P = 1.55. The above-mentioned N/P weight ratio of 1.64 corresponds to a capacity ratio of N/P = 2.08. The net results are

	<u>Capacity Ratios</u>	<u>Weight Ratios</u>
Ideal	1.0	0.79
Theoretical Minimum for a Sealed Cell	1.08	0.85
Minimum for 90 Percent Charging Efficiency	1.19	0.94
Minimum to Allow for 60 Percent Charging Efficiency After Cycling	1.55	1.22
Observed, Theoretical Negative Divided by Cycle 9P, Table 63	1.37	
Observed, Table 60, Item 7 Divided by Item 8	2.08	1.64
Published Industrial Practice <sup>(a)</sup>	2.15	1.7

(a) Alliegro, F., and Mundel, A., Proceedings of the 15th Annual Power Sources Conference (May 9-11, 1961), p 67.

\*"Batteries", Proceedings of the 3rd International Symposium, Bournemouth (October, 1962), Edited by D. H. Collins, MacMillan Company, New York (1963); "Kinetic Basis for the Operating Characteristics of Sealed Nickel Cadmium Cells", Upton B. Thomas, Jr., pp 123-125.



TABLE 30. ELECTROCHEMICAL DATA FOR SHAPED PORE ELECTRODES

(1) Experiment and Electrode	(2) Weight of Cd(OH) <sub>2</sub> , mg	(3) Cycle	(4) Current		(5) Discharge, ma	(6) 100 Percent Charge	(7) Theoretical Discharge	(8) Time, hours		(9) Discharging to 1.0 Volt	(10) Coulombic Efficiency, percent	
			Charge, ma	Discharge, ma				Charging to H <sub>2</sub> Evolution	Charging to H <sub>2</sub> Evolution		Charging to H <sub>2</sub> Evolution	Discharging to 1.0 Volt
101, commercial	152	1	3.7	111.2	111.2	16	1/2	n. d. (a)	n. d.	0.293	n. d.	59
		2	55.6	111.2	111.2	1	1/2	0.576	0.576	0.295	58	59
		3	55.6	55.6	55.6	1	1	0.550	0.550	0.660	55	66
102, 44	75.1	1	1.8	55.0	55.0	16	1/2	n. d.	n. d.	0.355	n. d.	71
		2	27.5	55.0	55.0	1	1/2	0.653	0.653	0.334	65	67
		3	27.5	27.5	27.5	1	1	0.616	0.616	0.705	62	71
103, 23B	14.4	1	0.34	10.6	10.6	16	1/2	n. d.	n. d.	0.385	n. d.	77
		2	5.3	10.6	10.6	1	1/2	0.720	0.720	0.372	72	75
		3	5.3	5.3	5.3	1	1	0.697	0.697	0.765	70	77
104, 34	17.9	1	0.42	13.1	13.1	16	1/2	n. d.	n. d.	0.362	n. d.	73
		2	6.55	13.1	13.1	1	1/2	0.658	0.658	0.362	66	73
		3	6.55	6.55	6.55	1	1	0.667	0.667	0.755	67	76
105, commercial	152	1	3.8	111.2	111.2	16	1/2	n. d.	n. d.	0.320	n. d.	64
		2	55.6	111.2	111.2	1	1/2	0.636	0.636	0.319	64	64
		3	55.6	74.1	74.1	1	3/4	0.670	0.670	0.501	67	67
		4	55.6	55.6	55.6	1	1	0.670	0.670	0.710	67	71
		5	111.2	111.2	111.2	1/2	1/2	0.345	0.345	0.334	69	67
		6	55.6	111.2	111.2	1	1/2	0.650	0.650	0.331	65	66
		7	111.2	222.4	222.4	1/2	1/4	0.317	0.317	0.142	64	57
		8	222.4	444.8	444.8	1/4	1/8	0.138	0.138	0.061	55	48
5A	27.8	55.6	55.6	2	1	1.29	1.29	0.698	64	70		
106, 45	40.7	1	1.5	46.4	46.4	10.3	0.31	n. d.	n. d.	0.218	n. d.	68
		2	23.2	46.4	46.4	0.62	0.31	0.368	0.368	0.204	59	64
		3	23.2	31.0	31.0	0.62	0.48	0.285	0.285	0.312	46	65
		4	23.2	23.2	23.2	0.62	0.62	0.345	0.345	0.418	56	65
		5	46.4	46.4	46.4	0.31	0.31	0.175	0.175	0.192	57	60
107, Hex 3	34.5	1	0.79	25.2	25.2	16	1/2	n. d.	n. d.	0.333	n. d.	67
		2	12.6	25.2	25.2	1	1/2	0.573	0.573	0.318	57	63
		3	12.6	16.8	16.8	1	3/4	0.502	0.502	0.458	50	61
		4	12.6	12.6	12.6	1	1	0.516	0.516	0.627	52	63
		5	25.2	25.2	25.2	1/2	1/2	0.250	0.250	0.290	50	58
		6	12.6	25.2	25.2	1	1/2	0.342	0.342	0.230	34	46
		7	25.2	50.4	50.4	1/2	1/4	0.178	0.178	0.113	36	44
		8	50.4	100.8	100.8	1/4	1/8	0.080	0.080	0.057	32	49
5A	6.3	12.6	12.6	2	1	0.695	0.695	0.468	29	47		

TABLE 30. (Continued)

(1) Experiment and Electrode	(2) Weight of Cd(OH) <sub>2</sub> , mg	(3) Cycle	(4) Current		(5) ma	(6) 100 Percent Charge	(7) Time, hours		(8) Charging to H <sub>2</sub> Evolution	(9) Discharging to 1.0 Volt	(10) Coulombic Efficiency, percent		(11) Discharging to 1.0 Volt
			Charge, ma	Discharge, ma			Theoretical Discharge	Charging to H <sub>2</sub> Evolution			Charging to H <sub>2</sub> Evolution	Discharging to 1.0 Volt	
108, 23B	12.4	1	0.28	9.0	16	1/2	n.d.	0.358	n.d.	72			
		2	4.5	9.0	1	1/2	0.660	0.348	66	70			
		3	4.5	6.0	1	3/4	0.655	0.520	66	70			
		4	4.5	4.5	1	1	0.600	0.705	60	70			
		5	9.0	9.0	1/2	1/2	0.290	0.315	58	63			
109, 26	11.5	1	0.26	8.2	16	1/2	n.d.	0.388	n.d.	76			
		2	4.1	8.2	1	1/2	0.675	0.352	68	69			
		3	4.1	5.5	1	3/4	0.653	0.512	65	67			
		4	4.1	4.1	1	1	0.630	0.658	63	66			
		5	8.2	8.2	1/2	1/2	0.287	0.288	57	58			
		6	4.1	8.2	1	1/2	0.320	0.180	32	36			
		7	8.2	16.4	1/2	1/4	0.185	0.095	37	38			
		8	16.4	32.8	1/4	1/8	0.085	0.046	34	37			
		5A	2.05	4.1	2	1	0.383	0.322	19	32			
		110, 34	No data										
111, Hex 2	52.0	1	1.2	38.0	16	1/2	n.d.	0.250	n.d.	50			
		2	19.0	38.0	1	1/2	0.342	0.234	34	47			
		3	19.0	25.3	1	3/4	0.342	0.346	34	46			
		4	19.0	19.0	1	1	0.338	0.453	34	45			
		5	38.0	38.0	1/2	1/2	0.150	0.200	30	40			
		6	19.0	38.0	1	1/2	0.315	0.200	32	40			
		7	38.0	76.0	1/2	1/4	0.145	0.090	29	36			
		8	76.0	152.0	1/4	1/8	0.063	0.040	25	31			
112, 23B	12.9	1	0.3	9.4	16	1/2	n.d.	0.379	n.d.	76			
		2	4.7	9.4	1	1/2	0.673	0.357	67	71			
		3	4.7	6.3	1	3/4	0.653	0.524	65	70			
		4	4.7	4.7	1	1	0.630	0.693	63	69			
		5	9.4	9.4	1/2	1/2	0.296	0.322	59	64			
		6	4.7	9.4	1	1/2	0.585	0.322	59	64			
		7	9.4	18.8	1/2	1/4	0.279	0.152	56	61			
		8	18.8	37.6	1/4	1/8	0.130	0.072	52	57			
113, 26	12.6	1	0.32	9.2	16	1/2	n.d.	0.315	n.d.	63			
		2	4.6	9.2	1	1/2	0.545	0.315	55	63			
		3	4.6	6.1	1	3/4	0.567	0.497	57	66			

TABLE 30. (Continued)

(1) Experiment and Electrode	(2) Weight of Cd(OH) <sub>2</sub> , mg	(3) Cycle	(4) Current		(5) ma	(6) 100 Percent Charge	(7) Theoretical Discharge	(8) Time, hours		(9) Discharging to 1.0 Volt	(10) Coulombic Efficiency, percent	(11) Charging to Discharging to 1.0 Volt
			Charge, ma	Discharge, ma				Charging to H <sub>2</sub> Evolution	Discharging to 1.0 Volt			
113, 26	12.6	4	4.6		4.6	1	1	0.575	0.667	58	67	
		5	9.2		9.2	1/2	1/2	0.282	0.322	56	64	
		6	4.6		9.2	1	1/2	0.580	0.316	58	63	
		7	9.2		18.4	1/2	1/4	0.274	0.150	55	60	
		8	18.4		36.8	1/4	1/8	0.128	0.071	51	57	
		1	0.43		12.8	15	1/2	n. d.	0.289	n. d.	n. d.	57
		2	6.4		12.8	1	1/2	0.500	0.289	50	57	
		3	6.4		8.5	1	3/4	0.508	0.447	51	59	
114, 34	17.6	4	6.4		6.4	1	1	0.610	0.610	52	61	
		5	12.8		12.8	1/2	1/2	0.252	0.297	50	58	
		6	6.4		12.8	1	1/2	0.508	0.289	51	58	
		7	12.8		25.6	1/2	1/4	0.245	0.137	49	55	
		8	25.6		51.2	1/4	1/8	0.117	0.063	47	52	
		1	1.2		35.4	15	1/2	n. d.	0.320	n. d.	n. d.	64
		2	17.7		35.4	1	1/2	0.492	0.280	49	56	
		3	17.7		23.6	1	3/4	0.453	0.411	45	55	
115, 46	48.4	4	17.7		17.7	1	1	0.434	0.542	43	54	
		5	35.4		35.4	1/2	1/2	0.197	0.237	39	49	
		6	17.7		35.4	1	1/2	0.395	0.246	40	49	
		7	35.4		70.8	1/2	1/4	0.185	0.109	37	44	
		8	70.8		141.6	1/4	1/8	0.083	0.046	33	37	
		1	0.26		8.2	16	1/2	n. d.	0.217	n. d.	n. d.	44
		2	4.1		8.2	1	1/2	0.417	0.253	42	52	
		3	4.1		8.2	1	1/2	0.480	0.266	48	53	
116, 23B	11.3	4	4.1		8.2	1	1/2	0.488	0.273	49	55	
		5	8.2		16.4	1/2	1/4	0.237	0.133	47	53	
		6	8.2		16.4	1/2	1/4	0.233	0.133	47	53	
		7	8.2		16.4	1/2	1/4	0.233	0.135	47	54	
		8	8.2		16.4	n. d.	0.226	n. d.	0.127	n. d.	n. d.	57(b, c)
		9	8.2		16.4	0.452	0.226	0.230	0.166	51	73	
		10	8.2		16.4	0.452	0.226	0.297	0.166	66	73	
		117A, 23B	10.15	1	0.26		7.4	15	1/2	n. d.	0.392	n. d.
2	3.7				7.4	1	1/2	0.671	0.365	67	73	
3	3.7				4.94	1	3/4	0.621	0.533	62	71	
4	3.7				3.7	1	1	0.595	0.708	60	71	
5	7.4				7.4	1/2	1/2	0.258	0.314	52	63	
6	3.7				7.4	1	1/2	0.545	0.312	55	62	
7	7.4				14.8	1/2	1/4	0.235	0.143	47	57	
8	14.8				29.6	1/4	1/8	0.103	0.067	41	54	

TABLE 30. (Continued)

(1) Experiment and Electrode	(2) Weight of Cd(OH) <sub>2</sub> , mg	(3) Cycle	(4) Current		(5) ma	(6) 100 Percent Charge	(7) Time, hours		(8) Charging to H <sub>2</sub> Evolution	(9) Discharging to 1.0 Volt	(10) Coulombic Efficiency, percent		(11) Discharging to 1.0 Volt
			Charge, ma	Discharge, ma			Theoretical Discharge	H <sub>2</sub> Evolution			Charging to H <sub>2</sub> Evolution	Discharging to 1.0 Volt	
117, 45	51.7	1	1.3	37.8	37.8	15	1/2	n. d.	0.222	0.222	n. d.	45	
		2	18.9	37.8	37.8	1	1/2	0.375	0.214	0.375	38	43	
		3	18.9	25.2	25.2	1	3/4	0.358	0.345	0.345	36	46	
		4	18.9	18.9	18.9	1	1	0.377	0.471	0.377	38	47	
		5	37.8	37.8	37.8	1/2	1/2	0.187	0.204	0.204	37	41	
		6	18.9	n. d.	n. d.	1	n. d.	0.345	n. d.	n. d.	35	n. d.	
118, Hex 3	35.4	1	n. d.	25.8	25.8	n. d.	1/2	n. d.	0.019	0.019	n. d.	4.3(e)	
		2	12.9	25.8	25.8	1	1/2	0.038	0.043	0.043	3.8	8.3(f)	
		3	12.9	6.45	6.45	1	2	0.068	0.295	0.295	6.8	15(f)	
119, Hex 2	47.2	1	4.0	34.6	34.6	4.32	1/2	n. d.	0.304	0.304	n. d.	61	
		2	17.3	34.6	34.6	1	1/2	0.480	0.275	0.275	48	55	
		3	17.3	34.6	34.6	1	1/2	0.095	0.075	0.075	9.5	15(g,h)	
		4	17.3	34.6	34.6	1	1/2	0.135	0.083	0.083	14	17	
		5	17.3	34.6	34.6	1	1/2	0.135	0.086	0.086	14	17	
		6	17.3	34.6	34.6	1	1/2	0.135	0.093	0.093	14	19	
		7	n. d.	34.6	34.6	n. d.	1/2	n. d.	0.177	0.177	0.177	n. d.	48(i)
		8	17.3	34.6	34.6	1	1/2	0.335	0.226	0.226	34	61	
		9	17.3	34.6	34.6	1	1/2	0.384	0.221	0.221	38	60(j)	
		10	17.3	34.6	34.6	1	1/2	0.372	0.204	0.204	37	55	
		11	17.3	34.6	34.6	1	1/2	0.187	0.157	0.157	19	42(k)	
		12	n. d.	34.6	34.6	n. d.	1/2	n. d.	0.139	0.139	0.139	n. d.	37(l,1)
		13	17.3	34.6	34.6	1	1/2	0.228	0.204	0.204	23	55	

(a) n. d. = not determined.

(b) 116 Electrode charged in cyanide solution after the completion of Cycle 7.

(c) All values based on new value of theoretical capacity. New value 3.71 is 10% lower than starting capacity.

(d) 117A Test 117A continued from Cycle 10 of Test 116.

(e) 118 After impregnation the electrode was charged in cyanide electrolyte, washed, dried and weighed. Weight after impregnation 44.4 mg; after cyanide 35.4 mg.

(f) Charged for only 32.5 minutes at 1-hour rate.

(g) 119 Electrode on open circuit stand over weekend after Cycle 2. New electrolyte used for Cycle 3. NO Ba(OH)<sub>2</sub> used Cycles 1 → 6.

(h) Charge time for Cycles 3, 4, 5 was 15 min. Charge time for Cycle 6 was 30 min. Charge time for Cycles 8, 9, 10 was 32 min.

(i) After Cycles 6 + 11 electrode charged in KCN. Loss of material noted - new value appears in Cycles 7 and 12. Electrode then discharged in 30% KOH containing Ba(OH)<sub>2</sub>.(j) After Cycle 8 electrolyte changed to 30% KOH containing ≥ 13 g/l K<sub>2</sub>CO<sub>3</sub>.

(k) After 1 week stand in discharged condition electrode was cycled in 30% KOH containing no additives.

(l) Electrolyte in Cycles 12 and 13 was 30% KOH + Ba(OH)<sub>2</sub>.

Newly designed electrodes with straight-through and shaped pores might increase the charging efficiency and decrease cycling loss. If this hope were to materialize, the N/P ratios might be substantially decreased toward the theoretical minimum of a capacity N/P of 1.08 and a weight N/P of 0.85. Any improvement in N/P ratios will improve the weight and size factors of batteries and the above calculations are intended to show that such improvements are a worthy goal.

### Experimental Screen Electrodes

A large amount of research effort with stacked-screen electrodes was performed in connection with impregnation studies. Since that work is described under Task E, Table 30 shows only selected data which relate to identifying optimum pore dimensions.

In Table 30, the experiment numbers (101 through 119 in Column 1) were necessitated because the same electrodes were used several times. Electrode 23B, for example, was used in six separate experiments. For reuse, the electrodes were stripped with chromate solution and reweighed before impregnation by the fused salt method. Table 31 shows the slight changes occurring with reuse of electrodes. The weight changes are small enough that an electrode might be reused 10 or 20 times. The changes are large enough that the weights cannot be considered to be constant.

TABLE 31. TYPICAL WEIGHTS OF REUSED ELECTRODES

Experiment	Weight of Electrode 23B Before Impregnation, mg
103	39.3
108	37.1
112	36.6
116, 117A	35.3

In Column 1 of Table 31, the electrode numbers are those of Table 7. Pore sizes, porosities, and other physical properties of each electrode are given in Table 7. Pertinent information from Table 7 will be repeated with data from Table 30 to permit convenient comparisons. Other explanatory notes for Table 30 are as follows:

- n. d. means "not determined". Usually this vacancy was caused by the intentional nonrecording of an overnight charge after impregnations.
- All experimental data are recorded in Battelle Laboratory Record Book No. 22547. Experiments were not necessarily run in the numerical order listed.
- All the electrodes were impregnated by the modified fused-salt method described under Task E. Cathodic polarization during impregnation was avoided for all experiments except Numbers 102, 103, 104, and 106. In these four exceptions, cathodic polarization, to destroy nitrate, was carried out at less than 1 ma/cm<sup>2</sup> to a cut-off voltage of -1.0 volt versus SCE in the hot KOH solution. With improved temperature control during

impregnation, less than 1 minute was observed to be needed to reach the cut-off voltage. For this reason, the cathodic polarization was deemed to be negligible in subsequent experiments.

- All electrodes for all cycles were charged to 100 percent of theoretical capacity based on the weights shown in Column 2. Thus, charging continued at the constant current shown in Column 4 for the theoretical time shown in Column 6 regardless of where hydrogen evolution commenced.
- Time to H<sub>2</sub> evolution, Column 8, was determined from a recorder chart by measurement of the time span between start of charging and the mid-point of the voltage inflection that occurs with commencement of hydrogen evolution. (See Figures 69 and 71 for details of charging voltages.)
- In experiments having six or more cycles, Cycle 2 and Cycle 6 of those experiments are duplications to measure reproducibility.
- For overnight charges, Columns 4 and 6, current was controlled approximately to require a nominal 15- to 16-hour charging time.

Minor details are listed by experiment and cycle numbers at the end of Table 30.

Reproducibility. Comparison of Cycles 2 and 6 in Table 30, for those experiments having similar No. 2 and No. 6 cycles, provides a measure of reproducibility. Only Experiments 105, 113, and 114 duplicated as desired. All other experiments showed a significant loss of coulombic efficiency, both charge and discharge, when Cycle 6 is compared with Cycle 2. This comparison is made in Table 32 for two reasons:

- (1) It seems desirable to emphasize that effects of rates, pore sizes, and other variables can be estimated best using those electrodes that gave reproducible results. Otherwise capacity losses caused by some unknown variable might mask the effects of pore size, rate, etc. It will be noted later, however, that the reproducible results were not always the best results.
- (2) It should be noted how the nonreproducible cycles exhibited consistently large decreases in both charging and discharging efficiencies.

Effect of Rates. Considering first the reproducible electrodes from Table 30, the efficiencies of Columns 10 and 11 are seen to decrease with the increase of rates given in Columns 4, 5, 6, and 7. Figure 67 is a semilogarithmic plot to illustrate the effect of rate on efficiencies. The most striking feature of Figure 67 is that the screen electrodes are much less sensitive to rate than the commercial electrode. This could be an important and practical discovery because it implies that straight-through pores could provide electrodes whose performance is relatively insensitive to rate. In Figure 67, for example, Screen 26 appears to be more efficient, at rates higher than 30 minutes; the commercial plaque appears to be the more efficient at rates lower than 30 minutes.

Included also in Figure 67 are the results from the two discharge rates of Experiments 101 through 104 of Table 30. These results are particularly interesting because they consistently show higher efficiency for the stacked screens, with straight-through

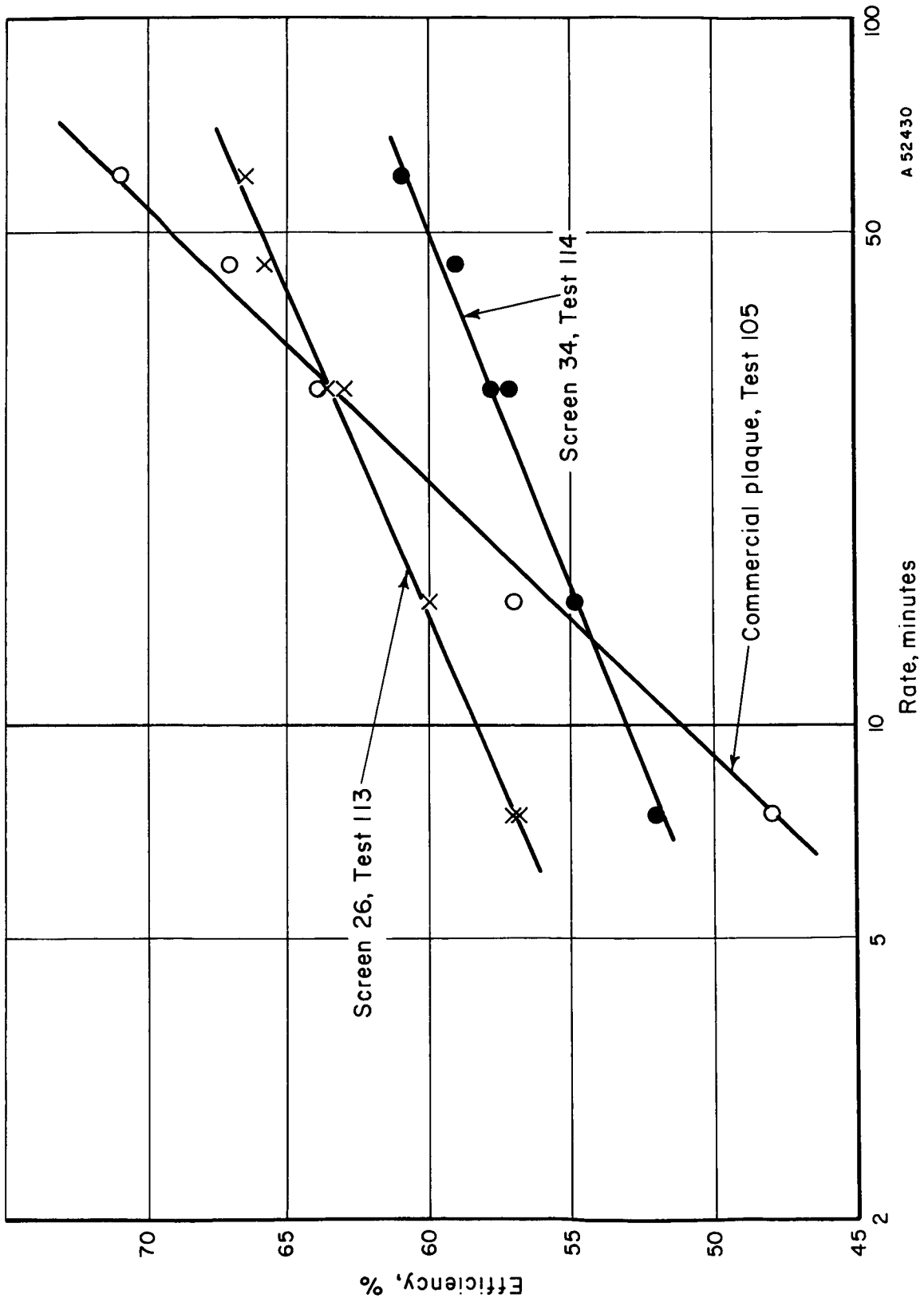
TABLE 32. REPRODUCIBILITY OF ELECTROCHEMICAL DATA

Experiment 1 from Table 30	Cycle	Input Efficiency, Column 10	Output Efficiency, Column 11	Efficiency
105	2	63.6	63.8	Reproduced
	6	65.0	66.2	
107	2	57.3	63.2	Decreased
	6	34.2	45.9	
109	2	67.5	68.8	Decreased
	6	32.0	36.0	
111	2	34.2	46.8	Decreased
	6	31.5	39.9	
112	2	66.3	71.0	Decreased
	6	58.5	64.0	
113	2	54.5	63.1	Reproduced
	6	58.0	62.8	
114	2	50.0	57.2	Reproduced
	6	50.8	57.9	
115	2	49.2	55.8	Decreased
	6	39.5	49.2	
117A	2	67.1	72.7	Decreased
	6	54.5	62.3	
119	2	48.0	55.0	Decreased
	6	13.5	18.6	

pores, compared with the efficiency of commercial screens. The results show that screen electrodes with uniform straight-through pores can be more efficient than the commercial screens with random pores.

A noteworthy feature of the results showing in Figure 67 is the consistently parallel lines for the screens and the powder plaques. These results provide additional evidence that screens are less sensitive to discharge rate than are sintered powder plaques.

All the screen electrodes in Figure 67 had straight-through pores. Therefore, the large differences in efficiencies cannot be attributed to pore shapes. Screen 34, a 1000-line/inch screen, shows parallel but widely different efficiencies in two experiments. Screens 23B and 44 are both 250 lines/inch and Screen 26 is 750 lines/inch. The efficiencies showing in Figure 67, therefore, are not controlled by pore sizes so much as by the impregnation and activation pretreatment as discussed in connection with Table 21 and Figure 55.



A 52430

FIGURE 67. DISCHARGE EFFICIENCY AS A FUNCTION OF RATE



Also, comparison of the efficiencies with electrode thickness from Table 7 show no direct relationship between efficiency and thickness. Rather, it appears, by comparing electrodes under conditions which displayed their highest efficiencies, that the ratio of electrode thickness to pore size may be important, as described under the next subheading.

The same effect of rate on charging efficiency occurs with electrodes of Experiments 105, 113, and 114; namely, the stacked screen electrodes are less sensitive to charging rate than is the sintered powder electrode.

Experiment	Electrode	Efficiency to H <sub>2</sub> Evolution, percent, at Indicated Charging Rates		
		1	1/2	1/4
105	Sintered powder	65.0	63.4	55.0
113	26 (750 lines/inch)	58.0	54.6	51.4
114	34 (1000 lines/inch)	50.8	49.0	46.6

With the charging rate data, however, the sintered powder plaque was consistently more efficient than the stacked screens for the reproducible electrodes. For Experiments 101 through 104, the opposite was observed, namely, the screen electrodes were consistently more efficient than the commercial electrodes.

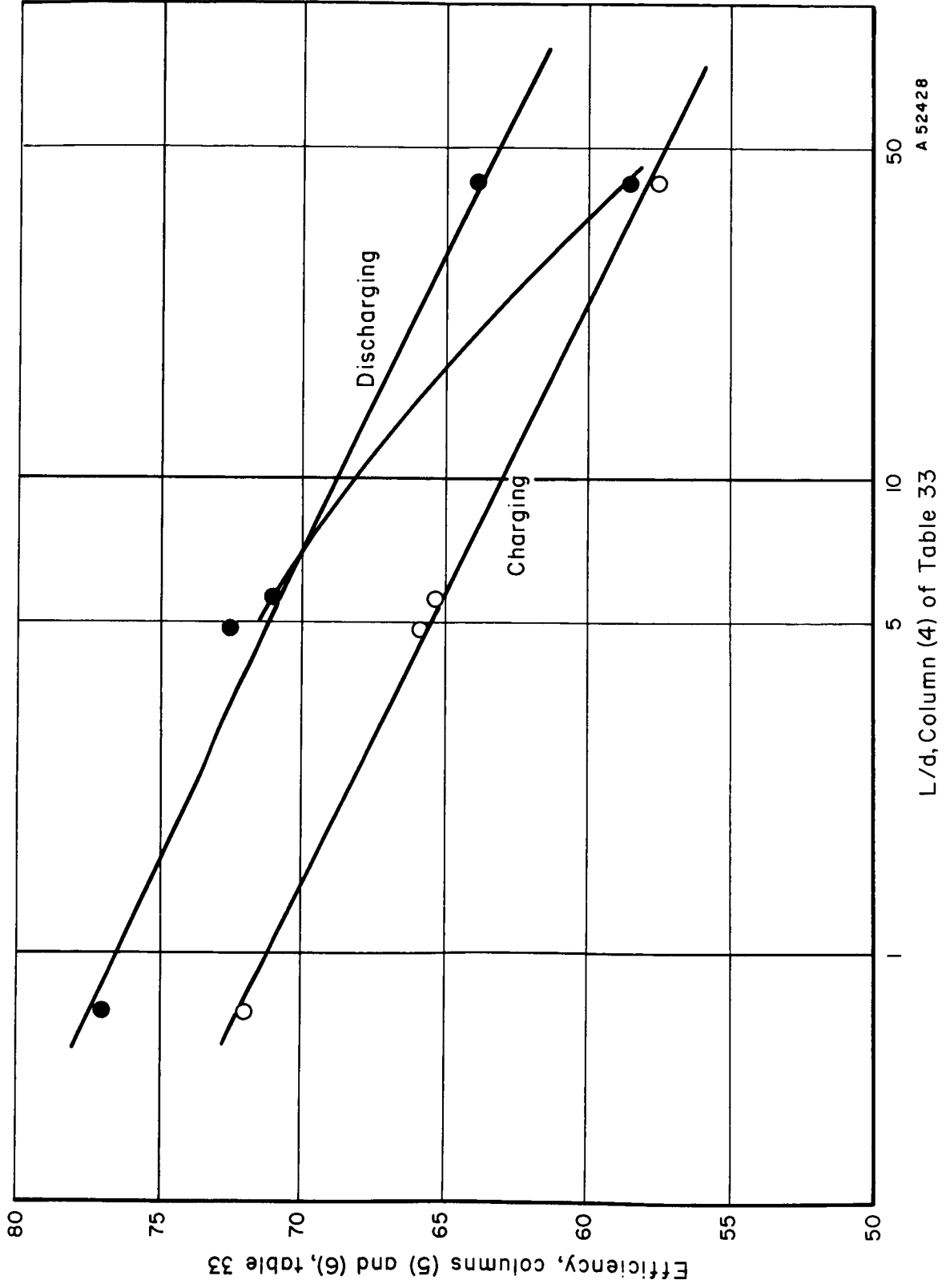
Effect of Pore Size and Electrode Thickness. The first four experiments in Table 30 were with electrodes 5.0 to 36 mils thick and with pore diameters from 0.63 to 3.2 mils. It is the ratio of the thickness to pore diameter that appears to be related to the charging and discharging efficiency. Designating one-half the electrode thickness as  $L$  and the pore diameter as  $d$ , Table 33 and Figure 68 show the relationship just mentioned. One-half the electrode thickness is taken as a pore length because the electrodes operate from both sides.

The straight discharging line in Figure 68 is drawn parallel to the charging line to imply a similar relationship for charging or discharging. The efficiency point on the discharging line at  $L/d = 42$  is from the first discharge cycle of Experiment 105, Table 30, Column 11, which was the highest first discharge efficiency for a commercial electrode for a 1/2-hour rate.

TABLE 33. RELATIONSHIP OF ELECTRODE THICKNESS AND PORE DIAMETER TO ELECTROCHEMICAL EFFICIENCY

(1) Experiment No. and Electrode Number	(2) Electrode Thickness, = 2 L, mils	(3) Pore Diameter = d, mil	(4) L/d	(5) Efficiency Percent		(6) Output, Cycle 1, Column 1 Table 30
				Input, Cycle 2, Column 10 Table 30	Output, Cycle 1, Column 1 Table 30	
101	36 <sup>(a)</sup>	0.63	42 <sup>(a)</sup>	57.6	58.6	
102	36	3.2	5.6	65.3	71.0	
103	5.0	3.2	0.75	72.0	77.0	
104	7.6	0.8	4.8	65.8	72.6	

(a) A tortuosity factor of 1.5 was used to calculate the L/d ratio.



A 52428

L/d, Column (4) of Table 33

FIGURE 68. RELATIONSHIP OF PORE LENGTH, L, AND PORE DIAMETER, d, TO ELECTRODE EFFICIENCY

Experiment 109 in Table 30 also had a high initial efficiency. This involved Electrode 26 with an L/d ratio of 2.4. The data have been added to Figure 68 to show that when the highest efficiencies are considered, the L/d ratio appears valid.

The relationship implied by Figure 68 has practical significance because it suggests an improved electrode will be obtained by using thin electrodes with wide pores. The extreme in efficiency would, therefore, be predicted for thin film on nonporous supports. However, two comments must be made about this conclusion: First of all, the simple relationship of Figure 68 is not always observed - thus suggesting that more than an L/d ratio is needed to make an efficient cadmium electrode. Second, the predicted high efficiency for flat nonporous electrodes was verified by the experiment described next.

A Flat-Plate Electrode. Because of this apparent advantage of a low L/d ratio for porous electrodes, it was assumed that a flat, negative electrode should perform well because flatness is the ultimate in a low L/d ratio. Weight ratios of nickel metal to active cadmium material can be made more favorable for this system than for sintered porous electrodes simply by using thin foil supports. However, nothing was known about the expected performance of a positive electrode of a flat-plate design. A cell was made to check out the idea and to see whether the positive electrode would perform well also.

Weighed amounts of cadmium and nickel oxides were sprinkled onto a flat plate and covered with filter paper. The amount of cadmium compound was selected to give a weight of cadmium hydroxide equal to 5 times the weight of a 0.1-mil nickel supporting foil. Commercial electrodes have about equal weights of cadmium hydroxide and nickel metal as shown in Items 7 and 9 of Table 25. The amount of nickel oxide was selected to give two-thirds the capacity of the cadmium electrode. The electrodes were clamped together, flooded with potassium hydroxide electrolyte, charged, and discharged. With a positive limited system, an efficiency of about 40 percent was obtained for a 1-hour discharge rate. Actual discharge time was 24 minutes. Literature for commercial sealed cells shows efficiencies from 40 to 60 percent for a 1-hour discharge rate. Subsequently it was observed that the nickel compound covered only about 10 percent of the electrode area and was 2 mils thick because the nickel oxide particles were about 2 mils in diameter. Uniform nickel oxide coatings 0.2 mil thick can be expected to increase the efficiency of discharge, and 0.2-mil positive material on a 0.1-mil support will increase the weight ratio of active material over that available from commercial porous electrodes. This prediction follows because Items 7 through 10 of Table 25 show commercial electrodes have more weight of inert plaque than weight of active materials whereas the proposed electrodes will have more active material than inert plaque. Based on this one quick test, the feasibility of making a sealed nickel-cadmium battery with very thin electrodes appears worthy of further consideration. Thin electrodes with corrugations up to 5 mils deep and 5 mils wide should be considered also.

The Effect of Carbonate Contamination. In addition to the detrimental effect of carbonate on the specific volume of the active material impregnated, a more serious effect is reported on the behavior of both the nickel hydroxide positive and cadmium negative electrodes on cycling. According to this recent literature\*, the effect of carbonate on the negative cadmium electrode is much greater than on the positive. The negative electrodes demonstrate both permanent and transient effects when cycled in the

\*Casey, E. J., Dubois, A. R., Lake, P. E., and Moroz, W. J., J. Electrochem. Soc., 112, 381 (1965).

presence of carbonate, both of which lower the coulombic or ampere-hour output, whereas the positive electrodes show only transient effects. Casey et al further report that the transient effects are a complicated function of the amount of carbonate in the electrolytes, depending also on current density and temperature.

Capacity losses in successive cycles were greatly decreased or eliminated by using a "carbonate-free" electrolyte. Data for cycling impregnated electrodes are given in Table 34.

TABLE 34. CAPACITY OF EXPERIMENTAL ELECTRODES

Electrode	Mesh	Capacity, percent of theoretical		
		First Cycle	Second Cycle	Third Cycle
23A	500	71(a)	78(b)	74(b)
26	750	62(a)	51(a)	Not checked
34	1000	64(a)	59(b)	76(b)

(a) Electrolyte, 30 percent KOH, about 0.3 percent  $K_2CO_3$ . Reagent KOH contained 0.85 percent  $K_2CO_3$ .

(b) Addition of  $Ba(OH)_2$  to electrolyte to precipitate most of the carbonate. An excess of 1.5 g/l  $Ba(OH)_2$  remained in the electrolyte.

Each electrode was first charged and discharged in 30 percent KOH containing about 3 g/l of potassium carbonate, a normal impurity in the reagent chemical. The 500-mesh screen electrode (Electrode 23A) had about 10 percent more available material than did the other two electrodes. However, this electrode (23A) was used soon after impregnation whereas Electrodes 26 and 34 were stored overnight in 30 percent KOH. Note in Table 34 that the third cycle was higher than the first cycle in both cases. Electrode 26 had a second cycle in the carbonate-containing electrolyte and the capacity dropped another 11 percent on a theoretical basis. This drop is consistent with prior work on both screen electrode and sintered-powder electrodes. The second cycle of Electrode 23A and the third cycle of Electrode 34 were the highest, respectively. Charging for these cycles was done overnight at a low charge rate with a large overcharge. Different charging rates and amounts of overcharge should affect the discharge capacity.

After obtaining the data in Table 34, an experiment was designed to demonstrate with one electrode both the detrimental effect of carbonate contamination and the advantageous effect of capacity recovery by means of a novel activation technique. The basic objectives were first to cycle an electrode in "carbonate-free" electrolyte until constant capacity was attained, then to add an excess of carbonate to a fresh electrolyte containing no  $Ba(OH)_2$  while cycling until constant capacity, and, finally, to attempt to recover the lost capacity by charging the electrode in a potassium cyanide electrolyte. The electrode would then be cycled in carbonate-free electrolyte and the capacity redetermined. Details of the experiment appear in Table 35. Cycles 1 and 8 were considered activation steps and were not recorded.

The data in Table 35 demonstrate that carbonate ion contamination in the electrolyte brings about a decrease in the available capacity of a negative electrode. This

"lost" capacity is not restored by open-circuit stand while in the discharged condition. However, more than the "lost" capacity was restored when the electrode was charged in a cyanide electrolyte and recycled in carbonate-free electrolyte. Thus, the electrode was somewhat passivated in Cycles 2 and 3.

TABLE 35. DETAILS OF CARBON-CONTAMINATION EXPERIMENT

Cycle	Charge Rate, hr	Discharge Rate, hr	Discharge Efficiency, percent
2	1	1/2	62 <sup>(a)</sup>
3	1	1/2	60 <sup>(a)</sup>
4	1	1/2	52 <sup>(b)</sup>
5	1	1/2	50 <sup>(b)</sup>
6	1	1/2	49 <sup>(b)</sup>
7	1	1/2	53 <sup>(b,c)</sup>
9	1	1/2	71 <sup>(a,d)</sup>

(a) Electrolyte 30% KOH + Ba(OH)<sub>2</sub> 5 g/l.

(b) Electrolyte 30% KOH + K<sub>2</sub>CO<sub>3</sub> 72 g/l.

(c) Electrode cycled after 8-day stand on open circuit in Electrolyte (b).

(d) Electrode charged in KCN electrolyte, then washed and discharged in Electrolyte (a).

It might seem that the electrode became passivated from the carbonate contamination to which it was exposed during its impregnation. However, chemical analysis showed that the material precipitated on impregnation was all Cd(OH)<sub>2</sub>.

The loss of capacity observed in Cycles 4 through 7 is attributed to a direct substitution of CdCO<sub>3</sub> for Cd(OH)<sub>2</sub> during the cycling.

The significance of the above experiment is that carbonates should be removed from both impregnating solutions and battery electrolytes to attain quantitative capacity data on negative cadmium electrodes. But the efficiencies in Table 35, Cycles 4 through 7, are still large compared to some of the low efficiencies shown in Columns 10 and 11 of Table 30. For example,

Experiment in Table 30	Lowest Efficiency in Column 11 of Table 30, %
109	32
111	31.4
115	36.7
118	14.3
119	14.9
120	33.0

There appear, therefore, to be additional and important efficiency factors that are yet to be described.

Item 2 - Energy InputInput Efficiencies

Comparison of charging efficiencies in Table 30, Column 10, with discharging efficiencies, Column 11, implies that charging is generally less efficient than discharging. Cycles 3, 5, 7, and 8, in the commercial electrode Experiment 105, are the only apparent exceptions that show slightly higher values in Column 10 than in Column 11. All other cycles in Table 30 show the higher values for Column 11, thereby indicating that discharging is more efficient than charging. In actuality, the above conclusion may be erroneous and misleading. Thus, if charging had been stopped at the point of first hydrogen evolution, the discharging efficiency would have been consistently lower than the charging efficiency. That is to say, the values in Column 11 are larger because some cadmium metal is produced on charging after hydrogen evolution. This complication is dealt with in connection with Figures 69 and 70, which follow immediately. The significant point here is to note that Columns 10 and 11 of Table 30 must be compared only under specially chosen conditions. Otherwise there appear to be few restrictions on use of the data.

When cadmium electrodes are charged for several cycles, at least two things happen: First of all, the apparent efficiency of the charging process decreases; second, the potential increases for hydrogen evolution. These effects are shown in Figure 69 with Cycles 1, 2, 8, and 9, for a commercial cadmium electrode. Note how the charging efficiency decreased between Cycles 1, 2, and 8, all at the same current density. The data for Cycle 9, when compared with Cycle 8, imply that cycling losses tend to diminish toward a constant low efficiency. Assuming this efficiency does tend to become stabilized with cycling, then Cycles 8, 11, 12, and 13 will show the effects of charging rate. Thus, increasing charging rate is seen decreasing the charging efficiency, as tabulated below:

<u>Cycle</u>	<u>Charging Rate, ma/cm<sup>2</sup></u>	<u>Efficiency to H<sub>2</sub> Evolution, percent</u>
8	4.8	72
12	24	66
11	48	64
13	96	62

Also notice in Figure 69 how the steady-state hydrogen evolution potential increased, first with cycling then with charging current density. Figure 70 shows how the hydrogen evolution potential, from Figure 69, varies logarithmically with current density. The straight line in Figure 70 is drawn with a slope of 0.12 volt per decade of current density because this is a commonly reported slope for the hydrogen evolution reaction - commonly called a "Tafel slope". Its practical significance is the implication that the effective surface area is decreasing with cycling. Thus, the 0.67-volt difference between the endpoints of Cycles 1 and 8 in Figure 69, corresponds to an area decrease of fivefold, assuming the same Tafel slope just described for Cycles 8 to 13. The same cadmium electrode after Cycle 8 seems to have only one-fifth, 20 percent, of its effective area at Cycle 1. This implication of loss of area in cadmium electrodes not only has the practical implication about cycling losses, it also shows why cadmium electrodes should be studied with cycling rather than without cycling.

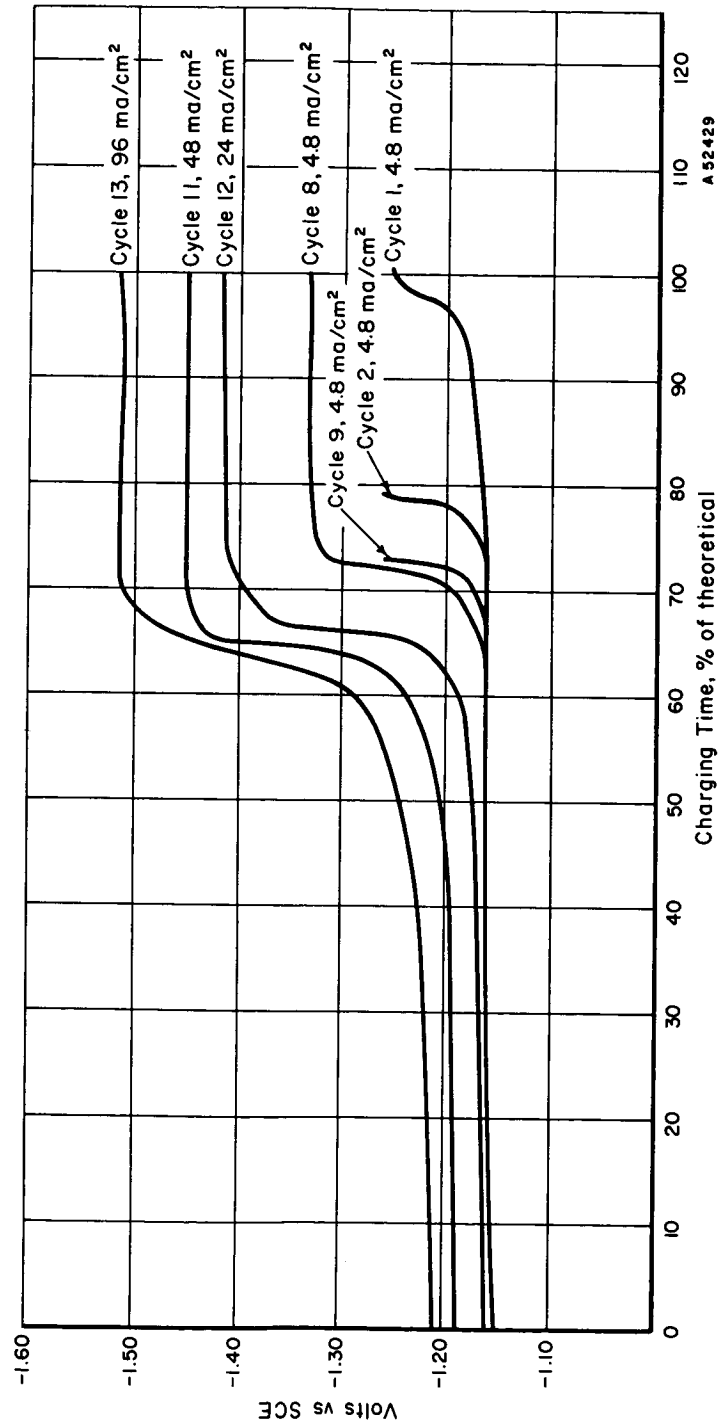


FIGURE 69. EFFECTS OF CYCLING ON THE CHARGING OF COMMERCIAL CADMIUM ELECTRODES

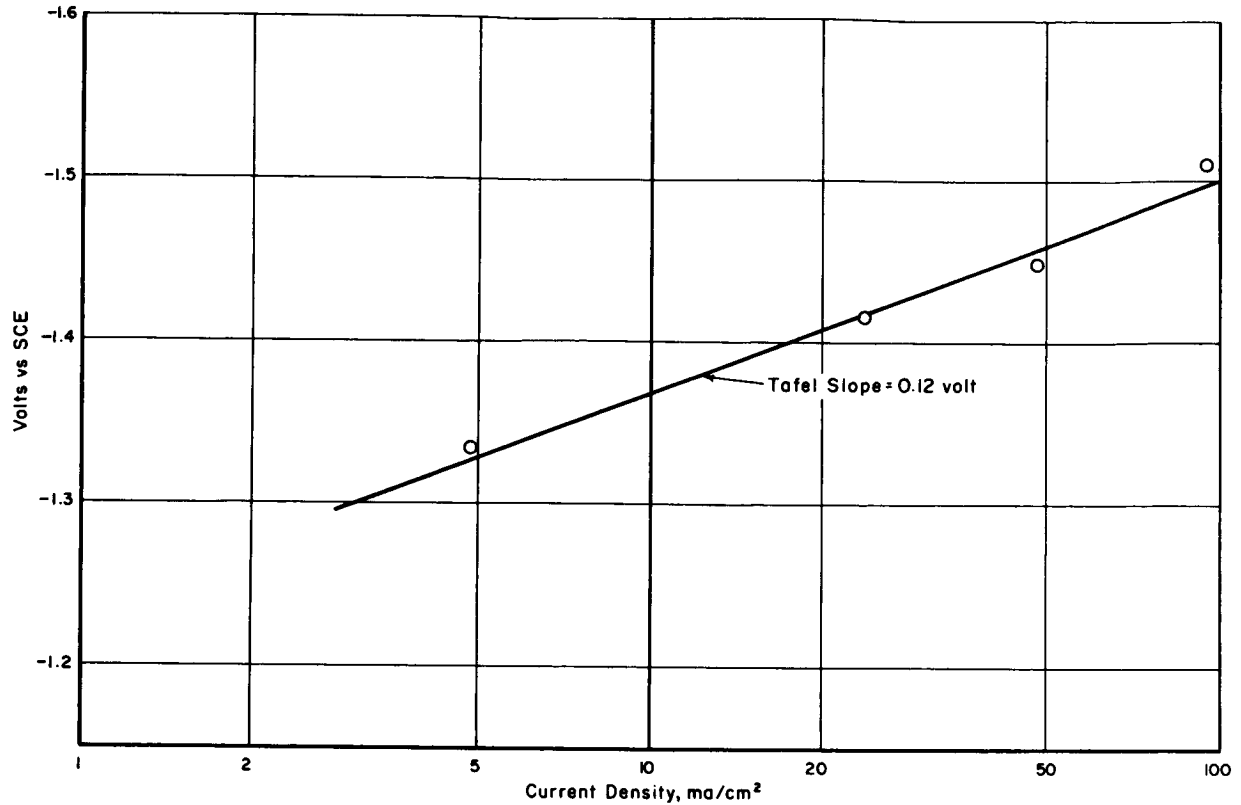


FIGURE 70. VOLTAGE FOR HYDROGEN EVOLUTION AS A FUNCTION OF CADMIUM ELECTRODE POTENTIAL

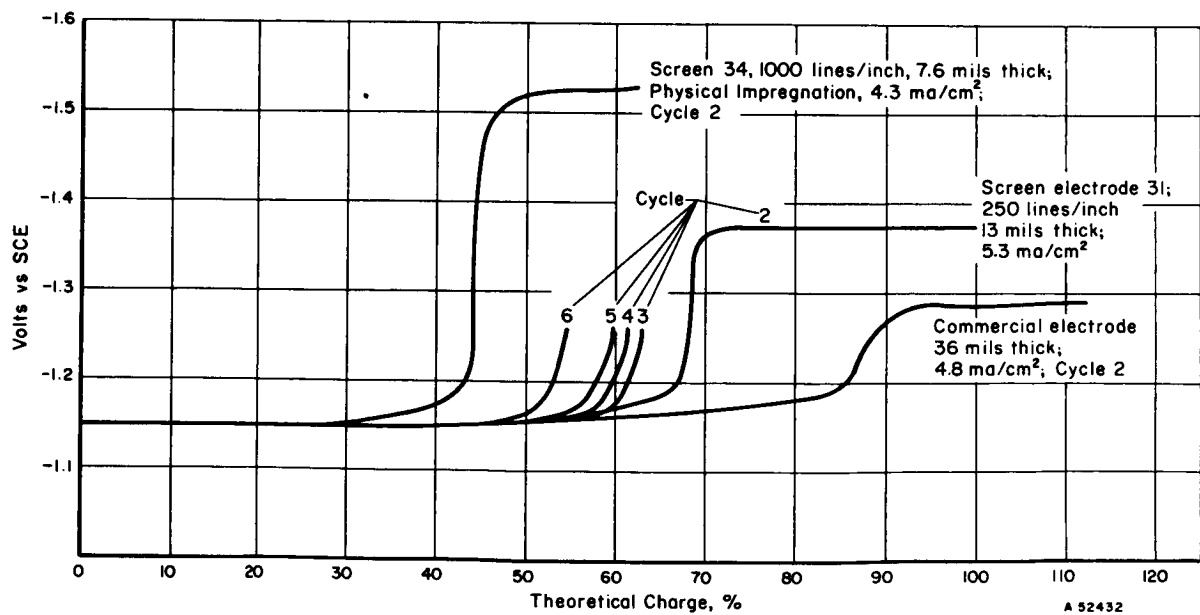


FIGURE 71. CHARGING CURVES FOR COMMERCIAL AND SCREEN ELECTRODES



Figure 71 shows additional data for experimental electrodes. Notice that all electrodes have about the same current densities and all start charging at the same voltage. Therefore initial or partial charging is independent of the electrode structure. Note that Screen Electrode 31 lost efficiency just as did the commercial electrode in Figure 69. The absolute changes are smaller for the screen electrodes but the absolute efficiencies are better for the commercial electrodes. The smaller changes with cycling suggest that shaped pores will be advantageous when one has learned how to achieve a high efficiency with them. The lower efficiency with the screen electrodes suggests that effective areas are less than in the commercial electrodes. Thus if one assumes the Tafel relationship of Figure 70, the hydrogen evolution voltages in Figure 71 imply the following relationships:

Electrode	Internal Surface Area, cm <sup>2</sup> /g (from Table 10)	Relative Internal Surface Area, cm <sup>2</sup> /g	Electrode Thickness, mils	Estimated Area, cm <sup>2</sup>	Relative Estimated Area	Relative Area, cm <sup>2</sup> (from Figure 71)
Commercial	880	1.0	21	410	1.0	1.0
Screen 31	140	0.16	18	57	0.14	0.18
Screen 34	560	0.64	7.6	100	0.24	0.009

The last column in the above tabulation was calculated by assuming the Tafel relationship:

$$E_{\text{comm.}} - E_{\text{screen}} = 0.12 \log (\text{area comm.} / \text{area screen}) \quad ,$$

where  $E_{\text{comm.}}$  and  $E_{\text{screen}}$  are the final voltages in Figure 71 at hydrogen evolution for Cycle 2 of each electrode, and the areas are effective areas rather than the approximate 2.0-cm<sup>2</sup> geometric area for each electrode. The most striking feature of the estimated effective areas is that they appear to bear little relationship to the estimated areas of the nickel metal plaques which were computed from the area for gram of electrode in the second column above, multiplied by the density of nickel, 8.9 g/cm<sup>3</sup>, and by the cm<sup>3</sup> of each electrode which was 1 cm<sup>2</sup> in geometric area. Thus, Screen 31 had more effective relative area (0.18 cm<sup>2</sup>) than expected (0.14 cm<sup>2</sup>), whereas Screen 34 had less effective relative area (0.009 cm<sup>2</sup>) than expected (0.24 cm<sup>2</sup>).

The voltage inflections on charging to hydrogen evolution appear to be one of the most sensitive indicators of changes within an electrode with cycling. The interpretation given above suggests the changes are due entirely to changes in and at which hydrogen can evolve. This interpretation needs to be challenged and verified, or modified, by further research because it suggests that significant area changes are causing losses of electrode capacity with cycling. If the interpretation is found to be true, then means to increase and control the effective area should be sought.

### The Effect of Pore Shapes

Contract work required a study on the effects of pore shapes on electrode performance. Table 36 shows selected data to illustrate the effects of pore shape. The data in the table seem to indicate that any restriction of the pore openings causes a decrease in efficiency. Thus, the "staggered taper", the "keyed", and the "random" sintered powder have both lower input and output efficiencies than the straight-through pores in Table 36. However, referring back to Electrode 39 in Table 21, it will be seen that a keyed opening electrode when properly impregnated and activated gave up to 71 percent efficiencies. Moreover, referring again to Figure 67, it is seen that efficiencies for the same electrode (Screen 34) can vary as much as all the variations in

Table 36. The net conclusion is that the effects of pore shape on the electrode performances were undetectable with the experiments performed. Extensive cycling tests are recommended as a preferred way to show the effects of pore shape.

TABLE 36. EFFECT OF ELECTRODE SHAPE ON ELECTRODE EFFICIENCIES

Electrode Shape	Experiment (Table 30)	Cycle 2 Efficiency, percent of theoretical	
		Input (Table 30, Column 10)	Output (Table 30, Column 11)
Straight	102	71.0	66.7
Straight	103	72.0	74.5
Random	105	63.6	63.8
Keyed	106	59.4	63.5
Staggered taper	115	49.2	55.8

Effects of Pore Volume Filled and Plaque Areas  
on Electrode Performances

Although care was taken to attain about the same porosity for all experimental electrodes and to fill all electrodes the same way, electrodes did not end with exactly the same percentages of pores filled. Thus, when the weights of  $\text{Cd}(\text{OH})_2$  in Column 2 of Table 30 are combined with the porosities of electrodes in Table 7, the values result as shown in Table 37. Even though there seems to be no connection between the percents of voids filled and the observed efficiency, it also seems that pores might be more completely filled without ill effects on electrode efficiency. The result would be a decrease in electrode and battery weights.

The last column in Table 37 was estimated using the  $\text{cm}^2/\text{gram}$  values from Table 10 multiplied by the weight values from Table 7. The commercial electrode area, Experiments 101 and 105, and the hexagonal-hole screens, Experiments 107, 111, 118, and 119 had their areas estimated in Table 22. All the electrodes in Table 37 were approximately 1 x 1-cm geometric area. There is no clear relationship between plaque internal surface areas and its efficiency as an electrode.

TABLE 37. RELATIONSHIP OF ELECTRODE EFFICIENCIES TO PERCENT OF PORE VOLUMES FILLED AND TO THE INTERNAL SURFACE AREA OF THE ELECTRODES

Experiment (from Column 1 of Table 30)	Calculated Percentage of Pore Volumes Filled	Observed Cycle 2 Discharge Efficiency (Column 11 of Table 30)	Estimated Internal Surface Area, cm <sup>2</sup>
101	40	59	150.
102	29	71	45
103	46	77	5.8
104	35	73	5.2
105	40	73	150.
106	22	68	29.
107	38	67	2.5
108	39	72	5.8
109	37	76	11.
111	58	50	2.5
112	41	76	5.8
113	41	63	11.
114	38	57	5.2
115	34	64	2.8
116	32	44	5.8
117A	32	78	5.8
117	29	45	29.0
118	49	4	2.5
119	50	61	2.5

### TASK G - CORROSION STABILITY

#### Objectives

Task G of the contract reads as follows:

"Not more than six selected electrode structures that show promise under Task F shall be given potentiostatic test for corrosion. Commercial sintered nickel plaques shall be used as controls."

The objective of this work was to show the inherent stability of electrode structures to electrochemical oxidation.

Active materials are well known to expand and contract with cycling of electrodes. These expansion processes might be expected to break sintered contacts apart - thereby opening up a porous powder plaque and leading to shedding of its active material toward the bottom of batteries. Even before this extreme condition prevails, it might be

expected further that sintered contacts would become areas of highly localized stress. Any chemical or electrochemical corrosion processes would then attack the sintered contacts preferentially. The result would be that a small amount of attack on the plaque could lead to a large amount of physical deterioration of its structure.

With the above reasoning in mind, a stacked screen electrode, a sintered powder electrode, and a solid nickel foil were given similar corrosion tests. The stacked screen electrode was Number 43 of Table 7, having 250 lines per inch. Both the commercial sintered powder plaque and the stacked screen were 21 mils thick. The general procedure was as follows:

Electrode specimens of about 1 x 1 cm had long platinum wires spot welded to them before placing in a three-compartment glass cell. The nickel electrodes were placed in an anodic compartment separated from the other compartments by a fritted disc or ground joint. The cathodic compartment contained a large platinized platinum counterelectrode. The third compartment contained hydrogen and saturated calomel reference electrodes. All compartments were filled with 30 weight percent potassium hydroxide and all experiments were performed at ambient room temperatures of about  $75 \pm 5$  F. A nitrogen atmosphere was maintained over the anodic compartment holding the nickel specimens.

An electronic potentiostat was connected to the various compartments so that current was caused to flow between the test nickel specimen and the large platinum counterelectrode in the direction and in sufficient quantity required to control the potential of the nickel test specimen at a preselected voltage with respect to the reference electrode. A recorder followed the current variations with time while the potentiostat maintained the constant potential.

Figure 72 shows the current density values for the three kinds of electrodes as a function of the anodic corrosion potentials. Each point on each curve shows the current density after 3 minutes, or more, at the given potential. The overlapping curves in the figure may appear somewhat complicated. Actually the result is simple from the viewpoint of corrosion stability, namely, all the curves in Figure 72 imply that all of the electrodes will show negligible corrosion.

Notice that each electrode exhibits hysteresis so that current density is less after the electrodes have been positive. Also, all the electrodes showed negative currents after being made anodic at +1.4 volts and return to potentials less than +0.7 volt. The above mentioned hysteresis is additional evidence of anodic passivation against corrosion. The negative currents mean that the passivating films can be reduced.

The general conclusion of negligible corrosion was confirmed by a longer corrosion test on a sintered powder plaque, as follows:

A commercial sintered powder plaque of 1.0-cm<sup>2</sup> geometric area was flooded with electrolyte after weighing at 44.0 mg. It was then potentiostatically set in the previously described three-compartment cell at +1.41 volts vs the hydrogen reference electrode for a total of 200 hours. There were four current interruptions of about 8 hours each. During the total experiment, 65 coulombs were passed. The 65 coulombs would have been enough to dissolve 19.7 mg of nickel, if the observed anodic currents of 50 to 120 microamperes were dissolving the nickel by corrosion rather than evolving oxygen. The final weight of the plaque was observed to be 43.7 mg. The 0.3-mg apparent loss of weight is

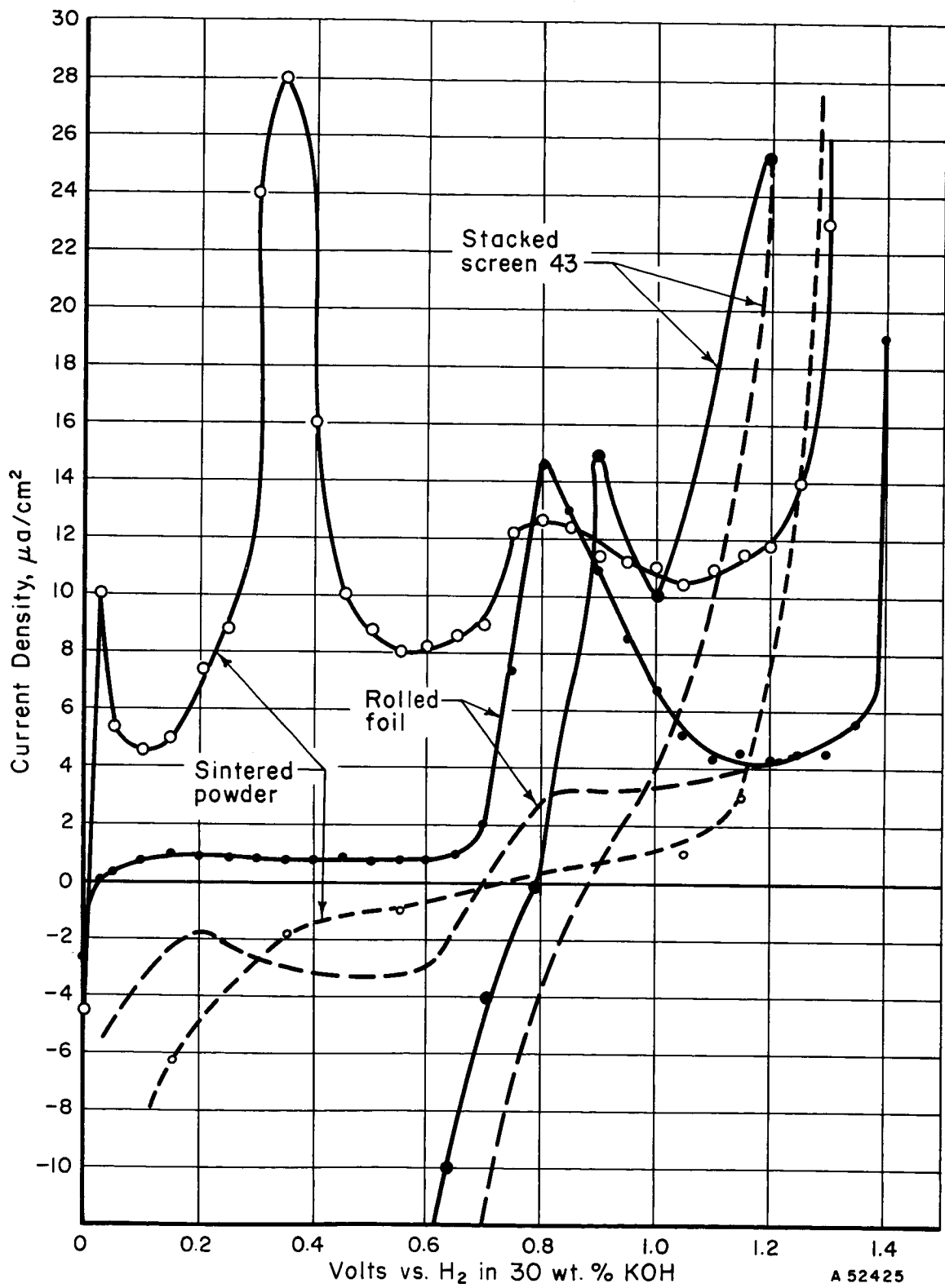


FIGURE 72. ANODIC-CORROSION MEASUREMENTS ON NICKEL ELECTRODES

equal to about the estimated experimental error thereby confirming the prediction from Figure 72 that corrosion would be negligible.

In view of the above findings, it was concluded that nickel corrosion will be a negligible process in the performance of nickel plaques in nickel-cadmium batteries.

All experimental data for Task G are on recorder charts filed with other detailed records of the project. The assistance of Mr. Carl H. Layer, who made the above experimental observations, is gratefully acknowledged.

JM/GRS/DGT/CLF:eh/all

DISTRIBUTION LIST

National Aeronautics & Space Administration  
Washington, D. C. 20546  
Attention: Ernst M. Cohn, Code RNW  
James R. Miles, Code SL  
A. M. Andrus, Code ST

National Aeronautics & Space Administration  
Scientific and Technical Information Facility  
P. O. Box 5700  
Bethesda, Maryland, 20014 (3)

National Aeronautics & Space Administration  
Ames Research Center  
Moffett Field, California  
Attention: A. S. Hertzog/J. R. Swain

National Aeronautics & Space Administration  
Goddard Space Flight Center  
Greenbelt, Maryland  
Attention: Thomas Hennigan, Code 636

National Aeronautics & Space Administration  
Langley Research Center  
Langley Station  
Hampton, Virginia  
Attention: S. T. Peterson  
John L. Patterson, MS 234

National Aeronautics & Space Administration  
Lewis Research Center  
21000 Brookpark Road  
Cleveland, Ohio 44135  
Attention: R. R. Miller, MS 500-202  
N. D. Sanders, MS 302-1  
Robert L. Cummings, MS 500-201  
Library  
B. Lubarsky, MS 500-201  
J. E. Dilley, MS 500-309  
J. J. Weber, MS 3-16  
M. J. Saari, MS 500-202  
W. A. Robertson, MS 500-201 (1 copy + 2 repro.)

National Aeronautics & Space Administration  
Manned Spacecraft Center  
Houston 1, Texas  
Attention: Robert Cohen - Gemini Project Office  
Richard Ferguson (EP-5)  
James T. Kennedy  
F. E. Eastman (EE-4)

National Aeronautics & Space Administration  
Marshall Space Flight Center  
Huntsville, Alabama  
Attention: Philip Youngblood

Jet Propulsion Laboratory  
4800 Oak Grove Drive  
Pasadena, California  
Attention: Aiji Uchiyama

U. S. Army Engineer R&D Labs.  
Fort Belvoir, Virginia  
Attention: Electrical Power Branch

U. S. Army Engineer R&D Labs.  
Fort Monmouth, New Jersey  
Attention: Arthur F. Daniel (Code SELRA/SL-PS)  
David Linden (Code SELRA/SL-PS)

Harry Diamond Labs.  
Room 300, Building 92  
Connecticut Avenue & Van Ness Street, N.W.  
Washington, D. C.  
Attention: Nathan Kaplan

Army Materiel Command  
Research Division  
AMCRD-RSCM T-7  
Washington 25, D. C.  
Attention: John W. Crellin

U. S. Army TRECUM  
Physical Sciences Group  
Fort Eustis, Virginia  
Attention: (SMOFE)

U. S. Army Research Office  
Box CM, Duke Station  
Durham, North Carolina  
Attention: Dr. Wilhelm Jorgensen

U. S. Army Mobility Command  
Research Division  
Center Line, Michigan  
Attention: O. Renius (AMSMO-RR)

Hq., U. S. Army Materiel Command  
Development Division  
Washington 25, D. C.  
Attention: Marshall D. Aiken (AMCRD-DE-MO-P)

Office of Naval Research  
Department of the Navy  
Washington 25, D. C.  
Attention: Dr. Ralph Roberts

Bureau of Naval Weapons  
Department of the Navy  
Washington 25, D. C.  
Attention: (Code RAAE)

Naval Ammunition Depot  
Crane, Indiana  
Attention: E. Bruess

Bureau of Ships  
Department of the Navy  
Washington 25, D. C.  
Attention: Bernard B. Rosenbaum (Code 340)  
C. F. Viglotti (Code 660)

Naval Ordnance Laboratory  
Department of the Navy  
Corona, California  
Attention: Mr. William C. Spindler (Code 441)

Naval Ordnance Laboratory  
Department of the Navy  
Silver Spring, Maryland  
Attention: Philip B. Cole (Code WB)

U. S. Naval Research Laboratory  
Washington, D. C. 20390  
Attention: Code 6160

Wright-Patterson AFB  
Aeronautical Systems Division  
Dayton, Ohio  
Attention: J. E. Cooper

AF Cambridge Lab.  
L. G. Hanscom Field  
Bedford, Massachusetts  
Attention: Francis X. Doherty

Rome Air Development Center, ESD  
Griffiss AFB, New York  
Attention: Frank J. Mollura (RASSM)

Office of the Deputy Commander AFSC  
for Aerospace Systems  
United States Air Force  
Los Angeles 45, California  
Attention: W. J. Bennison

Mr. Donald B. Hoatson  
Army Reactors, DRD  
U. S. Atomic Energy Commission  
Washington 25, D. C.

Defense Documentation Center Headquarters  
Cameron Station, Building 5  
5010 Duke Street  
Alexandria 4, Virginia  
Attention: TISIA

Institute for Defense Analyses  
1666 Connecticut Avenue, N. W.  
Washington 9, D. C.  
Attention: Dr. G. Szego

National Bureau of Standards  
Washington 25, D. C.  
Attention: Dr. W. J. Hamer

Power Information Center  
University of Pennsylvania  
Moore School Building  
200 South 33rd Street  
Philadelphia 4, Pennsylvania

Office of Technical Services  
Department of Commerce  
Washington, D. C. 20009

Mr. R. A. Eades  
D. R. S.  
British Embassy  
3100 Massachusetts Avenue, N. W.  
Washington 8, D. C.

Canadian Joint Staff  
Defense Research Member (WASA)  
2450 Massachusetts Avenue, N. W.  
Washington 25, D. C.

Power Sources Division  
Whittaker Corporation  
P. O. Box 337  
Newbury Park, California  
Attention: J. Rhyne

Aerospace Corporation  
P. O. Box 95085  
Los Angeles 45, California  
Attention: Library

Allis-Chalmers Manufacturing Company  
1100 South 70th Street  
Milwaukee 1, Wisconsin  
Attention: Dr. T. G. Kirkland

Atomics International  
North American Aviation  
Canoga Park, California  
Attention: Dr. H. L. Recht

Battelle Memorial Institute  
505 King Avenue  
Columbus 1, Ohio  
Attention: Dr. C. L. Faust

Buckbee Mears Company  
Park Square Building  
St. Paul, Minnesota 55101  
Attention: Norman C. Mears

Burgess Battery Company  
Freeport, Illinois  
Attention: Dr. Howard J. Strauss

Clevite Corporation  
Aerospace Research Division  
540 East 105th Street  
Cleveland, Ohio  
Attention: A. D. Schwobe

Delco Remy Division  
General Motors Corporation  
Anderson, Indiana  
Attention: Dr. J. J. Lander



Dynatech Corporation  
17 Tudor Street  
Cambridge 34, Massachusetts  
Attention: W. W. Welsh

Eagle-Picher Company  
P. O. Box 290  
Joplin, Missouri  
Attention: E. M. Morse

Electric Storage Battery Company  
Missile Battery Division  
Raleigh, North Carolina  
Attention: A. Chreitzberg

Electrochimica Corporation  
1140 O'Brien Drive  
Menlo Park, California  
Attention: Dr. Morris Eisenberg

Electro-Optical Systems, Incorporated  
300 N. Halstead  
Pasadena, California  
Attention: H. R. Erwin

Emhart Manufacturing Company  
Box 1620  
Hartford, Connecticut  
Attention: Dr. W. P. Codogan

Federal-Mogul Division  
20700 Mound Road  
Warren, Michigan 48090  
Attention: A. Beebe

Dr. Arthur Fleischer  
466 South Center Street  
Orange, New Jersey

General Electric Company  
Battery Products Section  
P. O. Box 114  
Gainesville, Florida

General Electric Corporation  
Schenectady, New York  
Attention: Dr. William Carson, ATL

Globe Union Incorporated  
900 East Keefe Avenue  
Milwaukee, Wisconsin  
Attention: Dr. C. K. Morehouse

Gould-National Batteries, Incorporated  
Engineering and Research Center  
2630 University Avenue, S. E.  
Minneapolis 14, Minnesota  
Attention: J. F. Donahue

Gulton Industries  
Alkaline Battery Division  
Metuchen, New Jersey  
Attention: Dr. Robert Shair

Huyck Metals Department  
P. O. Box 30  
Milford, Connecticut  
Attention: J. T. Fisher

IIT Research Institute  
10 West 35th Street  
Chicago 16, Illinois  
Attention: Dr. H. T. Francis

Leesona Moos Laboratories  
Lake Success Park, Community Drive  
Great Neck, New York 11021  
Attention: Dr. H. Oswin

Livingston Electronic Corporation  
Route 309  
Montgomeryville, Pennsylvania  
Attention: William F. Meyers

Lockheed Missiles & Space Company  
Sunnyvale, California  
Attention: Dr. J. E. Chilton, Dept. 52-30

P. R. Mallory & Company  
Technical Services Laboratories  
Indianapolis 6, Indiana  
Attention: A. S. Doty

P. R. Mallory & Company  
Northwest Industrial Park  
Burlington, Massachusetts  
Attention: Dr. Per Bro

Material Research Corporation  
Orangeburg, New York  
Attention: V. E. Adler

Melpar, Incorporated  
3000 Arlington Boulevard  
Falls Church, Virginia  
Attention: Dr. R. T. Foley

Monsanto Research Corporation  
Everett 49, Massachusetts  
Attention: Dr. J. O. Smith

Radiation Applications Incorporated  
36-40 37th Street  
Long Island City 1, New York  
Attention: Munroe F. Pofcher

Rocketdyne Division  
North American Aviation  
6633 Canoga Avenue  
Canoga Park, California  
Attention: Dr. R. P. Frohberg,  
Department 591

Sonotone Corporation  
Saw Mill River Road  
Elmsford, New York  
Attention: A. Mundel

Space Technology Laboratories, Incorporated  
2400 E. ElSegundo Boulevard  
ElSegundo, California  
Attention: Dr. A. Krausz

Metals & Controls Division  
Texas Instruments, Incorporated  
34 Forest Street  
Attleboro, Massachusetts  
Attention: Dr. E. M. Jost

Thompson Ramo Wooldridge, Incorporated  
23555 Euclid Avenue  
Cleveland, Ohio  
Attention: Librarian

Union Carbide Corporation  
Parma Research Center  
Box 6116  
Cleveland, Ohio  
Attention: Meredith Wright

Westinghouse Electric Corporation  
Research & Development Center  
Churchill Borough  
Pittsburgh, Pennsylvania  
Attention: Dr. A. Langer

Yardney Electric Corporation  
New York, New York  
Attention: Dr. Paul Howard